Design and Construction of an Experimental Apparatus to Assess the Performance of a Solar Absorption Chiller with Integrated Thermal Storage

by

Christopher Baldwin,

B.Eng., Carleton University, 2011

A thesis submitted to the Faculty of Graduate and Postdoctoral Affairs in partial fulfillment of the requirements for the degree of

Master of Applied Science

in

Mechanical Engineering

Carleton University
Ottawa, Ontario

Abstract

As the prevalence of mechanical space cooling in the residential sector increases in Canada, the amount of energy consumed and greenhouse gases released is increasing. Solar absorption cooling has the potential to significantly reduce the energy consumption for space cooling. Before widespread implementation of solar cooling can be achieved throughout Canada, the feasibility and optimization of these systems must be determined for the different climatic conditions within Canada. The design and construction of a complete experimental apparatus to assess the performance of an absorption chiller with integrated thermal storage was completed. The experimental set-up consists of a controllable, variable heat source capable of supplying water at 95°C and at flow rates up to 30 L/min, a heat rejection loop, which can dissipate 30 kW of thermal energy, and a building load simulator to create realistic residential cooling profiles. In addition, a model of the experimental set-up was created in TRNSYS. This model was used to create the experimental procedure for testing the absorption chiller. Through simulation it was determined that the chiller should be run for seven complete cycles and measurements taken at 30 second time intervals. Calibration was performed on the thermocouples and thermopiles to determine a set of equations that relates the voltage produced to the temperature and temperature difference. The error on the temperature readings was determined to be ±0.49°C while the temperature difference measured by the thermopiles has an uncertainty of ±0.15°C. An uncertainty analysis was conducted on the overall experimental set-up and the uncertainty of the thermal coefficient of performance can be determined to an overall uncertainty of ±3.8 percent, while the uncertainty on the electrical coefficient of performance was found to be ±3.3 percent.

Acknowledgements

I would like to thank my colleagues within the Solar Energy Systems Laboratory including Jenny Chu, Jayson Bursill and Ryan Dickinson as well as David Ouellette, Eric Duivesteyn, and Adam Wills for your friendship, guidance and assistance over the past two years. Additionally, I would like to thank Jacek Khan for his endless assistance throughout the construction, programming and calibration of the experimental set-up.

I would like to thank my supervisor, Dr. Cynthia Cruickshank, for the support, guidance and patience she has provided over the entire project.

I would like to acknowledge the financial support received from the NSERC Smart Net-Zero Energy Buildings Strategic Research Network, NSERC, and the Ontario Government through the Ontario Graduate Scholarship.

Lastly, I would like to acknowledge the support and encouragement of my family throughout my academic career.

Table of Contents

List of Tables

List of Figures

Nomenclature

Symbol	Description	Units
COP	Coefficient of Performance	
Q	Heat Transfer	kJ
e	Electrical energy consumed	kJ
T	Temperature	°C
HE	Heat Exchanger	
TC	Thermocouple	
TP	Thermopile	
FM	Flow Meter	
CV	Control Valve	
emf	Electromagnetic force	V
$\dot{m}$	Mass flow rate	kg/s
c_p	Specific heat	kJ/kg °C
$\dot{Q}$	Heat transfer rate	kJ/s
UA	Heat loss rate	W/°C
γ	Control signal	
η	Device efficiency	
ε	Heat exchanger effectiveness	
ϵ	Primary energy factor	
E	Energy	kJ
t	time	s
s_x	Standard deviation	
$s_{\bar{x}}$	Random standard uncertainty	

N	Number of measurements	
v	Degrees of freedom	
u	Uncertainty	
R	Resistance	Ω
CJC	Cold junction temperature	°C
$\dot{V}$	Volumetric flow rate	m^3/s
k	k-factor for flow meters	pulses/L
θ	Sensitivity factor	
δT	Change in temperature	°C
ρ	Density	kg/m^3

Subscripts

th	Thermal
el	Electrical
chiller	Chiller performance
system	System performance
cold	Change over cold side of chiller
hot	Change over hot side of chiller
in	Inlet conditions
out	Outlet conditions
amb	Ambient conditions
ave	Average
htr	Auxiliary heater
cool	Auxiliary cooler

c	Cold side of heat exchanger
h	Hot side of heat exchanger
r	Random uncertainty
T	Total uncertainty
s	Systematic uncertainty
pump	Change over pump
reject	Change over the heat rejection device

1 Chapter: Introduction

1.1 Background

In the last two decades, there has been rise in the use of residential cooling, causing an increasingly large demand on the electrical grid during the hot, humid summer months. As shown in Figure 1-1, from 1990 to 2010, the total cooled residential floor space in Canada has nearly tripled from 267 million square meters to 788 million square meters, while the total energy required for mechanical air conditioning increased by over 150 percent from 10.4 PJ to 26.5 PJ [1].

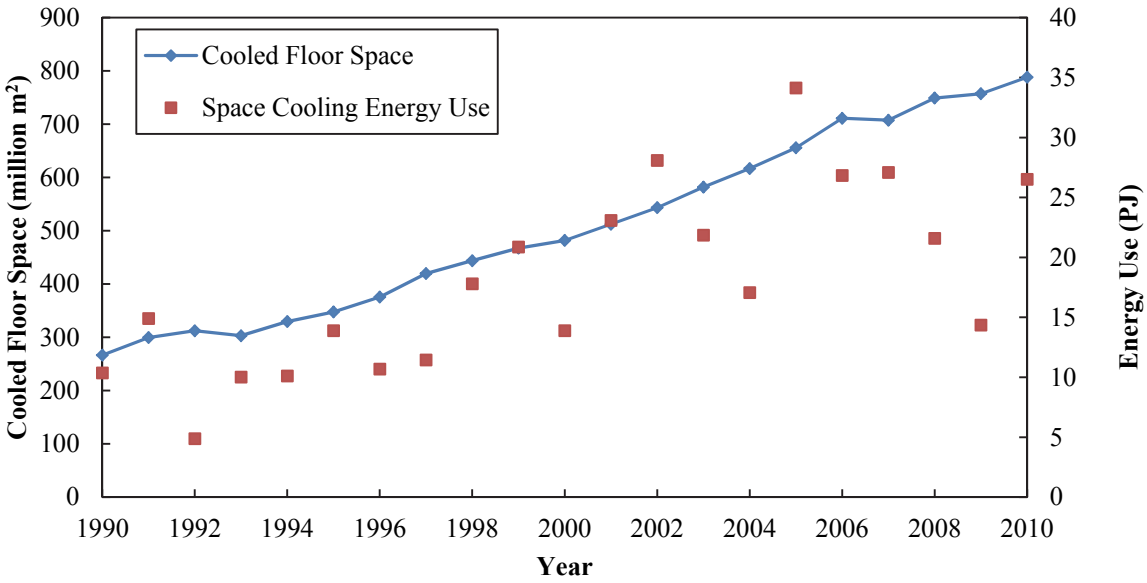

Figure 1-1: Comparison of energy use and cooled floor space in Canada

This increase in electrical demand has also caused greenhouse gas emissions to increase almost 140 percent from 0.6 Mt CO_2 equivalent in 1990 to 1.4 Mt CO_2 equivalent in 2010 [1].

Because of Canada's heating dominated climate, space cooling accounts for only two percent of the secondary energy (refined energy sources ready for end use e.g.,

electricity, natural gas) consumed by the residential sector in 2010 (as shown in Figure 1-2), and just under five percent of total residential electrical consumption [1]. Although the overall energy demand is a small percentage of the total residential annual energy consumption in Canada, this demand places a peak loading on the electrical grid during the late afternoons and early evenings of hot summer days [2]. In Ontario, the peak demand for the summer is forecast to be over 2000 MW, which is approximately nine percent higher than the winter peak [2]. To meet this peak demand, many provinces, including Ontario, use power plants to generate electricity from fossil fuels (e.g., natural gas), which produce large quantities of greenhouse gases. In Ontario, up to 50 percent more greenhouse gases per unit of peak electricity are released in the summer months to the winter months [3].

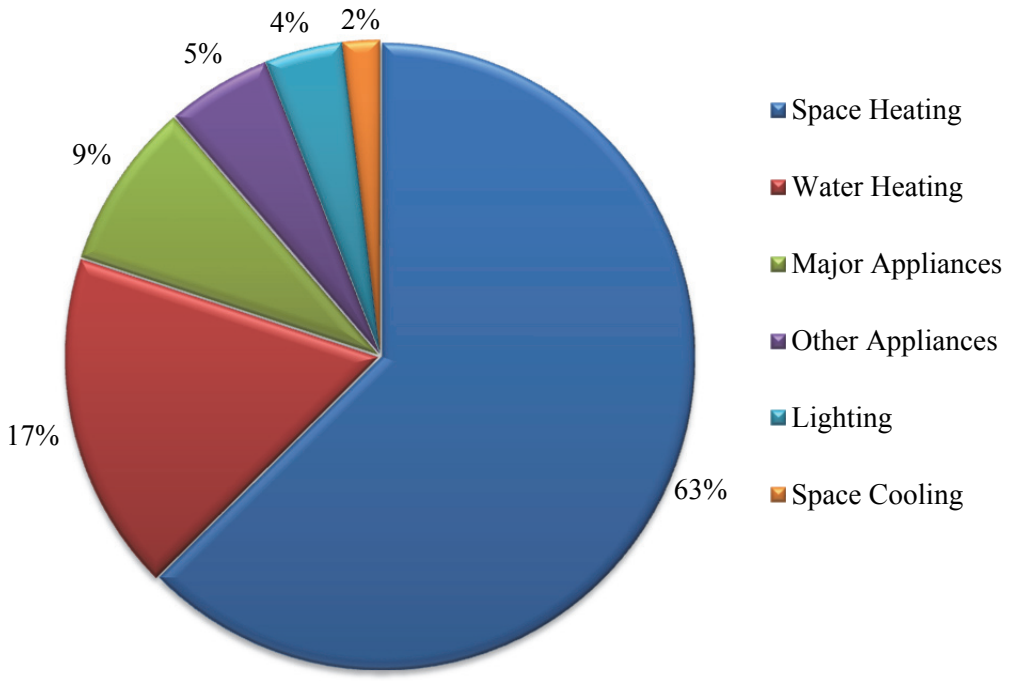

Figure 1-2: Residential secondary energy consumption in Canada

Solar cooling is a promising technology that could reduce the amount of electricity consumed by the residential sector for space cooling, and consequently reduce the amount of greenhouse gases produced in Canada. Although these systems are currently commercially available over a wide range of configurations and sizes, very few solar cooling systems have been installed in Canada as it is still a new and unproven technology. As a result, further work on the utilization and optimization of these systems in Canada is required before widespread implementation is possible.

1.2 Solar Cooling

Solar cooling systems can be broken down into two categories. The first uses photovoltaic panels to create electrical energy to drive a vapour compression cycle within an air conditioner or a heat pump, while the second category uses thermal energy collected from the sun as the principal energy input to cool and dehumidify a space [4]. Solar thermal cooling systems can be further broken down into two main categories: desiccant based systems and thermally driven chillers. Desiccant based systems are typically used to dehumidify incoming ventilation air by absorbing the moisture into a desiccant, and subsequently evaporating the moisture out of the desiccant using solar energy. Although latent cooling loads can be met, these systems are not able to provide sensible cooling and therefore are most effective in building with high ventilation rates in more humid climates [4].

Thermally driven chillers, on the other hand use a thermodynamic cycle to create chilled water, through either an absorption or adsorption process. These systems are applicable in almost all applications as they produce cold water that can then be used in

most standard air handling units with only minor changes required. The primary energy input into the chiller is solar thermal energy, while some electrical input is still required to operate the unit [4]. The difference between the absorption and adsorption chillers is the chemical process that takes place within the cycle. In an absorption process the refrigerant is completely absorbed into the absorbent forming a solution, while in an adsorption process, the refrigerant adheres to the outside of the adsorbent, staying as two separate states. The process which takes place is dependent on the pair of working fluids that are chosen, with different pairs of refrigerants and absorbent/adsorbents reacting differently. Typically, adsorption chillers use water-silica, zeolite-water, activated carbon-methanol or activated carbon-ammonia, while absorption chillers use a wider range of working fluids, with lithium bromide-water, lithium chloride-water and water-ammonia being some of the most common [5]. This thesis will focus on an absorption solar chiller using lithium chloride as the absorbent and water as the refrigerant.

An absorption chiller contains two different chemical components, with one of them acting as the refrigerant and the second acting as the absorbent. The absorption refrigeration cycle can be described as a modified version of the vapour refrigeration cycle, where instead of using a compressor between the evaporator and condenser, the vapour refrigerant is absorbed into an absorbent and pumped as a liquid to the generator where heat is added to the processes, causing the refrigerant to desorb from the solution as a vapour [6]. A comparison of a typical vapour compression cycle and an absorption cycle is shown in Figure 1-3. This is the most common commercially available thermally driven solar chiller [7].

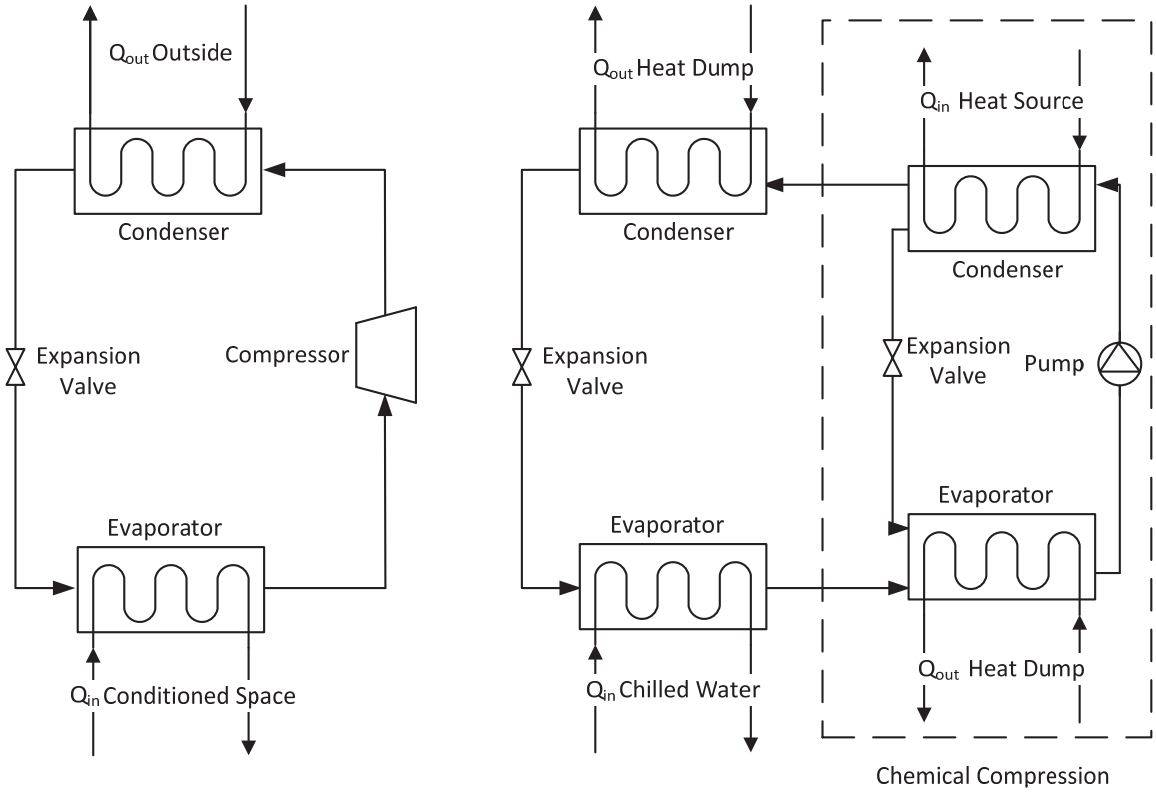

Figure 1-3: Traditional vapour compression cooling cycle (left) and an absorption cooling cycle (right) Adopted from [8]

An alternative to the typical absorption refrigeration cycle is an intermittent absorption cycle system shown in Figure 1-4. This system consists of only two independent heat transfer components, as opposed to the standard four heat transfer components in a traditional cycle (evaporator, absorber, generator and condenser). The two heat transfer components are piped together to allow the bi-directional flow of refrigerant between the two. The first heat transfer component is the generator and the absorber, while the second component is the evaporator and condenser, depending on the direction of the refrigerant flow (dictated by the heat source, whether the heat input or surroundings). These systems work in two distinct steps. The first step is the charging process. During this step, heat is inputted to the generator from the solar thermal

collectors to desorb the refrigerant (water in the case of the ClimateWell unit) from the absorbent (LiCl for the ClimateWell). As the refrigerant is desorbed, it converted to a vapour, and flows to the condenser. The refrigerant then condenses, which is an exothermic process, releasing waste heat which is rejected outside, typically using a cooling tower [8]. Once all of the refrigerant is desorbed, the unit switches from charging to discharging, where the system air conditions the building. The discharge cycle begins with heat being drawn from the surroundings to the evaporator (typically

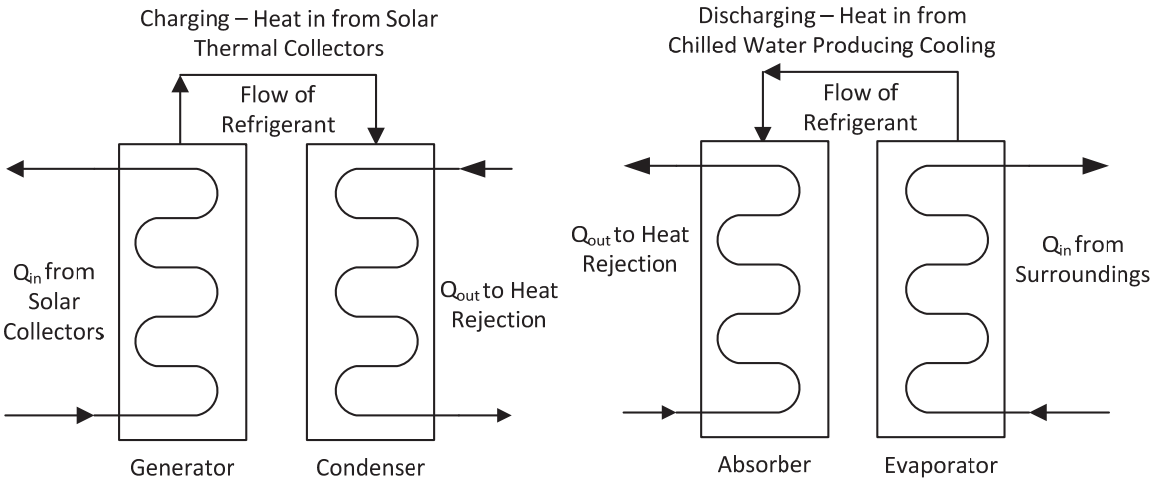

Figure 1-4: Schematic of an intermittent absorption cooling cycle

through the use of a cooling water loop) to evaporate the refrigerant. The evaporation is an endothermic reaction, removing hear from the air conditioning loop, cooling the water down. The refrigerant, now a gas, travels from the evaporator to the absorber, where it is absorbed back into the absorbent. The absorption process is also an exothermic process, releasing heat that is again rejected outside through a cooling tower. Once all of the refrigerant is absorbed back into the absorbent, the unit switches function and the processes starts over.

There are advantages and disadvantages to the intermittent system compared to the more traditional cyclical system. The main advantage to the system is that it allows for the "storage" of cooling capacity by storing the desorbed refrigerant in the evaporator/condenser, making it available for cooling when required. The main disadvantage is that continuous cooling cannot be provided, as it only cools the surrounding space while it is discharging. To overcome this, two intermittent absorption chillers need to be installed and controlled together as a pair. This allows one system to be charging, while the other system is discharging. The two systems would switch roles when the latter is completely discharged. This method is utilized by the ClimateWell solar absorption chiller, which was the focus of this experimental and modelling study [9].

1.3 Solar Absorption Cooling System Configuration

A complete solar cooling system consists of many individual components working together to provide space cooling. All solar cooling systems are comprised of solar thermal collectors, a heat rejection loop, a distribution system and a solar chiller as the minimum. Solar collectors are a special kind of heat exchanger that transforms radiant energy from the sun into useable thermal energy [10]. The type of collector selected for a specific solar cooling system is based on the type of cooling process (thermal chiller or desiccant and the working pairs within the system) and the temperature of the heat input required to drive the system. For lower temperature applications, flat plate collectors are often used, while evacuated tube collectors (having lower heat loss) are selected for applications requiring higher temperatures, which include most thermally driven chillers

[6]. Large scale solar cooling systems will typically use parabolic trough collectors which use a concentrating mirror to heat a working fluid to achieve very high temperatures.

Solar cooling systems also require a heat rejection loop or external heat rejection system, which is typically in the form of a cooling tower. This is critical for removing the excess heat created from the thermodynamic processes used in solar cooling, as both the condensing and absorption of the refrigerant are exothermic processes. To realize the cooling produced by the chiller, a distribution system or network is required. The most common distribution method is an air based system, where the air is blown over cooling coils, effectively creating a liquid-to-air heat exchanger. A second distribution method is using a hydronic system, where the chilled water is circulated through radiating ceiling or wall panels. Figure 1-5 shows a schematic of a typical absorption cooling system and depicts how the different components are installed and plumbed together.

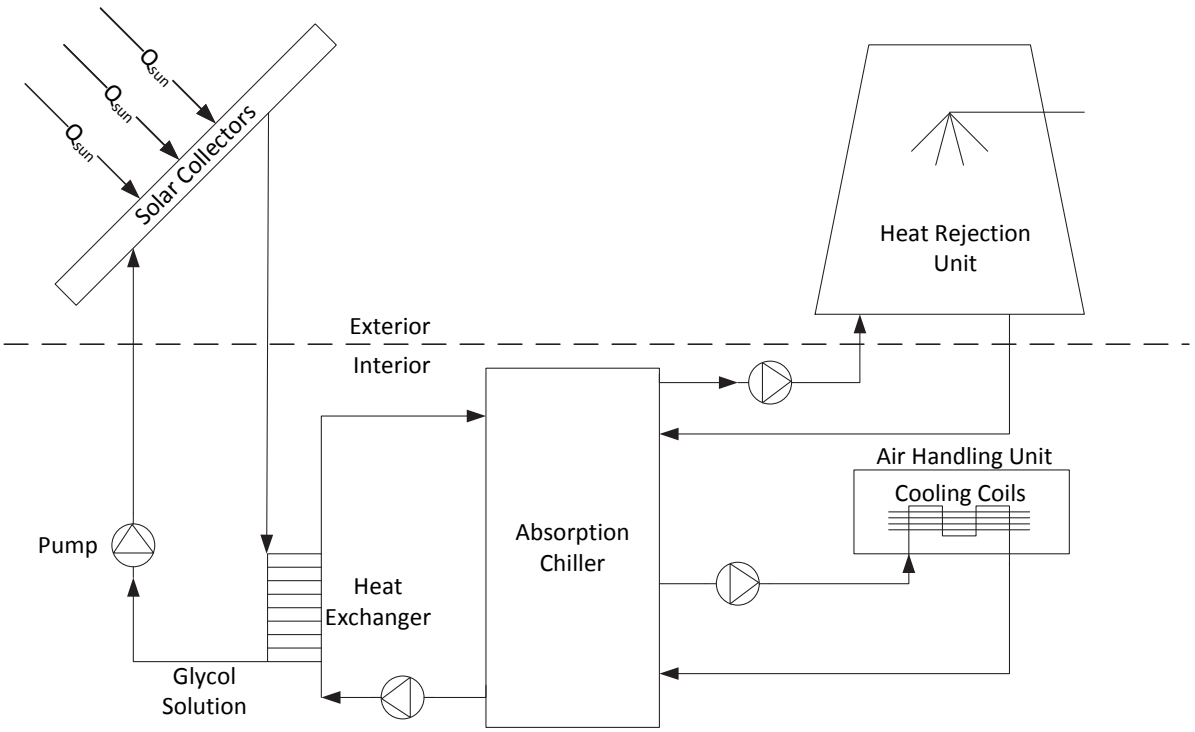

Figure 1-5: Typical solar absorption cooling system

To increase the effectiveness of the solar cooling system, thermal energy storage is generally needed to store energy for use when solar energy is not available [6]. This occurs at night or during cloudy days when the amount of solar radiation reaching the collectors is greatly reduced. Thermal energy storage systems can be achieved by: using a hot storage, generally by storing water at high temperatures; and through the use of a cold storage, where water or other liquid is kept at a low temperature to provide cooling as required at a later time [7]. Thermal storage can also be achieved using chemical storage, such as in a fully charged intermittent solar absorption chiller. Figure 1-6 shows a schematic of how a hot and cold thermal storage could be integrated into the complete system. This configuration allows chilled water to be stored, and when cooling is required, cold water is drawn from the storage, cooling the space through the distribution

system. As the cold storage heats up, the chiller engages, drawing energy from the hot storage which is charged when solar energy is available, and creates chilled water which is deposited into the cold storage, to be used when cooling is needed. Often, solar cooling systems use the same components as a solar thermal heating system, allowing a single system to provide both heating in the winter months and cooling in the summer months, simply by bypassing the absorption chiller and using the thermal energy from the collectors within the distribution system.

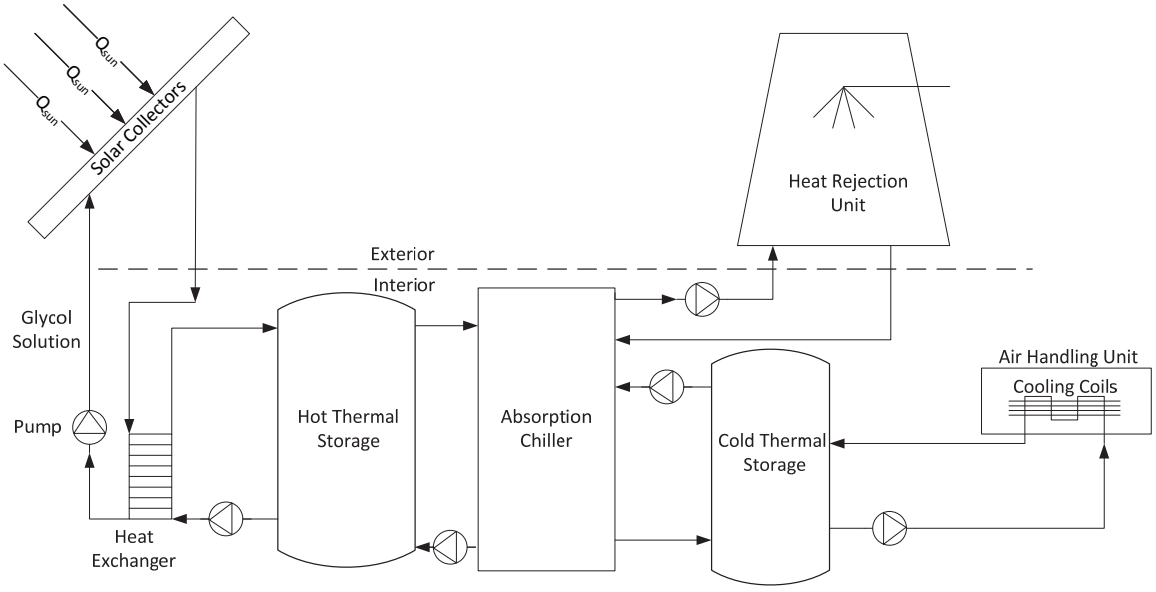

Figure 1-6: Typical solar absorption cooling system with hot and cold thermal storage

1.4 Research Objectives

The overall goal of the research presented in this thesis is to evaluate the performance of a solar absorption chiller through the design, construction, commissioning and modelling of an experimental apparatus. To meet the overall goal, the research had the following objectives of which the results are presented within this thesis.

- Create a conceptual design of an experimental test apparatus that can provide controlled steady state and transient operating conditions for the solar absorption chiller.
- Design heat input and heat rejection loops to simulate solar input.
- Design and size system components to be installed within the experimental test set-up.
- Construct four hydraulic networks within the laboratory and install and test equipment. Additionally, install and program the data acquisition and control system. Install and connect all of the instrumentation used to assess the performance of the absorption chiller.
- Calibrate instrumentation and determine the system uncertainty on the heat transfer rates in the absorption chiller and COP calculations.
- Develop a model in TRNSYS of the experimental apparatus to determine the design and experimental procedure and ensure the experimental apparatus will function over the entire test range.

This work is the first phase in a multi-year project to determine the feasibility of solar absorption cooling in Canada and subsequently determine the optimal system configuration for a residential installation. Future work will involve both experimental evaluation and computer simulation for different climatic and building load conditions across Canada.

1.5 Contribution to Research

This work included the:

1. design of a complete experimental testing apparatus to determine the thermodynamic and heat transfer rates within a solar absorption chiller;
2. construction and instrumentation of the experimental apparatus within the Solar Energy Systems Laboratory;
3. performance of calibration experiments on the thermocouples and thermopiles installed within the experimental apparatus;
4. completion of an uncertainty analysis on the complete experimental system to determine the uncertainty on the heat transfer rates and coefficient of performance; and
5. determination of the experimental procedure for testing the absorption chiller through simulation.

1.6 Organization of Research

The information outlined in this thesis documents research that has been conducted over the previous two years and is divided into the following chapters:

Chapter 1 – Introduction: An introduction of solar cooling technologies, typical system configurations and an outline of the thesis

Chapter 2 – Literature Review: A review of literature on solar cooling research including experimental testing, modelling studies and case studies of installed systems

Chapter 3 – Experimental Design: A detailed description of the hydraulic loops designed and constructed and description of the components installed

Chapter 4 – System Modelling: An outline of how the model was constructed in TRNSYS and how each of the key components function.

Chapter 5 – Modelling Results and Discussion: A summary of the results of the modelling studies including the experimental procedure determined through simulation.

Chapter 6 – Calibration and Uncertainty Analysis: A description of the calibration experiments and the uncertainty analysis conducted on the experimental apparatus.

Chapter 7 – Conclusion and Future Work: A summary of the conclusions from this thesis and an outline of future work.

2 Chapter: Literature Review

Solar cooling is an expanding field, with a significant potential to offset the amount of energy consumed and greenhouse gases released as a result of mechanical cooling. As a result, a large amount of research has been conducted on system design and optimization for the residential and industrial sector. To date, most research projects have focused on large scale installations for use in industrial and commercial complexes as opposed to the implementation of small scale solar cooling systems. Additionally, the bulk of the research has been conducted in Europe, with little research and very few solar cooling systems have been installed and tested within Canada.

This chapter contains a literature review of past and current research and demonstration projects focused on the implementation and performance assessment of solar cooling systems. The results of the International Energy Agency's programmes on solar cooling are presented, with the major advancements and results in small scale, residential sized solar cooling systems highlighted. Current research projects are also discussed, including those based on the simulation of solar cooling systems and those experimentally evaluating the performance of solar cooling systems either in a laboratory under controlled conditions or as a field study, where full scale systems are installed and the performance monitored over an extended period of time. Finally, a review of different performance metrics used to evaluate the performance of a solar chiller and the complete solar cooling system are outlined and will be used within the experimental evaluation of the system.

2.1 International Energy Agency – Solar Heating and Cooling Programme

Solar cooling has been investigated through the International Energy Agency (IEA) Solar Heating and Cooling (SHC) Programme. The IEA was established in 1974 as an autonomous agency within the framework of the Organization for Economic Co-operation and Development [11]. The IEA was created to carry out a comprehensive program of energy co-operation among the 25 member countries and the Commission of European Communities [11]. The Solar Heating and Cooling Programme was one of the first programmes established by the IEA in 1977 with a focus on advancing active solar, passive solar and photovoltaic technologies with a mission "to facilitate an environmentally sustainable future through the greater use of solar design and technology" [12]. Under the IEA-SHC programme, solar cooling has been investigated under three separate tasks; Task 25 from 1999 to 2004, Task 38 from 2006 to 2010 and since 2011, solar cooling has been studied under Task 48.

2.1.1 IEA-SHC Task 25

From June 1999 until May 2004, researchers from over 10 different countries collaborated on a project under IEA-SHC Task 25 Solar Assisted Air Conditioning of Buildings. This task sought to address the three principle problems with standard air conditioning systems. These problems were defined as follows:

- they consume a large quantity of energy
- they cause large electricity peak loads
- in general, they employ refrigerants which have negative impacts on the environment.

The main objectives of Task 25 were to improve the conditions for market entry of solar assisted cooling systems and to promote the reduction of primary energy consumption and peak electrical loads. The results of the Task were directed towards the air conditioning industry, planners, architects, and facility owners and managers.

In order to address the objectives laid out by Task 25, the study was broken down into 4 subtasks:

- Subtask A – Survey of Solar Assisted Cooling: this provided a review of the current technologies available as well as the evaluation of past completed projects
- Subtask B – Design Tools and Simulation Programs: this developed a detailed simulation tool to layout, optimize and determine the control strategies for solar assisted cooling systems
- Subtask C – Technology, Market Aspect and Environmental Benefits: this provided an overview of the current equipment suitable for solar cooling applications, as well as supported the development and market introduction of new systems
- Subtask D – Solar Assisted Cooling Demonstration Projects: this task carried out eleven demonstration projects to gain practical experience and at the same time provide real performance data of the systems

As a result of the work produced under these subtasks, several advancements were made in the area of solar cooling. Within Subtask C, a guideline was developed for the design and implementation of different solar assisted cooling systems [12]. This document presents a decision scheme to aid in the selection of the most applicable

technical solution for a given situation. The design scheme takes into consideration the climatic conditions, building factors, and the occupation and use of the building in selecting a system design. The design scheme uses easy to navigate flow charts to determine a technical solution based on the various factors as specified by the proposed building. Also Subtask C released a technical report that outlined recently completed and on-going research in the area of solar cooling [13]. One remaining obstacle identified within this report was the need to overcome the lack of small scale chillers currently on the market.

The results of Task 25 form the basis of the book titled "Solar-Assisted Air-Conditioning in Buildings – A Handbook for Planners" [14]. This book details many of the findings of the different subtasks under Task 25. It outlines the different system configurations and components, as well as different methods for characterizing the performance of solar-assisted cooling systems. It also highlights some of the demonstration projects completed within the Task.

2.1.2 IEA-SHC Task 38

More recently, a second Task under the IEA-SHC further looked at solar assisted cooling. From September 2006 until December 2010, Task 38 – Solar Air-Conditioning and Refrigeration studied technologies for producing cold water or conditioned air by the means of solar heat. Task 38 set out to meet a list of objectives, with the main objective being the accelerated introduction of solar assisted cooling system into the market place through the development and testing of cooling equipment for the residential and small scale commercial sector. Among other goals, Task 38 worked towards the development

of pre-engineered systems for small and medium sized applications, as well as the development of simulation tools for the evaluation of these systems.

Similar to Task 25, Task 38 was further broken down into four subtasks, each focusing on specific areas within the solar cooling field:

- Subtask A – Pre-Engineered Systems for Residential and Small Commercial Applications: this provided a report of current small scale solar cooling equipment and guidance on system implementation and maintenance.
- Subtask B – Custom Made Systems for Large Non-Residential Buildings and Industrial Applications: This provided a market overview and review of current system designs for large scale systems and guidelines for system design, installation and monitoring.
- Subtask C – Modelling and Fundamental Analysis: This looked at simulation thermodynamic evaluation of solar cooling systems.
- Subtask D – Market Transfer Activities: This focused on transferring the results of Task 38 to useable technology advancements in industry.

Through these subtasks, a wide range of work was conducted on different solar cooling technologies and systems. The overall results of Task 38 are outlined in the final position paper, and will be included in the release of the second edition of the previously mentioned handbook for planners (released as part of Task 25) [15]. An overview on installed solar cooling systems over 20 kW was also published to outline the types and locations of all large systems in the world [16]. In 2008, there were 81 large scale cooling systems installed in the world, with the largest system located in Viota, Greece, with a

total cooling capacity of 700 kW and 2,700 m^2 of flat plate collectors. Among all the solar cooling systems discussed, only one such system was located in North America (specifically, Mexico), with no large scale solar cooling systems installed in either the United States or Canada. Lastly, the publication outlined the distribution of cooling technologies, as well as the type of collectors used and the type of thermal storage implemented in the systems.

Another outcome of Task 38 was the creation of the "Checklist Method for the Selection and the Success in the Integration of a Solar Cooling System in Buildings" [17]. This checklist aims to help building operators determine if a solar cooling project is feasible or not at the design phase of the project. This checklist takes into consideration many factors that influence whether a project will be successful. These factors include the location of the project and the climate at that location, as well as the building logistics and required cooling load. The checklist also accounts for the economic feasibility of the project by factoring the energy costs for the given location as well as the motivation and ability for the owner to make the required investment for the solar cooling system. Finally, the checklist considers the technical skills of the building operational staff, as well as the ability to monitor the long-term performance of the system.

The checklist is comprised of several questions which address the previously mentioned factors, and awards a value to each question with a maximum score of 20. Based on the total score obtained, the feasibility of the project is determined (with a recommended minimum of 10 out of 20 to proceed with the project) [17]. This is an effective first step in determining whether a solar cooling system is a possibility for a given situation. However, after the completion of this checklist, a significant amount of

design work would still be required before a project can be successfully implemented. Although this is a useful tool, one significant limitation is that this checklist method is only applicable for projects being considered in Europe, as all climates and energy costs are for countries in Europe. As a result, this method cannot be used directly to assess the feasibility of projects within Canada and the United States.

Of particular interest for residential applications was the work conducted by Subtask A of Task 38. Through this subtask, a report titled "Market Available Components for Systems for Solar Heating and Cooling with a Cooling Capacity of < 20kW" was completed. The report outlines the current market availability of small scale solar cooling units (less than 20 kW) [7]. This report also outlines the components currently available for use within solar cooling systems including solar heating systems, thermally driven chillers, heat rejection methods and cold storage solutions. It was found that there are a limited number of thermally driven coolers currently available on the market, with a total of fourteen different systems either available, or that will be available in the near future on the market. Of these, five systems use an adsorption process with either water-silica gel or water-zeolite technology, while the remaining nine use an absorption process with either ammonia-water, lithium bromide-water or lithium chloride-water technology. These systems have nominal thermal coefficients of performance (COPs – a ratio of cooling produced compared to thermal heat input and is further discussed in Section 2.3) of 0.5 to 0.78 with the absorption systems typically having a slightly higher COP when compared to the adsorption systems.

As a final noteworthy aspect of Subtask A, thirteen small scale systems in Europe were monitored on an on-going basis with eleven providing enough data for analysis

[18]. Through the monitoring of these systems, the thermal COP of nine of the chillers were found to have COPs ranging from 0.5-0.7, which was in-line with the manufactures specifications. When the entire system is evaluated, the electrical COP of the system peaked at 8, with many systems having electrical COPs (a ratio of cooling produced compared to the amount of electrical input) between 5 and 6. It was also found that some systems had an overall electrical COP of less than 3, meaning that a traditional vapour compression refrigerator may be more energy efficient. The conclusion from this study was that many of these systems could achieve a higher COP if the systems were further optimized, and a COP of 3 should be obtainable in most, if not all of the systems. To be able to monitor these systems, a method had to first be developed and is detailed in a separate report entitled "Monitoring Procedure for Solar Cooling Systems" jointly released by Subtask A and B [19].

2.1.3 IEA-SHC Task 48

Currently the IEA-SHC is investigating solar cooling under Task 48 – QA and Support Measures for Solar Cooling. Although this Task is in its early stages, a report outlining the trends in solar cooling projects was released [20]. It found that in 2011, approximately 750 small scale solar cooling systems were installed worldwide and that in the last 7 years, there has been an annual worldwide growth of between 40 and 70 percent in the number of small scale solar installations. This showed that the small scale market is still a niche market, but is still growing and developing. Furthermore the report looks at the economic viability of small scale solar cooling systems, and found that the average cost was 4,500€/$kW_{cooling}$ (approximately \$CAD6,200/$kW_{cooling}$) and while not

economically viable at this time, the cost of these systems has decreased between 40 and 50 percent in the last five years. This Task will continue until March of 2015 with a focus on market development of solar cooling systems.

2.2 Research Projects

In addition to the work conducted as part of IEA-SHC Tasks 25, 38 and 48, a number of studies have been conducted to examine the performance and feasibility of solar absorption chillers. These studies for the most part can be broken down into three major categories; experimental evaluation of the chiller, simulation of the chiller performance and long term monitoring of installed systems. Each of these will be further discussed in the coming sections.

2.2.1 Experimental Evaluation of Solar Chillers

In recent years a number of studies have been conducted to experimentally evaluate small scale solar absorption within a laboratory setting.

A study conducted by Florides et al. looked at the performance of a domestic absorption chiller installed in Cyprus that consisted of a solar collector array, a storage tank, a back-up boiler and a lithium bromide-water absorption chiller [21]. The heat transfer coefficients of the absorption chiller were obtained experimentally, and the entire system was modelled using the TRNSYS simulation program with varying collector array size, orientation and type, as well as varying thermal storage capacity of the system. The optimal system configuration for the Cyprus climate and 11 kW absorption chiller

was found to have a 15 m^2 compound parabolic trough collector and a 600 L hot water storage tank.

A small scale solar thermal absorption cooling system was built and instrumented by Kalkan et al. [22] The system was designed to test the electrical and thermal COP of a 4.5 kW Rotartica LiBr/H_2O absorption chiller. To thermally drive the chiller, a 15 m^2 evacuated tube collector array was installed. In addition to the heat source, a 1000 L thermal storage tank was installed on the cold side of the chiller to store cold water for cooling when solar energy is not available. Through experimental runs, a maximum output of 4.98 kW with a COP of 0.63 was observed. Over the period, when solar thermal energy was available, the average thermal COP of the chiller was 0.65, with an overall system COP (electrical and thermal) of 0.46.

A 35 kW LiBr/H_2O Yazaki absorption chiller was experimentally evaluated by Johnson within controlled laboratory settings [23]. The system consisted of the chiller, a 40 kW in-line heater as the thermal input, a 30 kW in-line heater to simulate the building load, and an externally chilled glycol line that is capable of rejecting up to 70 kW of heat. Through this experimental set-up, a map of heat transfer rates in the evaporator, condenser and generator were experimentally determined, as well as the thermal COP of the absorption chiller. This information was later used by Edwards [24] to calibrate a computer model of the system to determine the optimal system performance (see Section 2.2.2 Modelling and Simulation).

In addition to powering absorption chillers using solar thermal energy, a number of studies have been conducted using micro-cogeneration units to power small scale absorption chillers. The performance of these chillers is often examined and these results

are directly applicable to the performance of the chiller while using solar energy at the same heating and cooling conditions. Work conducted by Rosato and Sibilio, Angrisani et al. and through the Center for Urban Energy have all looked at pairing a 10 kW ClimateWell solar absorption chiller with a micro-cogeneration unit in a residential setting [25 - 28].

These experimental studies were used to help guide the design of the experimental apparatus constructed within the Solar Energy Systems Laboratory. Although each of these studies experimentally tested the absorption chiller with different methods, all of the experimental tests were conducted either using steady state conditions from an auxiliary heater, or using a solar array, testing the chiller under actual power conditions. None of the tests looked at both the performance of the chiller under transient solar conditions and steady state lab conditions. Additionally, some of the systems were tested with thermal storage tanks, however none of the chillers tested had integrated thermal storage, and therefore the effect this has on the daily and seasonal performance of the cooling system was not evaluated. Finally, most of the studies had little emphasis on the experimental uncertainty of the derived quantities, which could have a large impact on the presented results, and any models created using the experimental data.

2.2.2 Modelling and Simulation

A recent Canadian study conducted by Edwards [24] looked at the performance of an absorption chiller in Ontario, Canada. The study used ESP-r, a building modelling tool that uses simulation to predict energy performance, to determine the optimal system configuration comprised of solar collectors, a cooling tower, hot and cold thermal

storages and a 35 kW absorption chiller. Experimental data from the study conducted and previously discussed by Johnson [23] was used to first create a custom component in TRNSYS to perform preliminary system sizing, and then the data was subsequently used to create a custom plant network in ESP-r to model the absorption chiller as part of a house. From this study, it was determined that a collector array of 50 m^2, a hot storage tank of 0.5 m^3 and a cold storage tank of 1.5 m^3 would be required to meet the cooling loads of a typical residential home in an Ontario climate. Although both of these storage volumes are quite large, they can be accommodated by larger houses in Canada. It was also determined within this study that the implementation of a solar cooling system in a house in Ontario would reduce the amount of greenhouse gases released in the generation of the electricity consumed by the house by approximately 12% and would reduce the amount of peak loading on the electricity grid during the summer months.

Mateus and Oliveira conducted a study to evaluate the performance of a solar absorption cooler for use in different building types and climatic locations in Europe [29]. Through the use of the TRNSYS simulation software, the performance of an absorption heating and cooling system was evaluated for three building types: a residential building, an office building, and a hotel. In addition, each of these simulations was conducted for Berlin, Lisbon and Rome climate regions. It was found that for all three locations, the annual costs were lower when compared to a standard cooling system, even though a 60% solar fraction only accounted for an annual saving of 35-45% due to the increase in maintenance costs and an increase in water consumption. It was also found that at the current cost of energy and the current start-up costs of a solar cooling system, the lifetime cost of the system (including capital investment, annual costs and maintenance) would be

higher compared to conventional cooling system even when used over many years and for prolonged periods of time.

Udomsri et al. performed a parametric study which uses a ClimateWell 10 for district cooling, in an attempt to increase the thermal COP of the chiller and electrical COP of the cooling system [30]. The study looked at going from the fourth generation of the chiller to the fifth generation of the chiller, where the internal pumps are removed through changes in the process. The fifth generation chiller is very similar to the unit installed and studied within this research. The system was tested using realistic boundary conditions (inlet and outlet conditions) experienced by the chiller as if it was installed in Borlange, Sweden. The chiller was modelled operating over the cooling season starting in mid-May and ending in mid-September. The study found that the overall thermal COP of the system over this period to be 0.43, while the electrical COP of the system was 7.46.

These studies all showed the value in creating a model and simulating the performance not only of the chiller, but the entire cooling system. Simulation allows for the rapid evaluation of different system configurations, which is ideal for system optimization. Additionally solar cooling systems can be modelled and evaluated in any building and climatic zone, allowing for the evaluation of the systems at low costs and in a short time frame. To ensure accurate results, validation of the model must be conducted through either monitoring of installed systems or preferably within a laboratory under controlled conditions. Validation and creation of TRNSYS models of the various components within a solar cooling system is the main purpose for constructing the experimental apparatus. This will ensure an accurate assessment of the potential for implementation of solar cooling devices within Canada.

2.2.3 Installed System Monitoring

The third main type of study conducted on solar absorption cooling systems is the performance monitoring of installed systems under real weather and building load conditions in actual residential or small commercial applications. One of the largest monitoring studies was conducted by the IEA-SHC Task 38 and has been previously discussed in Section 2.1.2.

A separate study by Thomas et al. monitored the performance of a solar adsorption chiller used to cool a laboratory in the temperate climate of Belgium [31]. The system contained 14 m^2 of flat plate collectors, a 300 L hot storage and a 500 L cold storage. The adsorption chiller had a nominal cooling power of 9 kW with a dry cooler used for heat rejection. The system was monitored for over 50 days in 2011 and from this data the system was further refined and tested again in the summer of 2012. Based on the experimental results, a TRNSYS model was created and tuned to the system. Using the monitored results, the performance parameters of the system was determined. It was found that the thermal COP of the system was highly dependent on the weather, and the daily average COP ranges from 0.44 to 0.6, with peaks during the day reaching 0.7.

In February 2007, ClimateWell AB installed a ClimateWell solar absorption cooling system within a single family detached home in Madrid, Spain [32]. The system was integrated into a solar heating system utilizing a 35.54 m^2 solar collector array, maximizing the benefit of the solar heating infrastructure by supplementing the heating and domestic hot water traditionally produced with air conditioning. The system used the existing in-ground pool as a heat sink to remove the need for a cooling tower, and to reduce the initial capital costs. The radiant floor system originally designed for heating

was used to distribute the air conditioning by passing through chilled water. The house was further monitored by Borge-Diez et al. and the performance of the system was reported [33]. It was determined that the system COP was slightly lower than predicted by simulation and that a 68% reduction in greenhouse gas production can be achieved. Further evaluation on the performance of system was conducted using financial analysis. It was found that the initial capital costs were approximately 30,000 EUR higher then installing a traditional cooling system. This was offset by realizing an energy saving of 117 EUR per month. When the repayment of the capital cost is factored in, the home owners saved 52 EUR a month, or over $850 Canadian a year, making this a worthwhile investment.

2.3 Performance Parameters

A solar absorption cooling system can be evaluated using a number of different performance parameters to evaluate the thermal and electrical performance of both the chiller and the cooling system as a whole. An extensive list of performance parameters was developed as part of the IEA-SHC Task 38 under Subtask A and B [19]. This was done to ensure all systems are evaluated using the same method allowing the results from different systems to be compared. In addition to the work under Task 38, a study conducted by Nowag et al. [34] have expanded on some of the key performance parameters and have also defined target values using the climate conditions and the type of solar cooling system installed. Some of the key performance parameters used within this work are discussed in detail in the following paragraphs.

The most widely used and reported parameter for an absorption chiller is the thermal coefficient of the performance which compares the amount of cooling produced to the amount of energy input on the hot side and is defined as:

$$COP_{th} = \frac{Q_{cold}}{Q_{hot}} \tag{2.1}$$

Similarly to the thermal COP, the electrical coefficient of performance compares the amount of cooling produced with the amount of electricity consumed by the absorption chiller and is defined as:

$$COP_{el,chiller} = \frac{Q_{cold}}{e_{chiller}} \tag{2.2}$$

In addition to determining the performance of the chiller as a unit, it is important to determine the performance of the cooling system as a whole. The first parameter compares the amount of cooling produced to the total electrical consumption in the system including the chiller, pumps and heat rejection unit (dry cooler or cooling tower) and is defined as:

$$COP_{el,system} = \frac{Q_{cold}}{e_{pump} + e_{chiller} + e_{reject}} \tag{2.3}$$

While it is important to quantify the total electricity consumption within the system, it is also important to consider the primary energy that is required to produce the electricity. This is also important if a non-electric auxiliary heat source is implemented (e.g., natural gas boiler) to supplement the solar thermal energy. For the case where there is no auxiliary heater, the primary energy ratio is defined as:

$$PER = \frac{Q_{cold}}{e_{total}/\epsilon_{elec}} \tag{2.4}$$

where ϵ is the primary energy factor which relates the amount of primary energy required to produce the electricity consumed, or the amount of fossil fuels used to produce thermal energy. In the case of electricity, a value of 0.4 is recommended while a value of 0.9 is used for fossil fuels [19]. Equation 2.4 is valid only when electricity is used within the system, while Equation 2.5 must be used when any form of fossil fuel is used.

$$PER = \frac{Q_{cold}}{e_{total}/\epsilon_{elec} + Q_{hot,fossil}/\epsilon_{fossil}} \tag{2.5}$$

While the performance parameters defined by Equations 2.1-2.5 can be used to determine the electrical or thermal performance of the chiller and the system as a whole, there are many additional performance parameters that can be used. These parameters address the performance of the solar collectors, thermal storage, water consumption (for systems with a cooling tower) and effectiveness of the air handler among others. For this work, the focus will be on determining the COP_{th} and $COP_{el,chiller}$ though experimental evaluation.

3 Chapter: Experimental Design

This chapter provides a detailed description of the experimental apparatus which was designed and constructed to test the performance of a solar absorption chiller. The chapter begins with an overall description and schematic of the experimental set-up, followed by a detailed description of each of the main components installed within the system. Next, a description of the data acquisition system and all of the instrumentation installed within the system. Last, the steps taken to commission the air conditioning and building loop will be presented.

The experimental apparatus was constructed in the Solar Energy Systems Laboratory (SESL) in the Canal Building lab at Carleton University. The detail design, drawings, certification and construction of heat rejection and heat input loop within the mechanical room were completed by a consulting engineer and certified contractor as per Carleton University's regulations. This includes the dry cooler installation and all connections to the building systems (steam and chilled water). Once complete, the heat input and heat rejection loops will be connected to the test apparatus constructed in the lab.

3.1 Overview of Experimental Set-Up

An experimental apparatus was designed to determine the thermal performance of a ClimateWell solar absorption chiller. The experimental apparatus contains four main hydraulic loops which are the heat input, heat rejection, air conditioning and the building load simulator. These hydraulic loops are instrumented to record the inlet and outlet

temperatures of the chiller as well as the flow rates and the data collected will be used to determine the thermodynamic performance and heat transfer rates of the chiller. In addition to the four primary hydraulic loops, the experimental apparatus contains three secondary hydraulic loops which provide heat input or rejection for the four primary loops. These include the steam line from the building (heat source), the chilled water from the building and the glycol loop to the dry cooler.

Before any design work could be conducted, a set of design parameters had to be determined. The goal of this experimental apparatus is to test the chiller at various temperatures and flow rates, and therefore the system has to be adaptable and be able to function over the entire range of test conditions. To start, a single design condition was determined for sizing of the various system components. The inlet and outlet conditions as well as the flow rates for the chiller were determined based on the specifications provided by the manufacturer of the unit and are outlined in Table 3-1 [9].

Table 3-1: Design conditions at chiller

Hydraulic Loop	T_{in} (°C)	T_{out} (°C)	Flow Rate (L/min)	Heat Transfer (kW)
Heat Input	90	81	25	15.20
Air Conditioning	20	15	25	8.73
Heat Rejection	20	27	55	26.83

In addition to the design parameters listed in Table 3-1, it was also important to ensure that all of the components of the system function and are able to provide the desired temperature and flow rate ranges for each of the three hydraulic loops. The range of temperatures and flow rates that the chiller will be tested over are listed in Table 3-2.

Table 3-2: Testing range

Hydraulic Loop	T_{in} Range (°C)	Flow Rate Range (L/min)
Heat Input	70-95	20-30
Air Conditioning	10-25	15-25
Heat Rejection	10-30	45-70

Based on these design parameters, the experimental apparatus was designed. The remainder of this Chapter will provide details on the hydraulic loops and main components installed within the system. An overall schematic of the system design can be found in Figure 3-1.

3.1.1 Heat Input

The heat input loop uses the Canal Building's built-in steam line as the main heat source, and has been designed to replace and mimic a solar collector array. The steam line was used instead of collectors because a controllable heat source that can operate 24 hours a day, 365 days a year was required. This also allows for a variety of collector types and array sizes to be simulated, so the chiller can be tested under a variety of heat input patterns and conditions. In addition, if solar collectors were used and no tests were being conducted, then the collectors may overheat. Additionally, stagnation prevention measures would have to be installed to avoid damaging the collectors. This would require the heat to be continuously dumped, consuming a significant amount of energy to run the pumps and dry cooler.

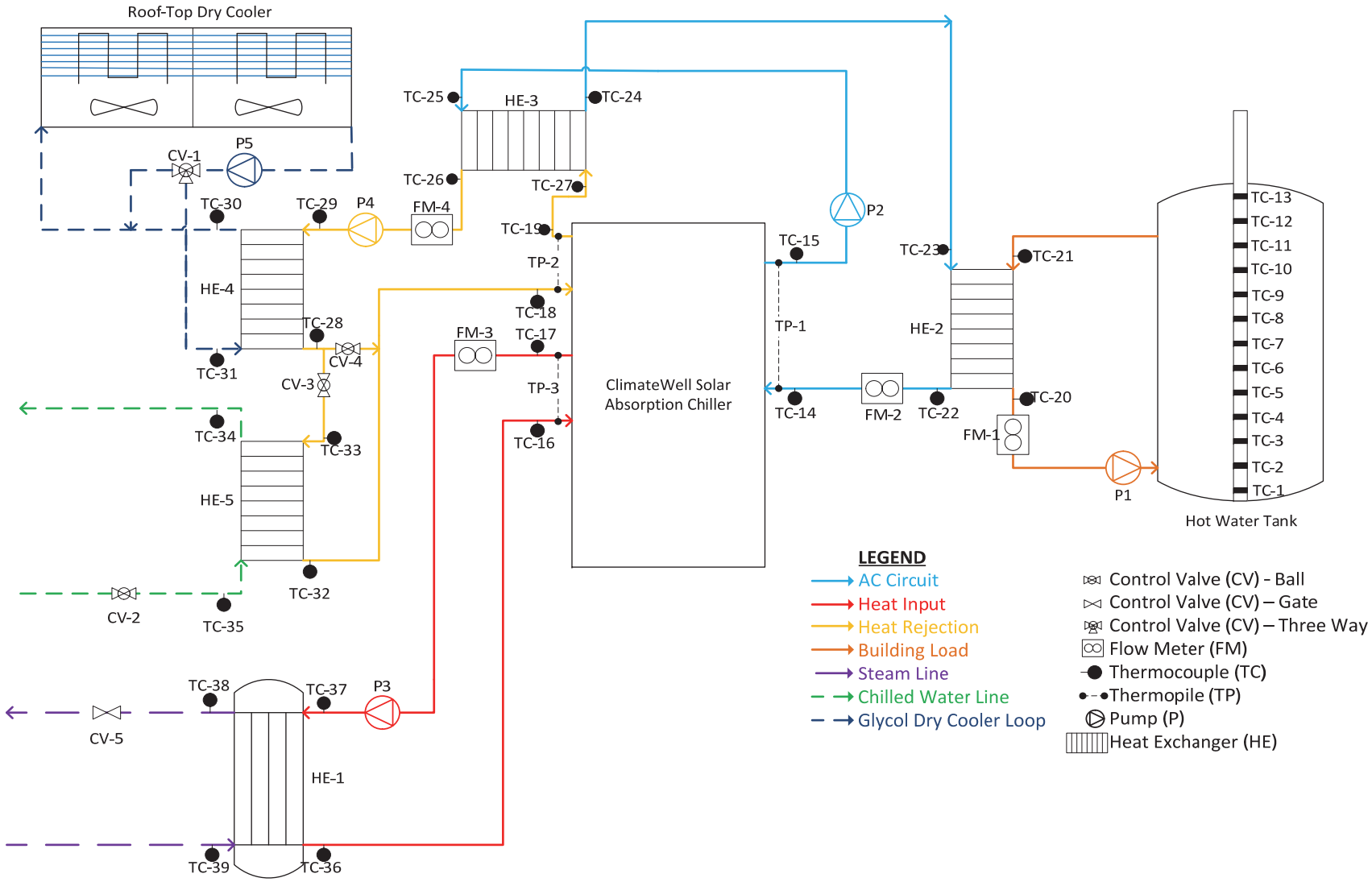

Figure 3-1: Schematic of experimental test set-up

The steam enters a shell and tube heat exchanger (HE-1 in Figure 3-1) located in the mechanical room, where heat is transferred from the steam to a variable flow water loop that transports the heated water into the lab and subsequently to the chiller. This heating system is capable of providing a completely controllable and variable heat input from 0 to 30 kW of thermal energy. Control of the power input is provided by varying the flow of the steam from the building into the heat exchanger, and can be used to mimic actual power profiles of solar thermal collectors based on real solar profiles collected by the 5 pyranometers on a weather station on the adjacent building (see Appendix A).

3.1.2 Heat Rejection

Solar absorption chillers generate a large quantity of waste heat which must be rejected outside. In a typical solar cooling installation, the heat is usually rejected using a cooling tower, or in some cases, to heat a swimming pool. Cooling towers and swimming pools are only able to provide heat rejection during the summer as they would freeze during the winter months in Ottawa. Because the experimental set-up will be tested year round, a dry cooler was selected to provide heat rejection as it can operate in both the summer and winter. A 10 ton (30 kW) Krack dry cooler, shown in Figure 3-2 was installed on the roof of the Canal Building.

Figure 3-2: Installed dry cooler

To prevent freezing, a glycol loop was installed between the heat rejection loop that circulates between the chiller and the mechanical room and the dry cooler with the heat being transferred from the water line to the glycol through HE-4, as shown in Figure 3-1.

Since a dry cooler is more effective in the winter than the summer, a second heat exchanger (HE-5) was installed between the heat rejection loop and the building's chilled water line (used for building air conditioning) to provide extra heat dissipation in the summer. This will provide the additional cooling capacity required to dissipate the necessary heat from the absorption cooling unit when operated during the summer months.

3.1.3 Air Conditioning

The purpose of a solar absorption chiller is to air condition a building space by producing chilled water which is then circulated through cooling coils within an air handling unit or a hydronic distribution system to provide cooling. To mimic the distribution system, the chilled water produced by the absorption chiller goes through two water-to-water heat exchangers (HE-2 and HE-3 in Figure 3-1). In the first heat

exchanger, HE-3, the chilled water is on the cold side, and the heat rejection loop is on the hot side. This heat exchanger does not only warm up the chilled water, it also simultaneously reduces the amount of heat that needs to be rejected by the dry cooler, reducing the required size of the unit. This heat exchanger is designed to transfer 5 kW of thermal energy to increase the temperature of the chilled water from 15°C to 18°C, providing a baseline heating of the chilled water, while the building load simulator through HE-2 provides a variable heat transfer for finer control of the cooling load being simulated. For simplicity and compactness, this water-to-water heat exchanger was used in place of an air handler.

Once the chilled water exits the first heat exchanger, it then enters a second water-to-water heat exchanger, HE-2. The 18°C chilled water enters the cold side, while hot water from the domestic hot water tank, supplies water to the hot side of the heat exchanger. Two 4500 W heating coils within the hot water tank keep the hot side entering at 55°C. A variable speed pump in the building load loop was installed to alter the flow rate between 10 L/min and 25 L/min. As a result, the heat transfer rate can be controlled to match the amount of cooling power produced by the unit in order to keep the unit operating at steady state.

3.2 Main Components

All four of the main hydraulic loops were built out of a number of individual components piped together. This section will discuss the major components within the experimental absorption cooling set-up, including the solar absorption chiller, the pumps, heat exchangers and the control valves.

3.2.1 Solar Absorption Chiller

The purpose of the entire experimental set-up is to test the thermal and electrical performance of a solar absorption chiller. A ClimateWell V 9.34 Solar Chiller, with a maximum cooling capacity of just over 9 kW, was procured and installed within the laboratory and can be seen in Figure 3-3. This chiller is a triple state absorption chiller, meaning that during the cooling process, the LiCl is in solid state, and the water is in both liquid and gaseous state. The system consists of two independent intermittent absorption chillers, referred to as barrels. Each barrel contains two reaction chambers, and the two barrels are plumbed together and controlled with the ClimateWell plumbing unit. This unit controls the cycling between charging and discharging of the two separate absorption

Figure 3-3: ClimateWell solar absorption chiller installed within the lab

cycles that make up the unit and controls the flow from the heat source, the heat rejection system and the air conditioning loops.

3.2.2 Pumps

Five pumps were installed within the experimental set-up to circulate the fluid between the various components and are detailed in Table 3-3. All five pumps are equipped with on-board variable speed drives and are controlled using a 0-10 V control signal. This allows the pumps to operate over a wide range of flow rates, and allow the chiller to be tested under different flow conditions. The pump design curves were used for sizing and selection and are available online [35-37].

Table 3-3: Installed pumps

Pump	Hydraulic Loop	Design Flow Rate (L/min)	Maximum Power (W)	Manufacture	Model
P-1	Building Load	15	62	Grundfos	UP 26-96F/VS
P-2	Air Conditioning	25	180	Grundfos	Magna 32-100
P-3	Heat Input	25	373	Grundfos	CR 3-2
P-4	Heat Rejection	60	1119	Grundfos	CR 5-4
P-5	Glycol Dry Cooler	75	1119	Grundfos	CR 5-4

3.2.3 Heat Exchangers and Heaters

To supply heat to and remove heat from the experimental set-up, as well as between the air conditioning loop and the building load simulator, five heat exchangers were installed. Four of these heat exchangers are flat plate heat exchangers, while HE-1

in Figure 3-1, located between the steam line and the heat input loop is a shell and tube heat exchanger. Table 3-4 outlines the size and specification for all five heat exchangers.

Table 3-4: Installed heat exchangers

Heat Exchanger	Hot Side	Cold Side	Capacity (kW)	Manufacture	Model
HE-1	Steam Line	Heat Input	200[†]	Preston Phipps Inc.	PPSCF-300-11W
HE-2	Building Load	Air Conditioning	3.5	HEX	BL14-30H
HE-3	Heat Rejection	Air Conditioning	5	HEX	BL26C-30H
HE-4	Heat Rejection	Glycol Dry Cooler	42.8	Alfa Laval	CB30-70H
HE-5	Heat Rejection	Building Chilled Water	46.5	Alfa Laval	CB27-34L

[†] Although HE-1 has a capacity of 200 kW due to the latent heat released by the steam as it condenses within the heat exchanger, during regular use, the maximum energy transfer will not exceed 30 kW.

In addition to the five heat exchangers installed within the system, a 270L domestic hot water tank with two internal 4500 W heaters was installed within the experimental test set-up as shown in Figure 3-1. This provides the heat input into the building load simulator, acting as the cooling load typically placed on the unit. The hot water tank is designed to keep the water at a constant temperature of 55°C which is circulated through HE-2.

3.2.4 Control Valves

To control the flows within the experimental system, five automated control valves were installed within the system. A three way valve, CV-1, was installed within the glycol dry cooler loop to bypass flow from HE-4 when the temperature is very cold outside (lower than -25°C). When the exterior temperature reaches these low

temperatures, the glycol solution (50% by volume) may freeze and cause significant damage to the dry cooler. To prevent this, when the exterior temperature reaches -25°C, pump P-5 in the glycol loop starts up at a very low speed to ensure no freezing occurs. The glycol solution could still be below 0°C as it enters HE-4, and therefore could potentially cause the water on the warm side (heat rejection loop) to freeze, damaging the heat exchanger. The ability to bypass the heat exchanger will ensure that no freezing will occur in either the glycol loop as well as the heat rejection loop.

Control valves 3 and 4 (CV-3 and CV-4) are used as a pair to switch the system from summer mode to winter mode. During the winter months, when all of the heat is rejected through the dry cooler, CV-4 is opened and CV-3 is closed to bypass the flow from HE-4 as the chilled water line is not operational. During the warm summer months, when the dry cooler alone cannot reject enough heat, CV-4 is closed and CV-3 is opened, to allow the fluid to first pass through HE-4 to reject some of the heat, and then pass through HE-5 to reject the remainder of the heat to the chiller water line before returning to the solar absorption chiller in the Solar Energy Systems Laboratory.

The final two control valves have been installed to regulate the flow of steam and chilled water from the building systems into HE-1 and HE-5. CV-2 has been installed on the chilled water line and is an on/off valve. This valve will be opened while the system is running in the summer mode, and will remain closed during the winter months and when there is no heat to reject through the chilled water heat exchanger (HE-5). While CV-2 has been installed to turn on and off the flow of the chilled water, CV-1 has been installed to regulate and stop the flow of steam through HE-1. CV-1 is a sliding stem control valve, allowing a variable flow of steam and is controlled with a 0-10 VDC

analog signal. The amount of steam that the valve allows through is proportional to the signal. This has been designed to allow both constant temperature input by allowing a constant flow of steam, as well as a variable power input by varying the amount of steam through HE-1. This will be controlled using a program built within the building automation system, allowing the actual power that would be produced by a real solar thermal collector array to be mimicked. In addition to CV-5, a second control valve has been installed on the steam line and is tied directly to a resistance temperature detector (RTD) on the water outlet of HE-1. If the temperature of the outlet exceeds 100°C, the steam line flow will automatically shut down, protecting the system from any possible thermal or pressure overload.

3.3 Instrumentation

In addition to the equipment installed within the hydraulic loops, each loop is also instrumented to determine the thermal performance of each of the components. To determine the performance of the absorption chiller, the heat transfer rates into and out of the chiller must be determined. To achieve this, the mass flow rate and the change in temperature across each of the three hydraulic loops connected to the chiller are measured. Thermopiles, in conjunction with the thermocouples are used to accurately determine the temperature change within the chiller. Flow meters were installed within each of the hydraulic loops to measure the volumetric flow rate. To determine the mass flow rate, the temperature of the water is measured with the thermocouples and the density is found using standard tables. Once the heat transfer into the chiller from the heat input and air conditioning loop is determined, the overall performance of the chiller is

calculated using the thermal COP. Section 3.3.1 to Section 3.3.4 describes each of the instruments installed within the system, including how they functions and their purpose.

3.3.1 Thermocouples

Thermocouples are temperature measurement devices that use the principle that when two dissimilar metals are joined together, an electromotive force (emf) is generated. This emf would be proportional to the temperature between the measurement junction and a reference junction with a known temperature (commonly called the cold junction) [38]. Using the measured emf (typically in the mV range) and the known temperature at the cold junction, the measured temperature can be determined either using pre-constructed tables (such as those created by the National Institute of Standards and Technology), or through a mathematical relation determined through a calibration experiment [39]. The standard tables are only accurate to 0.5°C before taking into account the accuracy of the cold junction temperature measurement and the resolution of the voltage readings and therefore, a calibration test was conducted on the thermocouples. The calibration procedure and the results are outlined in Section 6.1.1. The thermocouples were constructed using Type-T thermocouple wire consisting of copper and constantan (a copper-nickel alloy). Two different gauges of thermocouple wire were used for different areas of the experimental apparatus. A 30 gauge wire was used within the lab to allow for a large number of wires to be bundled within the hot water tank probe and to ensure the thermocouples fit within the small diameter, custom thermocouple wells. The thicker 24 gauge wire was used for the thermocouple in the mechanical room where there is more space and durability was a larger concern.

To immerse the thermocouples within the fluid stream, custom thermowells, shown in

Figure 3-4, were constructed by drilling a 0.125 inch hole through the center of a standard brass threaded cap and inserting a 4 inch long, 0.125 inch (outer diameter) pipe, with one end pinched shut and sealed with solder. Once the pipe was inserted, it was soldered into place ensuring a completely watertight seal was formed. These assemblies were then installed into the piping network. Whenever possible, they were installed with the probe pointing into the flow to allow for maximum contact of the thermowell with the flowing fluid. This was possible at the entry and exit of the heat exchangers and an example is shown in Figure 3-5. To prevent any air from entering the thermowell from the exterior surroundings, the thermocouple is sealed into the thermowell using electrical tape.

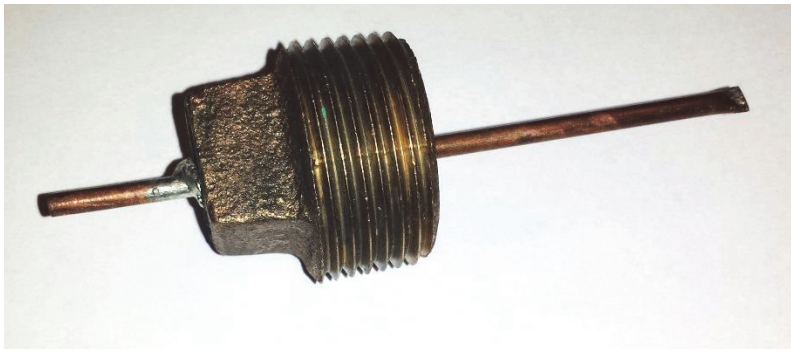

Figure 3-4: Custom built thermowell to take point temperature measurements

Figure 3-5: Thermowell at the entrance of a heat exchanger with the flow direction indicated

In addition, a thermocouple probe was constructed to fit into the hot water tank to monitor the interior temperatures of the tank. The thermocouple probe consists of 13 thermocouples, spaced at 10 cm intervals and was constructed and inserted into the hot water tank where the sacrificial anode is typically installed. The outer shell is a 0.625 inch stainless steel pipe with one end welded shut and the other open. The sealed end is inserted into the tank until it just touches the bottom of the tank, and the probe is then held in place using a compression fitting at the top of the tank, resealing the tank. The thermocouples are fed through a half inch plastic tube (the outer diameter of the poly tube is approximately the same as the inner diameter of the stainless steel tube), which has small slits cut into it at 10cm intervals. The completed probe before being inserted can be seen in Figure 3-6 while a close-up picture of one of the thermocouples is shown in Figure 3-7. The thermocouple end is pulled out through the slit and taped using kapton tape to the outside of the plastic tube. Once all 13 thermocouples have been fed through and taped to the outside of the tube, the plastic tube is inserted into the stainless steel

tube, with the thermocouples being sandwiched between the stainless steel and the plastic tube. Electrical tape has been wrapped around the plastic tube between each thermocouple to prevent any airflow between the stainless steel pipe and the plastic tube. This allows the thermocouples to read the temperature at specific heights, and allows any thermal stratification to be observed (although not expected due to the high flow rates in the building load simulator loop).

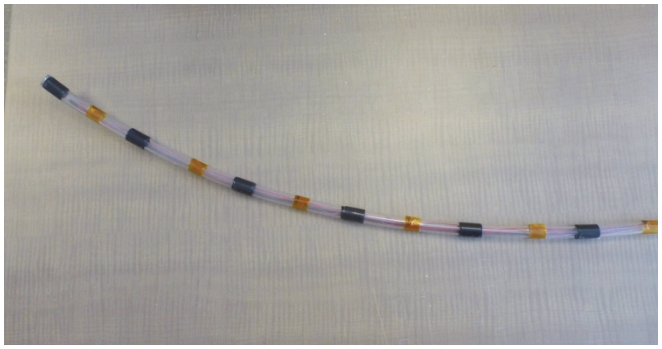

Figure 3-6: Thermocouple probe before being inserted into the stainless steel pipe

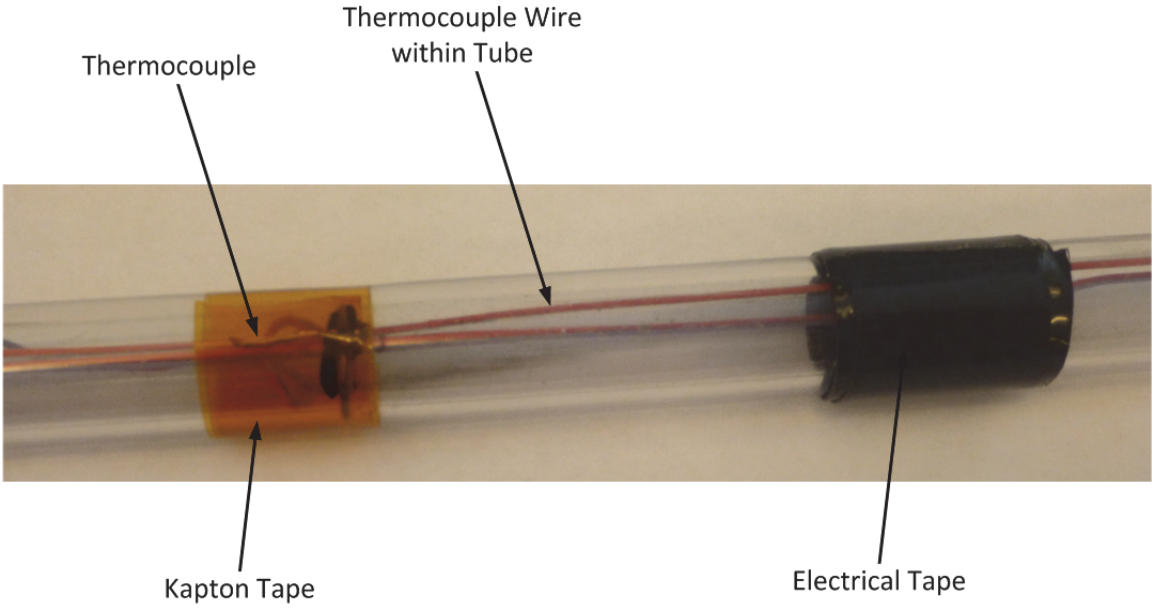

Figure 3-7: Picture of a single thermocouple within the thermocouple probe

In total, 39 thermocouples were installed within the system to measure the temperature at the key points within the system, with 13 being installed within the hot water tank, 6 monitoring the temperatures at the inlet and exit of the solar absorption chiller and the remaining 20 monitoring the inlet and exit of the five heat exchangers installed within the set-up. In addition to the 39 thermocouples installed, additional thermocouples were installed to monitor the status of the experimental set-up and troubleshoot any problems that may arise, including where the pipes enter and exit the mechanical room and the SESL. These are not included in Figure 3-1 as they are not used in calculating the performance of the chiller or the system.

3.3.2 Thermopiles

While thermocouples are able to accurately measure the absolute temperature at any given point (to within 0.5°C – see Section 6.1.1), when measuring a difference in temperature across a piece of equipment, the error on the two measurements compounds, and the resulting error is 0.7°C on the difference. For the design conditions, when measuring the temperature difference across the inlet and exit of the chiller for the air conditioning loop, a reading of 5°C ± 0.7°C would be obtained, which equates to a significant error of 14%. To reduce the error on the difference of temperatures, which is used to calculate the amount of energy transferred within the chiller, three thermopiles were built and installed within the system. A thermopile contains multiple thermocouples in series to amplify the voltage created. This set-up reduces the error on the difference in temperature in two ways. First, because the voltage is amplified by the number of junctions, the error caused by the resolution of the voltage reading is reduced by a factor

equal to the number of junctions. Secondly, because the thermopile is looking simply at the temperature difference across the hot and cold side and that the cold side acts as the cold junction, all sources of error associated with determining the cold junction temperature is eliminated. These two factors combined, reduce the error from ±0.7°C to ±0.15°C, or from 14% to 3% for a temperature difference of 5°C. The detailed procedure and results of the calibration tests performed on the thermopiles can be seen in Section 6.1.2.

Thermopiles can be built with any number of pairs of thermocouples, with each thermocouple amplifying the emf signal being produced equivalent to approximately that of a single thermocouple. This increase reduces the error on the emf reading from the data acquisition, however, there is a point where adding additional junction has a diminishing return on reducing the error. Using the sensitivity value of the voltage determined through the thermocouple calibration, and the reading error on the data acquisition system of 8 nV, the reading error on the thermopiles was determined for one to ten pairs and is displayed in Table 3-5. Although the reduction in error was the principal reason for selecting thermopiles, a balance between error reduction, complexity and ability to install the thermopiles within the piping network had to be examined, and a balance between all three determined.

Table 3-5: Error on differential temperature measurements based on number of junctions

Number of Junctions	Voltage Sensitivity (°C/mV)	Error on Measurement (°C)
1	21.819	0.175
2	10.910	0.0873
3	7.273	0.0582
4	5.455	0.0436
5	4.364	0.0349
6	3.637	0.0291
7	3.117	0.0249
8	2.727	0.0218
9	2.424	0.0194
10	2.182	0.0175

To install the thermopiles within the system, a similar thermowell to those used for the thermocouples was built, however, instead of a single 0.125 inch pipe, multiple individual pipes were drilled and sealed into the 1 inch brass cap. Instead of using solder to seal the thermowells to the brass caps, 24 hour epoxy was used. This change was made as all pipes had to be sealed simultaneously which could not be achieved through soldering. To determine the correct balance between the ability to install the thermopiles and the error results, a test was conducted to determine how many thermowells could be installed on a single 1 inch brass cap, which could then be installed within the system. Figure 3-8 shows the possible configuration that could be used for three, four, and five thermowells being installed.

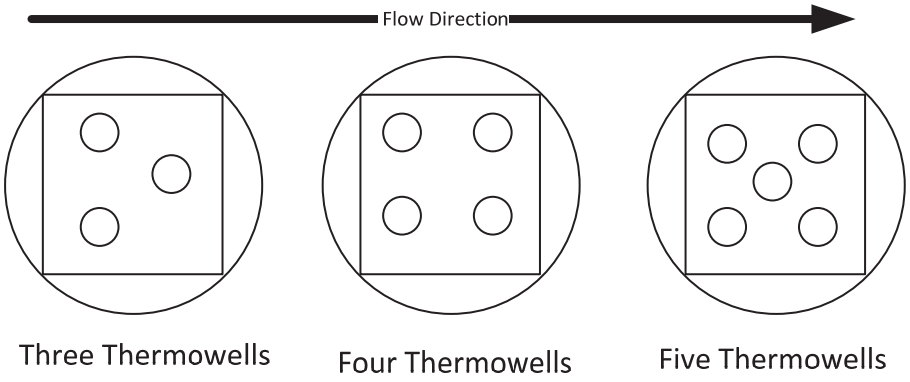

Figure 3-8: Layout for three, four and five thermowells in one brass cap

Once the configuration with five thermowells was built and tested, it was determined that no additional thermowells could be installed as there was minimal cap material left to drill through and at five thermowells, the ends were almost touching, leaving no room within the fluid stream for an additional test point. Since a thermocouple reading is also required at the hot and cold side of the thermopile, a brass cap with five thermowells, will actually house a four junction thermopile using the four thermowells around the outside of the brass cap, while the center pipe houses the thermocouple for that location. In comparing the error going from a four junction thermopile to a five junction thermopile, the reduction in error is less than 0.01°C, and therefore it does not justify the added complexity of adding a second brass tee and cap in series with the first to add the additional thermowells required. Because of this, it was determined that a four junction thermopile would be used to measure the temperature difference across the inlets and outlets of the three chiller loops.

3.3.3 Flow Meters

To measure the flow in each of the four hydraulic loops installed within the lab, oval gear, positive displacement flow meters were installed. As the flow passes through

the flow meters, it forces the calibrated gears to rotate and each rotation allows a certain volume of flow through. A 24 V signal is continuously supplied to the flow meter, and the oval gears are equipped with a reed switch to turn the signal on and off for each rotation the gears make. The data acquisition system then counts those pulses created by the turning on and off of the 24 V signal and the volumetric flow rate is calculated using the k-factor (number of pulses per unit of volume), as well as the elapsed time. The flow meters are factory calibrated with a one percent uncertainty of the total flow. An additional error is introduced through counting the pulses and will be discussed in Section 6.1.3. Figure 3-9 shows an installed flow meter within the hydraulic network, while the models and specifications of each of the flow meters are shown in Table 3-6.

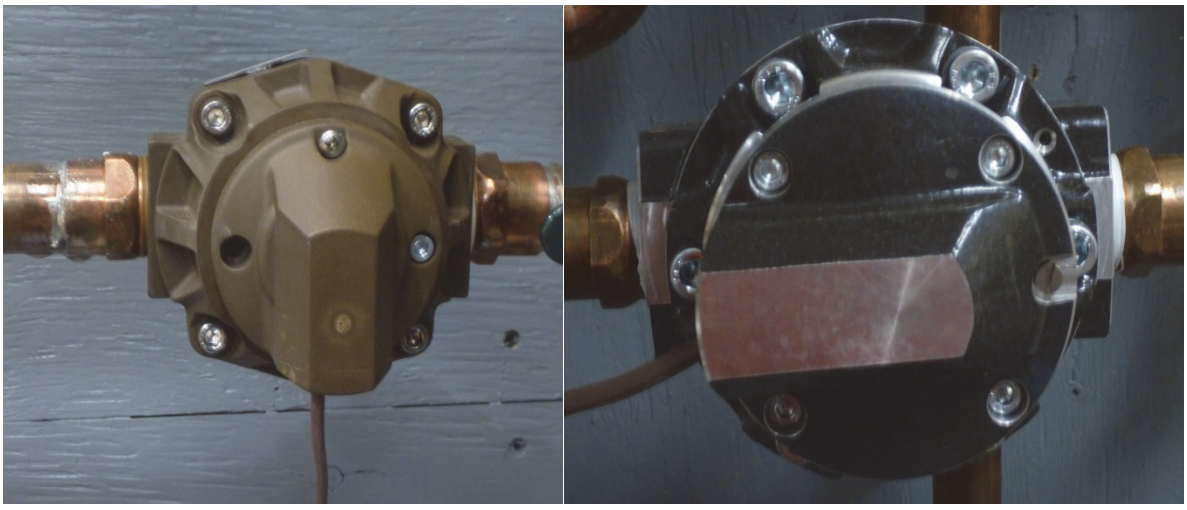

(a) *(b)*

Figure 3-9: Installed flow meters - (a) BM-07 and (b) BM-10

Table 3-6: Installed flow meters

Flow Meter	Hydraulic Loop	Capacity (L/min)	K-Factor (pulse/L)	Manufacture	Model
FM-1	Building Load	8-70	52	Brooks	BM-07
FM-2	Air Conditioning	8-70	52	Brooks	BM-07
FM-3	Heat Input	10-100	36	Brooks	BM-10
FM-4	Heat Rejection	10-100	36	Brooks	BM-10

3.3.4 Data Acquisition

To monitor all of the instrumentation installed within the four hydraulic loops, as well as to provide the control signals during experimental tests to the control valves and the pumps, a National Instruments NI cRIO 9024 CompactRIO data acquisition system was installed and wired to all of the devices and instruments. The cRIO has swappable I/O modules, often referred to as cards, which perform specific measurements or control functions. This allowed the data acquisition to be customized for the needs of the system being built. In addition to the primary chassis that houses the cards in the lab, an expansion chassis (NI 9144) was obtained to monitor the instrumentation and control the equipment installed within the mechanical room. Table 3-7 outlines the configuration of the main chassis installed in the lab while Table 3-8 shows the configuration of the expansion chassis installed in the mechanical room.

Table 3-7: I/O modules installed in the lab

I/O Modules	Function	Number of Modules	Total Number of Channels	Purpose
NI 9214	Isothermal Thermocouple Input	3	48	Measure thermocouples and thermopiles
NI 9476	24V Digital Out	1	32	Provide power to flow meters
NI 9264	0-10V Analog Out	1	16	Provide control signals to pumps
NI 9422	24V Sink/Source	1	8	Digital pulse counter for flow meters

Table 3-8: I/O Modules installed in mechanical room

I/O Modules	Function	Number of Modules	Total Number of Channels	Purpose
NI 9214	Isothermal Thermocouple Input	2	32	Measure thermocouples
NI 9476	24V Digital Out	1	32	Control signal for control valves
NI 9264	0-10V Analog Out	1	16	Control signals to pumps and control valves

To monitor the system performance and control the installed equipment, a custom Virtual Interface (VI) was created within LabVIEW. LabVIEW is a software developed by National Instruments, that interfaces with the NI cRIO data acquisition system and provides a development environment to create applications for experimental testing and control. This VI displays the live measurements being recorded in the system for ease of control, as well as logging them to a .csv file that can be imported into Excel or MATLAB for data analysis. Figure 3-10 show a screen shot of the LabVIEW VI as it records data.

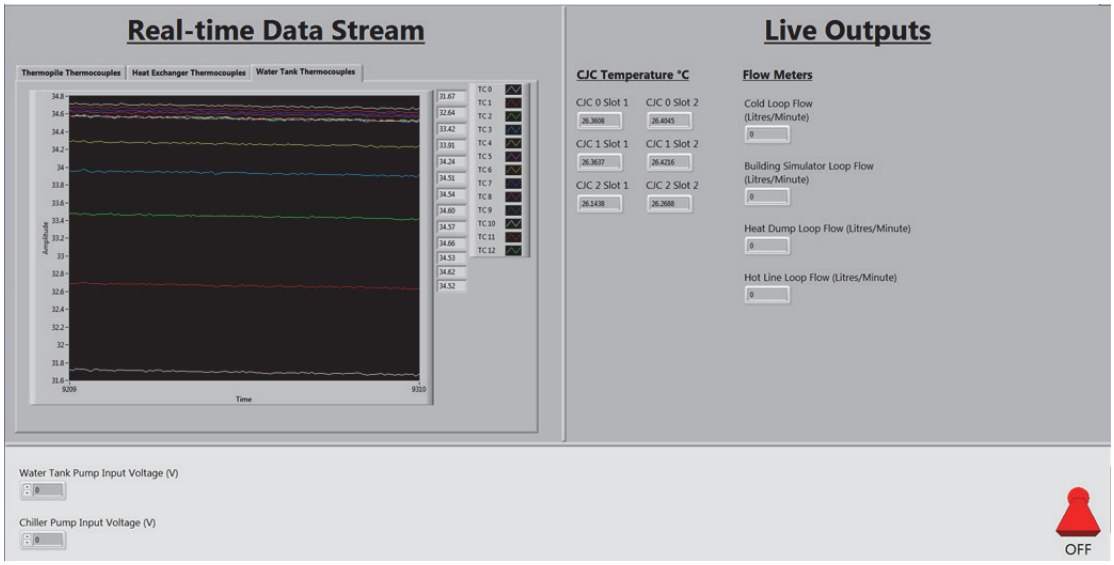

Figure 3-10: LabVIEW VI created for and system monitoring and control

3.4 Commissioning

Upon completion of the system design, the hydraulic networks within the lab, including all connections to the absorption cooling unit were constructed, instrumented and tested. The detailed plumbing diagram for the lab is shown in Figure 3-11, while photos of the installed system in the lab are shown in Figure 3-12 and Figure 3-13 (prior to insulation). The portion of the system within the SESL contains all of the instrumentation responsible for quantifying the thermal and electrical performance of the chiller, including the thermopiles measuring the temperature difference across the inlets and outlets, as well as the four flow meters, allowing the candidate to install and test all of the necessary instrumentation. The building load simulator and air conditioning loop were filled with water and pressurized to enable the testing of the pumps, flow meters and heat exchangers.

In addition to the equipment installed in the SESL, a mechanical contractor was hired to construct and install the hydraulic network and equipment within the mechanical

room and on the roof of the building. This included the dry cooler as well as connecting the hydraulic network into the building's base systems, such as, the steam and the chilled water lines. Figure 3-14 shows the piping network, steam to water heat exchanger and pumps installed within the mechanical room.

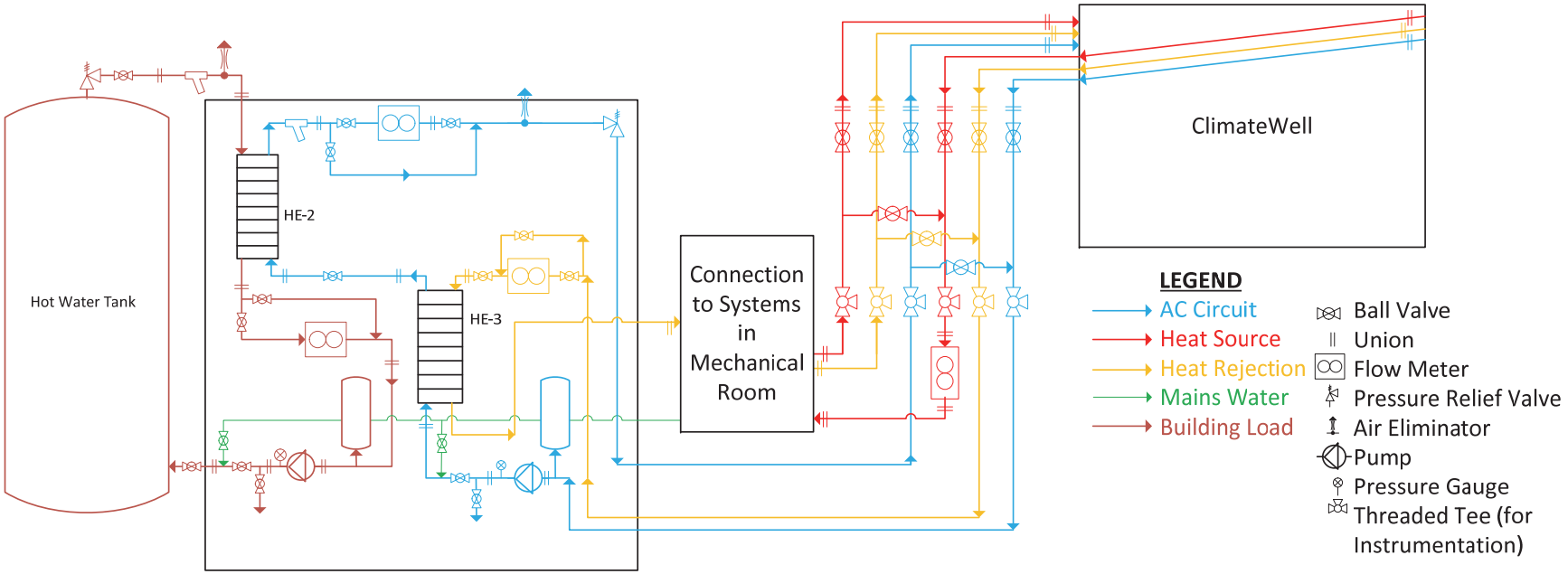

Figure 3-11: Detailed plumbing schematic

Figure 3-12:Hydraulic network installed within the lab

Figure 3-13: Connections into the chiller and thermopile installation

(a)

(b)

(c)

Figure 3-14: Equipment installed within the mechanical room - (a) steam-to-water heat exchanger, (b) heat input pump, (c) control valves, instrumentation, and heat exchangers

4 Chapter: System Modelling

To support the design of the experimental test set-up and to run sensitivity studies on the configuration and experimental procedure, a model of the system was created in the TRNSYS (TRaNsient SYstem Simulation) environment [40]. TRNSYS was selected to conduct the modelling for its capabilities to model complex, transient energy systems. TRNSYS contains a library of components, called "Types", which represent physical components, control devices, schedules and utility components for the simulation. The model is built within the simulation studio, which is a graphical interface where Types are imported and connected through links, which transfer data from one type or component to the subsequent one. The output of one linked Type acts as the input of the next Type with each Type having built in mathematical functions, which take the inputs and using these functions to calculate the outputs.

Once the model is built within the simulation studio and the simulation is initiated, an input file, called a deck file, is created to represent the components and initial conditions. An example of a deck file created for this model can be seen in Appendix B. This file is read into the TRNSYS simulation engine, which steps through the simulation in user-defined time steps, solving the model iteratively until the system converges, and then moves onto the next time step. This process continues until the model has been solved at all of the time steps. TRNSYS then outputs the results both graphically and as an output file that can be used for further analysis. This chapter provides a detailed description of the model of the experimental set-up built in TRNSYS, with the results of the modelling work presented in Chapter 5.

4.1 Description of System

A model representing the experimental set-up was built in the TRNSYS simulation software to ensure the system component sizing was adequate both at the design conditions as well as over the entire range of conditions that will be tested experimentally. Additionally, the experimental procedure was determined using the simulation model. Similar to the experimental set-up, the model consists of four hydraulic loops, creating the overall hydraulic network. These hydraulic loops include the heat input, air conditioning, heat rejection and building simulator loops. In addition to the four hydraulic loops, the model also contains four plotters with output files, which record the performance of the chiller, the stratification within the hot water tank, the state of charge within the chiller and the heat transfer rates across each of the heat exchangers installed within the system. A schedule controller was connected to the heat input loop, turning off the auxiliary heater and heating pump (P3) at the end of the test. Figure 4-1 illustrates the model created in TRNSYS. The following sections describe each of the components in detail.

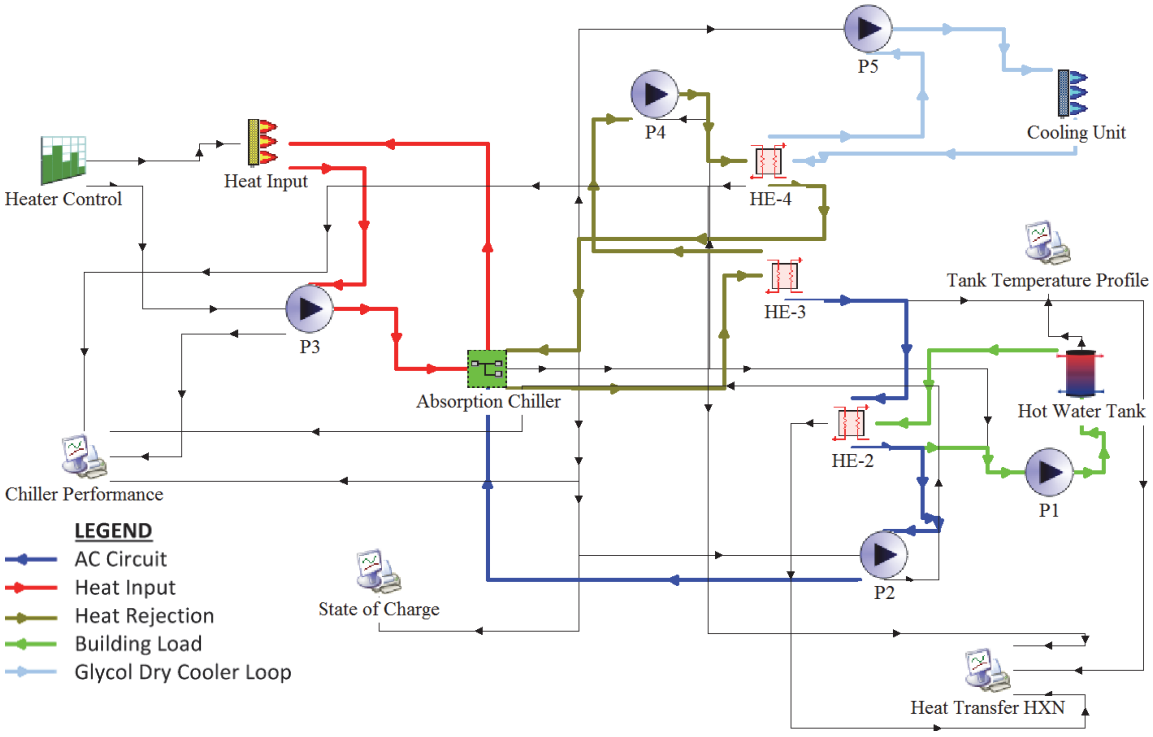

Figure 4-1: Model of experimental system built in TRNSYS

4.2 Heat Input

To simplify the complexity of the model without limiting its accuracy, the steam to water heat exchanger providing the heat input into the system has been replaced with an auxiliary fluid heater (Type 659). This Type was selected over the Type 6 auxiliary heater as it allows the heating capacity to be proportionally controlled unlike Type 6, which can only be turned on and off. Although this proportional control was not used within this model, the capability was included so that in the future, when testing the system under varying power conditions, a proportional controller can be attached to vary the power input. This heater will transfer heat into the system at the same rate as the heat exchanger, but without the requirement of modelling the steam line and a flooded shell and tube heat exchanger that could create additional error within the model. The auxiliary

heater has been set to transfer heat to the water flow at a maximum rate of 20 kW. This is the design of the heat transfer rate in the steam-to-water heat exchanger (although capable of higher heat transfer rates). The auxiliary heater operates by using the incoming temperature and flow rate of the fluid flow and performs an energy balance over the heater to determine the output temperature. The energy balance of the heater is depicted in Figure 4-2.

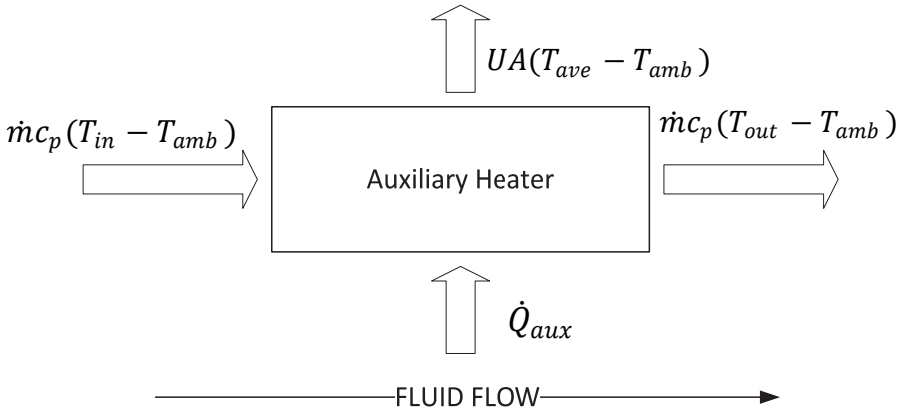

Figure 4-2: Energy balance on the auxiliary heater

Using this energy balance, Equation 4.1 can be derived to determine the temperature of the exiting fluid.

$$T_{out} = \frac{\dot{m}c_p T_{in} - UA\frac{T_{in}}{2} + UAT_{amb} + \gamma_{htr}\eta_{htr}\, CAP_{htr}}{\dot{m}c_p + \frac{UA}{2}} \qquad (4.1)$$

where UA is the heat transfer coefficient of the heater to the surroundings, γ is the control signal to the heater, CAP is the capacity of the heater and η is the heater effectiveness

The auxiliary heater is designed to have a proportional control that regulates the rate of heat transfer to the fluid, accepting a control signal, γ, between 0 and 1 which proportionally scales the capacity of the heater. Within this model, because it was only representing the heat transfer rate from the steam to the heat input hydraulic loop, it was assumed that the heat loss coefficient, UA, is 0, signifying there is no heat loss from the heater. Additionally, the heater effectiveness is assumed to be 1, signifying it is a perfect system and all of the heat added is transferred to the flowing fluid. These values were chosen as the auxiliary heater has been designed solely to mimic the performance of the heat exchanger and not to determine the performance of a heater.

In addition to the variables defined in Equation 4.1, a set-point temperature is defined within the simulation, and when calculating the output temperature, if the calculated temperature is greater than the set point temperature, the set point temperature is taken as the output temperature, and the amount of energy required to reach the set-point temperature is calculated. The set-point of the heater sets the temperature of the hot flow into the absorption chiller, and this value was varied to determine how the hot temperature affected the performance of the chiller.

4.3 Heat Rejection

Like the heat input, the heat rejection system was simplified to reduce the model complexity and to remove the weather conditions from the model. This was done to allow steady state, stable conditions with no reliance on the time of day, or day of the year the simulation takes place. The dry cooler is simulated with an auxiliary fluid cooler (Type 1246). This Type was chosen over Type 92, auxiliary cooling device, as Type 92 can

only be controlled on and off, while the auxiliary cooler in the model is proportionally controlled by the chiller control unit (Type 826). The capacity of Type 1246 is scaled by the control signal, and when only one barrel of the chiller is in operation, a control signal of 0.5 is supplied, as only half the heat rejection capacity is required. Since the auxiliary cooler in the model functions independent of the outdoor conditions, it will always provide the required cooling capacity and therefore the water to water heat exchanger between the heat rejection loop and the building's chilled water line (HE-5) is not included in the model. The auxiliary cooler has a capacity of 30 kW, which is equivalent to the design cooling capacity of the dry cooler installed within the experimental set-up (10 tons).

Like the auxiliary heater, the auxiliary cooler performs an energy balance over the device using the fluid flow rate, inlet temperature and the heat capacity of the fluid to determine the exiting fluid temperature. Since the auxiliary cooler represents the dry cooler, the fluid in the loop is a 50/50 by volume mixture of water and propylene glycol, with a heat capacity of 3.55 kJ/kg K [41]. A graphical representation of the energy balance of the auxiliary cooler is shown in Figure 4-3.

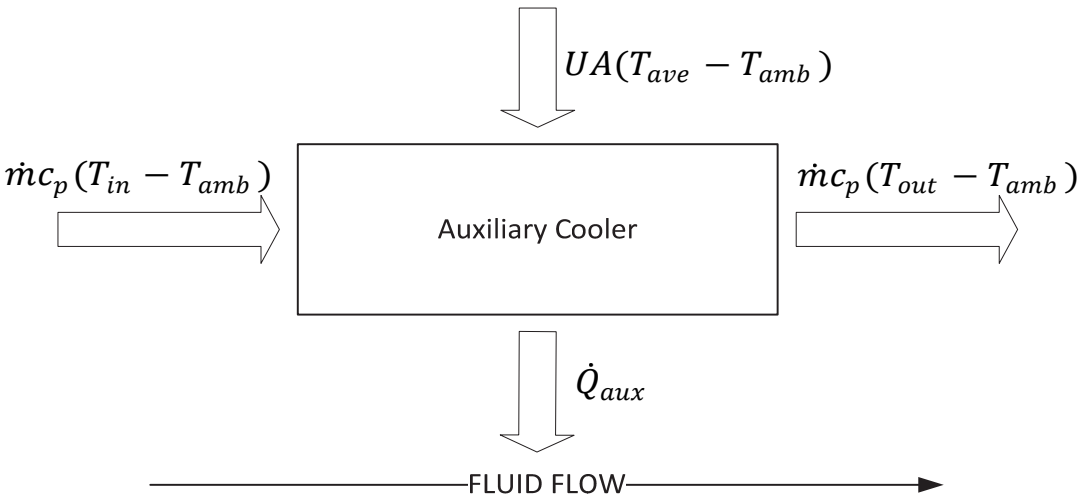

Figure 4-3: Energy balance for auxiliary cooler

Using this energy balance, Equation 4.2 is derived where UA is the heat transfer coefficient of the cooler to the ambient conditions, γ is the control signal to the cooler, CAP is the capacity of the cooler and η is the cooler effectiveness

$$T_{out} = \frac{\dot{m}c_p T_{in} + UA\frac{T_{in}}{2} - UAT_{amb} - \gamma_{cool}\eta_{cool}\, CAP_{cool}}{\dot{m}c_p - \frac{UA}{2}} \qquad (4.2)$$

Since the purpose of the auxiliary cooler is to provide constant heat rejection for the chiller, and not to determine the performance of the cooler, it was assumed that it was a perfect system. As a result, the effectiveness was assumed to be 1, indicating that all energy input is used to cool the fluid. In addition, the UA value was set at 0, indicating no heat gain or loss through the auxiliary cooler.

A set-point for the auxiliary cooler was set within the model, where if the set-point is reached, the set point temperature is used as the output temperature and the cooling required to achieve this temperature is calculated. The cooler is designed to work

with a proportional controller, with a control signal, γ_{cool}, supplied to the unit be 0 and 1, proportionally controlling the cooling capacity of the unit. This signal is provided by the chiller and varies between 0 (when neither barrel is charging or discharging), 0.5 (when only one barrel is charging or discharging), and 1 (when both are charging or discharging.)

4.4 Chiller

To model the chiller, a custom built TRSNYS Type was obtained from the supplier of the unit (Figure 4-4). The model of the chiller contains two separate Types, connected together to create a complete model of the solar absorption chiller. The first is Type 826, the chiller control unit, which represents the piping unit of the absorption chiller and controls the flow from the different hydraulic networks (heat input, heat rejection and air conditioning loops) between the two separate barrels of the chiller. It also determines when to switch between the charging and discharging of the barrels, and provides the control signal to the pumps in the air conditioning and heat rejection loop. The second component is the solar chiller barrel, Type 825, which represents a barrel of the ClimateWell solar absorption chiller. Two Type 825 chiller barrels were implemented into the model to represent the actual chiller and were connected to the chiller control unit (Barrel A and Barrel B). Figure 4-4 shows the configuration of the absorption chiller macro that was created and implemented into the overall model.

This model was developed by Chris Bales and Svante Nordlander from Solar Energy Research Center at Dalarna University in Sweden [8]. The original model was developed and validated under the PolySMART (POLYgeneration with advanced Small and Medium scale thermally driven Air-conditioning and Refrigeration Technology)

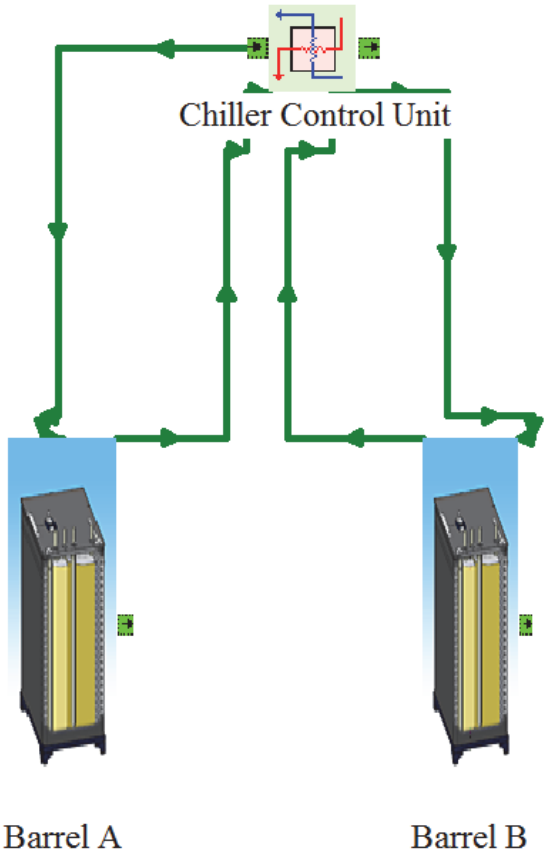

Figure 4-4: Solar absorption solar chiller macro for model of experimental set-up

program in Europe from 2006-2010 [42]. The source code and exact mathematical equations used within the model are proprietary and not available. The component was developed using a detailed resistance network for the external and internal heat transfers taking into account the properties of the solid salt and salt solution [42]. In addition,

sensible heat capacity, the heat of dilution, heat of vaporization and enthalpy of crystallization of the substances are taken into consideration.

4.5 Heat Exchangers

In total, three heat exchangers were included within the model. All three heat exchangers are parallel plate heat exchangers, and are modelled as such, using Type 5. The heat transfer coefficients were taken from the design specifications of the heat exchangers at the design conditions within the system. The overall heat transfer coefficient for each of the heat exchangers, as well as the heat capacity of the hot and cold fluid are listed in Table 4-1.

Table 4-1: Overall heat transfer coefficient for modelled heat exchangers

Heat Exchanger	Hot Side Heat Capacity (kJ/kg K)	Cold Side Heat Capacity (kJ/kg K)	Heat Transfer Coefficient (W/K)
HE-2	4.2	4.2	120
HE-3	4.2	4.2	281
HE-4	4.2	3.55	3097

The TRNSYS Type 5 component uses an effectiveness minimum capacitance approach to determine the outlet conditions, based on an effectiveness that is calculated using the overall heat transfer coefficient – product area, UA, value and the inlet conditions of the hot and cold fluid streams. A graphical representation of the heat exchanger model is presented in Figure 4-5.

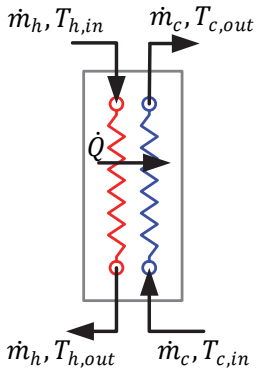

Figure 4-5: Schematic of the heat exchanger model

To calculate the effectiveness of the heat exchanger, the capacity for the fluid flow to contain thermal energy, which is the product of the mass flow rate and the heat capacity of the fluid, for both the hot and cold fluid must first be determined using Equations 4.3 and 4.4.

$$C_c = \dot{m}_c c_{p,c} \tag{4.3}$$

$$C_h = \dot{m}_h c_{p,h} \tag{4.4}$$

Once the capacity of the hot and cold side are determined, the larger of the two values is defined as C_{max} and while the smaller of the two values is defined as C_{min}. Using these values and the defined heat transfer coefficient, the model calculates the effectiveness of the heat exchanger using Equation 4.5.

$$\varepsilon = \frac{1 - \exp(-\frac{UA}{C_{min}}\left(1 - \frac{C_{min}}{C_{max}}\right))}{1 - \left(\frac{C_{min}}{C_{max}}\right)\exp(-\frac{UA}{C_{min}}\left(1 - \frac{C_{min}}{C_{max}}\right))} \tag{4.5}$$

Using the calculated effectiveness the outlet temperatures are calculated using Equations 4.6 and 4.7, and the heat transferred across the heat exchanger is calculated using Equation 4.8.

$$T_{h,o} = T_{h,i} - \varepsilon(\frac{C_{min}}{C_h})(T_{h,i} - T_{c,i}) \quad (4.6)$$

$$T_{c,o} = T_{c,i} + \varepsilon(\frac{C_{min}}{C_c})(T_{h,i} - T_{c,i}) \quad (4.7)$$

$$\dot{Q} = \varepsilon C_{min}(T_{h,i} - T_{c,i}) \quad (4.8)$$

These values are the output from the heat exchanger components and consequently form the input values for the subsequent component. The heat transfer rate is recorded by an online printer within the model, and will be compared to the heat transfer rates calculated during the experimental tests to validate the heat exchangers within the model.

4.6 Additional Components

In addition to the main heat transfer components discussed in the previous section, five variable speed pumps, Type 3, were integrated into the model of the experimental set-up and represent the five pumps listed in Table 3-3. A variable speed pump was chosen so that the flow rate could be regulated by the control signal produced by the chiller. This allowed for the heat rejection loop and dry cooler loop (P4 and P5) to operate at full capacity (55 L/min) when both barrels were in operation (one charging, one discharging), half capacity (22.5 L/min) when only one barrel was operating (either one charging or one discharging) or off when neither barrel was charging or discharging. Additionally, the chiller control unit controlled the pump in the air conditioning and building load simulator loop (P1 and P2), by turning the pumps on when one of the barrels started to discharge, and turning the pumps off when no air conditioning was available, or when the unit was switching between which barrel was charging and which

was discharging. The pump within the heating loop (P3) was controlled by a schedule which turns the pump on at the beginning of the simulation and remains on until the end of the heating phase.

The final component included within the model is a 270 L domestic hot water tank based on the design and configuration of the hot water tank included in the experimental set-up. This tank was modelled using a Type 4 thermal storage tank with two internal auxiliary heaters. The tank is modelled with 30 nodes, each 0.05 m in height. The auxiliary heaters are each 4.5 kW and are placed at node 3 (top of the tank) and node 15 (half way down the tank) to represent actual locations of the heating coils within the building load simulator tank. The top heater is set to heat to 60°C while the lower element is set to heat to 55°C, working in a master/slave configuration meaning the lower element will only go on when the top element is satisfied, ensuring that both elements are not on at the same time.

Although Type 4 is designed to determine the stratification within a thermal storage tank, no stratification was observed (fully mixed tank) due to the high flow rates (15 L/min) used within the building load loop and the fact that the tank starts completely charged at the beginning of the simulation. The model was created with 30 nodes, to compare with the thermocouple probe placed within the tank in the experimental set-up. The primary purpose of these measurements is to ensure there is adequate hot water in the tank to ensure it can provided the required energy to accurately mimic a building's cooling load.

4.7 Simulation Control

To control the simulations, TRNSYS's control card was predominantly used. The control card was used to set the overall length of the simulation. The length varied simulation to simulation and was dependent on the test being run and the charge and discharge rate when looking at the number of cycles. In addition to controlling the length of the simulation, the control card was used to set the time step of the simulation. The auxiliary heater was controlled independently of the simulation time, using a forcing function, TRNSYS Type 14 was used. Type 14 produces a control signal that is read in by the auxiliary heater and pump. At the start of the simulation, the auxiliary heater and pump are running, providing heat to the chiller, charging the chiller. At the end of the pre-determined charging period, the control signal from the forcing function switches from 1 to 0, turning the auxiliary heater and pump off, and allowing the unit to discharge through the remainder of the simulation. The length of the simulations and temperature ranges tested are further discussed in the following chapter.

4.8 Modelling Studies

Upon completion of the model within TRNSYS, a number of modelling studies were conducted. The first was to determine the experimental procedure, while the second was to ensure the experimental apparatus is capable of assessing the performance of the chiller over the desired test range. To determine the length of time the chiller should be operated to accurately determine the performance, a sensitivity study was conducted varying the experimental run time between 10 and 24 hours. Through this study, it was determined that the length of time the chiller operates is not the only factor that must be

considered when determining the experimental run time. As a result, a second sensitivity study was conducted to look at the performance of the chiller compared to the number of charge and discharge cycles of the chiller. In addition to determining the length of time the chiller will be operated, the measurement time step must be determined. To do this, simulations were run changing the simulation time steps from 1 second to 300 seconds and the results were compared with the results of the uncertainty analysis, and an experimental time step was determined.

A second modelling study was conducted to ensure that the system will operate over the entire desired test range for the solar absorption chiller. The heat input temperature was varied between 70°C and 95°C while the heat rejection temperature was varied between 10°C and 30°C. The results of the simulations were analyzed and any necessary changes to the experimental procedures and apparatus were determined. The results of the two modelling studies are presented in detail in Chapter 5.

5 Chapter: Modelling Results and Discussion

This chapter discusses the evaluation of the performance of the chiller through simulation, as well as the steps taken to determine the optimal experimental procedure for evaluating the performance experimentally. Finally it presents the results of a modelling study that was conducted over the entire test range.

5.1 Model Output and Result Files

The system performance was evaluated by recording the mass flow rate through the chiller and the entry and exit temperatures of the chiller to determine the amount of heat that is transferred to or from the chiller.

Once the simulation was completed, a spreadsheet was created to tabulate the temperatures and flows at each time step of the simulation. Using these temperatures and mass flow rates, the heat transfer rate for each simulation time step was determined. The total amount of energy that is transferred into, or out of the chiller for each time step, *t*, was determined using Equation 5.1.

$$E = \dot{m} c_p (T_{out} - T_{in}) t \tag{5.1}$$

Once the energy transferred during each time step is calculated, for each of the three hydraulic loops connected to the chiller, the total energy transfer for the simulation was calculated by summing the energy transferred for all of the time steps. The overall COP_{th} of the chiller was quantified using the total energy transfer in the heat input and air conditioning loops. Once all of the energy transferred during the simulation is calculated, the overall COP_{th} of the chiller is calculated using Equation 5.2.

$$COP_{th} = \frac{\sum E_{cold}}{\sum E_{hot}} \tag{5.2}$$

In addition to calculating the COP_{th} of the system, additional parameters are monitored, recorded and analyzed when determining the optimal experimental procedure. These include the length of time the heat input is on charging the chiller, the number of charge and discharge cycles and the state of charge in the two barrels. The state of charge is the fraction of charge in the barrel, presented as a decimal between 0 and 1, with 0 representing no cooling potential, or no charge, and 1 represents a fully charged barrel with the maximum amount of cooling potential. Both the model and the unit installed in the experimental set-up have a built-in condition where the barrel cannot switch from charging to discharging, unless the state of charge reaches a minimum of 0.7 in the charging barrel, and a barrel must remain charging for a minimum of two hours. These are implemented to ensure adequate charging occurs, and reduces the frequency of switching between charging and discharging, where no cooling can be produced.

5.2 Determining Experimental Procedure

To determine the experimental procedure, and subsequently the conditions for the remainder of the simulations, a sensitivity study was conducted to determine the optimal length of run time and time step for measurements. The experimental procedure includes the settings of the experimental apparatus, the steps taken for evaluation and the method for collecting experimental data to determine the system performance. The purpose, method, and results of these two sensitivities studies are presented in the following sections.

5.2.1 Experimental Run Time

The first step in creating the experimental procedure was to determine the length of time the experimental test should last. The length of time the auxiliary heater is on, providing heat input to the chiller, is considered the experimental test time. Following the operation of the heat input system (turning off the pump and auxiliary heater), the chiller is allowed to continue to operate for an additional four hours. This is to ensure that all of the energy stored within the chiller is discharged in the form of chilled water. The ClimateWell chiller is able to store energy in the form of desorbed refrigerant, and thus it is imperative that all of the stored energy is discharged. Any energy remaining in the unit at the end of the simulation will skew the calculated COP_{th} value obtained, returning a lower value then what is actually experienced by the chiller.

A time step of 30 seconds was selected to perform the sensitivity study as a first approximation, and had it been needed, the study would have been repeated if it was later found that this introduces a significant error in the overall test results. This means that for every 30 second period, one mass flow rate and the inlet and outlet temperature is recorded for each of the three hydraulic loops connected to the chiller. It was assumed that these values are constant through the entire time step, and represents a constant heat transfer rate, which is the same method that will be used to experimentally determine the performance of the chiller.

To test how long the chiller should be operated to obtain an accurate measurement of the COP_{th}, simulations were conducted allowing the heat input to run from six hours to twenty hours (total simulation time of ten to twenty-four hours). These values were chosen as it was desired that a minimum of one charge and discharge cycle occurs in each

of the two barrels. Based on the required minimum time between switching from charging and discharging (minimum of 2 hours) and the time required for switching (3 minutes), six hours was chosen to ensure two cycles are completed. The high end of a total simulation time of twenty-four hours was chosen as it was desired that any single experimental test never exceed a single day, allowing one test to be conducted daily. The two hour increment between tests was chosen as it was thought to represent approximately one additional cycle.

The total heat input to the chiller and the total amount of energy removed from the chilled water line was calculated for each of the eight simulation lengths. Using these values, the COP_{th} was calculated for each simulation length. The total heat input and cooling produced, along with the COP_{th} are presented in Figure 5-1.

It was expected that as the time increases, the results would converge to a given COP_{th}, however, as it can be seen in Figure 5-1, the COP_{th} does not converge and instead creates a sinusoidal cycle. The simulations for 10, 14, 18 and 22 hours have a lower thermal COP_{th} when compared to the results from the 12, 16, 18, 20 and 24 hour simulations.

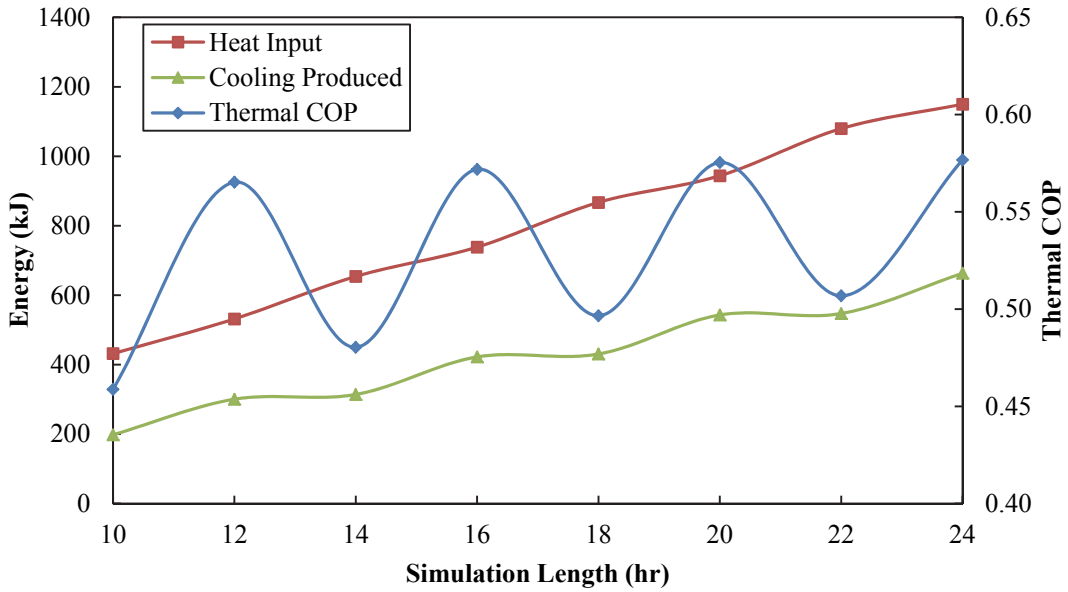

Figure 5-1: COP_{th} of the chiller and the heat input and cooling produced during the simulations

Further investigation was required to determine what was causing the fluctuations in the values obtained and that not only the total experimental run time needs to be considered when developing the testing procedure. Further work was conducted to determine the cause of this discrepancy and presented below.

The next aspect was to examine the state of charge (SOC) of each of the barrel in the cooling unit during each of these simulations. This was done as it was hypothesized that the change in COP_{th} was caused by not all of the energy stored within the unit being discharged in the form of chilled water. To see what effect the SOC, of the charging barrel when the heat input system was turned off has on the performance of the chiller, it was plotted and compared to the calculated COP_{th} in Figure 5-2.

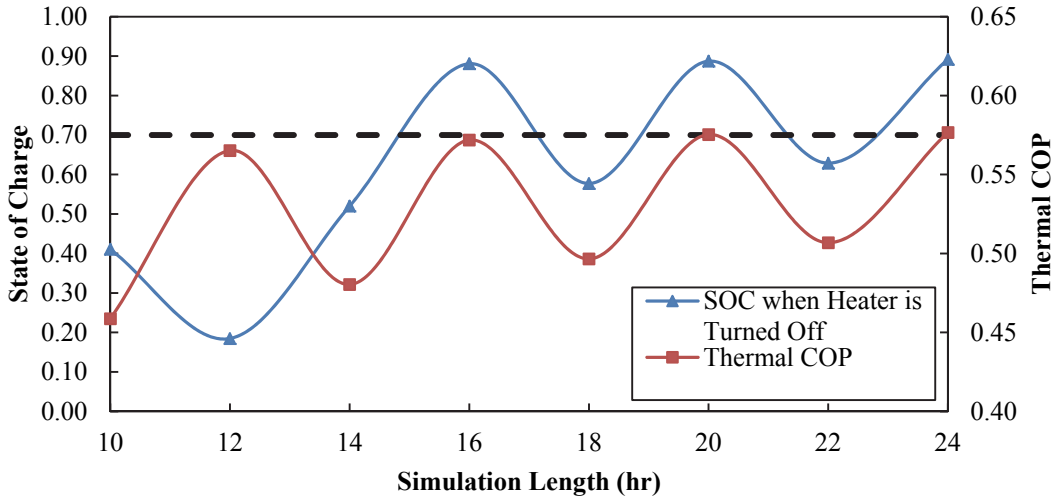

Figure 5-2: Comparing COP_{th} and the state of charge in the barrel

In addition to showing the COP_{th} and SOC for each simulation, a dashed line has been drawn at a SOC of 0.7, which is the previously discussed minimum threshold that the barrel must reach in order for discharging of the barrel to occur.

From Figure 5-2, it can be seen that the state of charge is below the 0.7 in the 10, 14, 18 and 22 hour tests, where the COP_{th} was lower than expected, meaning that the barrel could not switch from charging to discharging. As a result, energy from the heat input has been collected in the partially charged barrel, but is not able to discharge and hence the simulation ends with energy remaining in the chiller. The total heat into the unit takes into account the charging; increasing the heat term of the COP equation, while, the cooling produced as a result of this heat input by the chiller is not realized in the cooling produced term, causing the COP_{th} to be lower.

In contrast, for the simulations lasting 16, 20 and 24 hours, the threshold of 0.7 was reached before the auxiliary heating system was turned off as it ended up taking just

over 3 hours per charging cycle. As the charging barrel reached a SOC of 0.7, the barrels switched from charging to discharging and all of the energy was discharged as chilled water. Finally, the 12 hour simulation ended with a very low SOC in the charging barrel, meaning very little energy was absorbed before the heater was turned off. Consequently the amount of energy absorbed but not discharged is very small in comparison to the total amount of energy absorbed and therefore, the stored energy has little effect on the calculated COP_{th}, giving the appearance that all of the stored energy was discharged.

Based on these results, it was determined that of greater importance than the total length of time the chiller runs is that the barrels are not interrupted during a charging cycle. As a result of this conclusion, it was determined that the experimental test would not last a predetermined time, but rather last a certain number of charging and discharging cycles. To determine the number of cycles an experimental test should last a second sensitivity study was conducted. Simulations were run at the design conditions from two charge and discharge cycles, through twelve cycles. The $COPs_{th}$ of the sensitivity study are shown in Figure 5-3. In addition to showing the relationship between the COP_{th} and the number of cycles, the length of time the auxiliary heater is activated to fulfill the required number of charging cycles is also shown. From this data, it can be seen that for each cycle, a charging period of just over 3 hours is required. This time period is only valid at the design conditions, and the charging time for each cycle will vary based on the temperature of the heat rejection loop and the heat input. Shorter times will be experienced when the heat input temperature is higher, or the heat rejection input temperature is lower. A comparison of charging time is included in Section 5.3 which

looks at the effect of varying inlet temperatures on performance and experimental procedure.

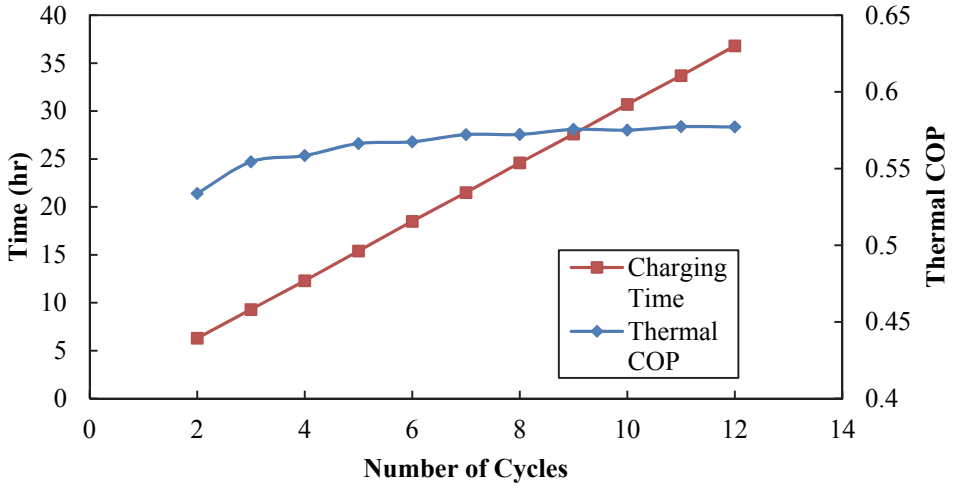

Figure 5-3: Number of cycles compared to COP_{th} and total charging time

In addition to looking at the COP_{th} in relation to the number of cycles, the total heat input and air conditioning produced are also examined to determine the relationship between the total energy transfer and the number of cycles. It was expected that the total energy transferred would increase linearly with time, however when the cooling produced was compared to the simulation time (Figure 5-1), it was found that there was no linear relationship for the cooling produced. When the same plot is produced (Figure 5-4) comparing the amount of heat input and air conditioning produced against the number of cycles, the relationship is linear. There is an initial offset in the heating, with an intercept of about 27,000 kJ, showing that the chiller requires an initial energy input at start-up to reach steady state conditions. This is also evident from the first cycle taking 3.3 hours, while every charging cycle after that takes slightly less than 3.1 hours.

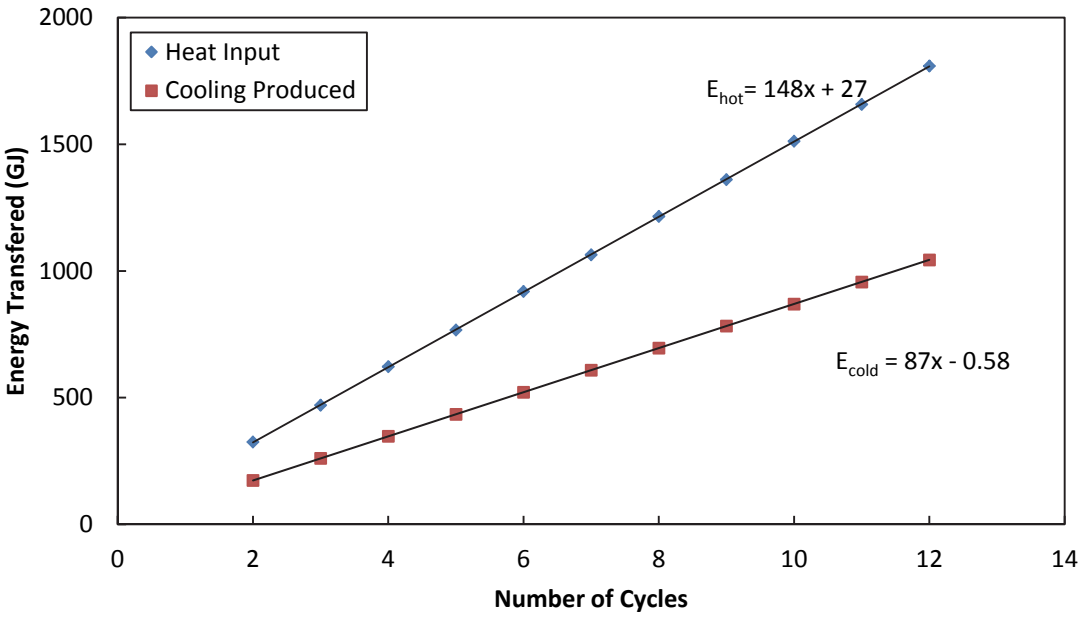

Figure 5-4: Comparison of number of cycles to energy transfer

Based on the results of the two sensitivity studies it was determined that the experimental run time would be seven cycles. This conclusion was determined based on a number of factors. The first, and most important, was at seven cycles, the COP_{th} has levelled off, with only a 0.005 increase in the COP_{th} between seven cycles and the maximum number of cycles tested (twelve). This value of 0.005 is equivalent to less than 1% of the calculated COP_{th} at seven cycles and is four times less than the uncertainty on the COP_{th} calculated with experimental data (see Chapter 6 for uncertainty analysis). Additionally, seven cycles met the initial target of having a single test lasting no more than 24 hours, with the auxiliary heater on for just over 21 hours, and then taking approximately three hours for the final barrel to discharge after the heater is switched off.

5.2.2 Simulation Time Step

After determining the experimental test length, the next step was to determine the experimental time step to be used in the remainder of the simulations and during experimental testing. The shorter the time step, the more accurate the simulation and experimental test will be as a shorter time step will more accurately measure any transient or sudden changes in the system. These changes will most commonly occur during the changing over between charging and discharging. Although a shorter time period can more accurately model and evaluate the sudden changes, a shorter time step will also create a larger uncertainty on the experimental measurements. The error on the flow meter reading increases as the averaging time used to calculate the volumetric flow rate decreases. In addition to the decrease in accuracy, as the time step decreases, the quantity of data collected during a simulation or experiment increase, and therefore if the time step is too small, the quantity of data becomes overwhelming and files become very large and difficult to use. For these reasons, a balance between accuracy and ability to track transient changes must be determined.

A sensitivity study was performed to examine the effect of the time step length and to determine an optimal time step length for the experimental evaluation of the system. The shorter the time step, the more accurate the simulation, and because of this, the purpose was to determine the variation in results as the time step is increased. Simulations were conducted at the design conditions and for seven complete cycles, with time steps of 1, 5, 10, 15, 30, 60, 120 and 300 seconds. The results of these simulations were tabulated and the heat input, cooling produced and the calculated COP_{th} are presented in Table 5-1. In addition to the results of the simulation, the experimental

uncertainty on the COP_{th} as calculated per the steps presented in Chapter 6 is included in Table 5-1.

Table 5-1: Simulation results compared to experimental uncertainty for different time steps

Time Step (s)	*Heat Input (kJ)*	*Cooling Produced (kJ)*	*COP_{th}*	*Experimental Uncertainty (%)*
1	1 046 767	606 123	0.579	9.48
5	1 051 959	605 685	0.575	4.80
10	1 055 984	605 671	0.573	4.60
15	1 062 687	606 164	0.570	4.55
30	1 063 746	608 598	0.572	4.53
60	1 072 771	606 484	0.565	4.53
120	1 071 933	605 696	0.565	4.52
300	1 081 880	535 660	0.495	4.52

A comparison between the results of the simulation and the experimental uncertainty at different time steps was conducted to determine the optimal time. From the results in Table 5-1, it was observed that there is very little change in the simulation results between the 1 second to 30 second time step, however, there is a significant change in the experimental uncertainty over this same range. There is a marked reduction in the experimental uncertainty between the 1 second and 15 second time steps and then little change as the time step increases beyond 15 seconds. As the time averaging period increases, the error on the flow rates will no longer be the dominant error in the COP_{th} calculation and a further increase in time has limited reduction in the overall uncertainty. As a result, both 15 second and 30 second time steps produce similar results both in terms

of the simulated performance of the chiller and in terms of the experimental uncertainty, indicating that both are acceptable time steps to use for the experimental procedures. The 30 seconds time step was chosen for the experiments, as it performs well based on simulation, has a low experimental uncertainty, and when compared to the 15 second time step, it will allow a 50 percent reduction in the quantity of data that needs to be recorded, stored and analyzed.

5.3 Simulation of Experimental System Over the Complete Test Conditions

After the experimental procedure was determined, simulations were conducted over the range of heat input and heat rejection temperatures to be experimentally tested. The main purpose of this modelling study was to ensure that each component was sized correctly, and capable of testing the chiller not only at the previously mentioned design conditions, but over the entire test range. A secondary purpose of the study was to determine the projected time that each test would take, and if any special considerations need to be taken into account when determining the experimental procedure. These results will give an indication of the time the chiller will need to operate under each test condition, and provide a simulated COP_{th} to compare the experimental results to.

These simulations were conducted with a target inlet temperature of the air conditioning loop of 20°C and under the previously developed simulation conditions of a 30 second time step and lasting seven complete charging and discharging cycles. With the exception of inlet temperature of the heat input and heat rejection loops, all other parameters were held constant at the design conditions. Simulations were run for heat input temperatures of 75°C to 95°C, at 5°C intervals while the heat rejection set-point

was varied from 10°C to 30°C at 5°C intervals. When the two variables were combined, a total of 25 different scenarios were simulated. The results of these simulations are presented in Figure 5-5, which shows the calculated COP_{th} of the chiller for each condition. Additionally, Figure 5-6 compares the length of time it takes for seven complete charging cycles between each scenario.

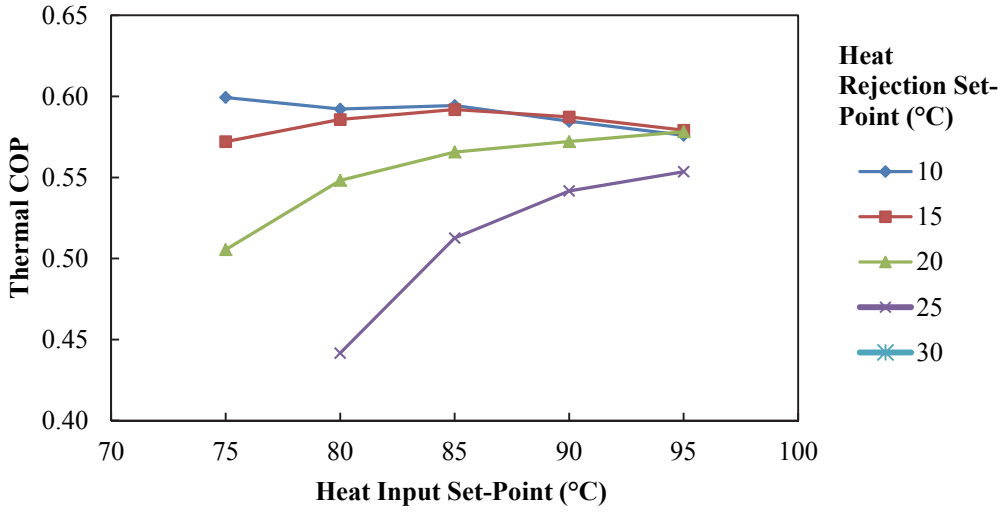

Figure 5-5: COP_{th} for varied heat input and heat rejection temperatures

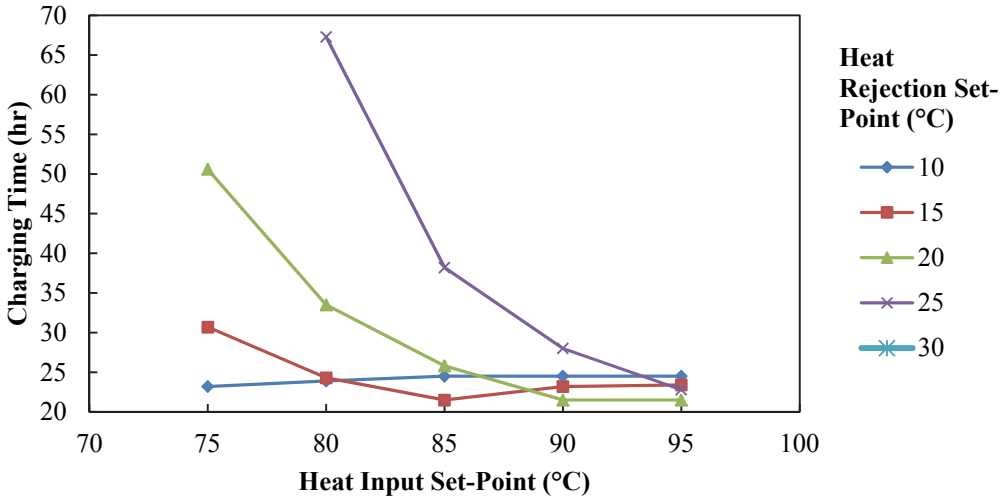

Figure 5-6: Charging time for seven cycles for varied heat input and heat rejection temperatures

Although simulations were run for 25 different conditions, only 19 are plotted in Figure 5-5 and Figure 5-6. This is because during the simulations, when a set-point of 30°C was tested in the heat rejection loop, there was an insufficient ability for the chiller to reject heat and therefore the chiller was unable to charge. This consequently caused no cooling to be produced. In addition to being unable to charge when the heat rejection was set to 30°C, the unit was unable to charge when the heat rejection was set to 25°C and the heat input was at 75°C. These results also showed that the heat rejection temperature has a larger influence on the performance of the chiller. Therefore, during the experimental testing, it is of equal or greater importance to control the temperatures and flows within the heat rejection loop.

In addition to examining the performance and the experimental time, each simulation was examined to ensure the experimental set-up was able to meet the demands and keep the temperature constant throughout the test. It was found that at the higher input temperatures and low heat rejection temperatures, the cooling capacity was greater than the cooling provided at the design conditions. Compounding this increase in cooling capacity, the temperature of the heat rejection loop leaving the chiller is also lower, reducing the amount of heat that can be transferred through HE-3. As a result of the lower temperatures and higher cooling capacity, it was found that the heat inputs from HE-2 and HE-3 do not equal the cooling provided by the chiller. Because of this, a slow cooling of the air conditioning loop was observed, with the entering temperature dropping as low as 8°C. Because of this, a periodic shutdown of the chiller occurred as there is a safety mechanism built in that will shut-off the cooling process if the temperature leaving the chiller drops below 5°C. This caused a reduction in the

performance of the chiller and led to a decreasing chiller performance with an increasing heat input temperature when the heat rejection loop is set to 10°C and 15°C.

To address this issue within the experimental design, when the heat rejection is set to 10°C or 15°C, the flow rate within the building load simulator must be increased to 25 L/min, to increase the amount of heat transfer through HE-3. This will cause an increase in the return temperature, keeping it well above the 5°C shut-off threshold. To determine the effect this change has on the performance of the chiller and to ensure the new configuration satisfies the testing requirements, the simulations were re-run using the new conditions. The increased flow rate was used for all of the simulations with a heat rejection temperature of 10°C and for the simulation with a heat rejection temperature of 15°C and a heat input temperature of 85°C, 90°C, and 95°C. The results using the new flow rates in the building load simulator were combined with the original results for the remainder of the simulations and are presented in Figure 5-7.

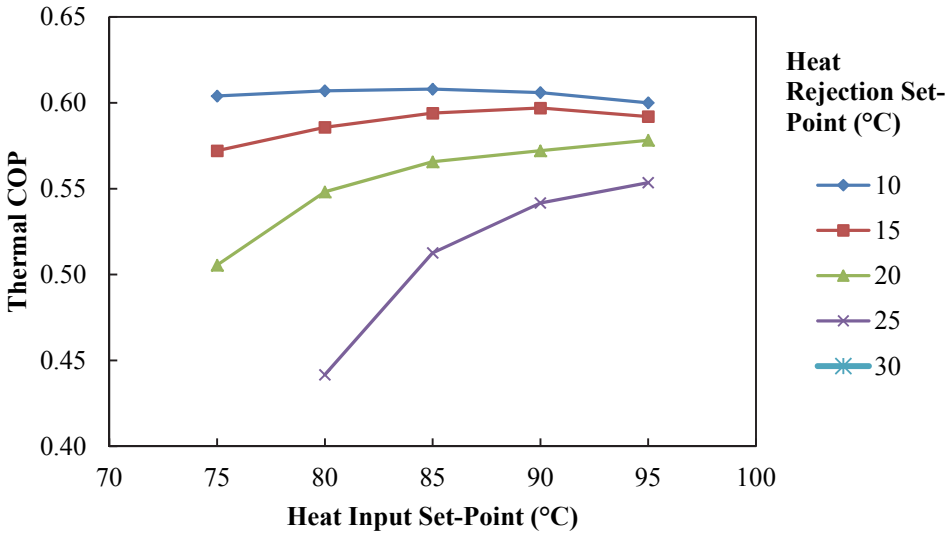

Figure 5-7: Thermal COP with varied temperatures and different building simulator flow rates

Analyzing the new results presented in Figure 5-7, the change in the flow rate and subsequent higher heat transfer rate across has resolved most of the issues seen in the first iteration. There is still a small drop off when the heat input is 95°C as a result of the slow overall cooling of the return temperature in air conditioning loop. These results are more aligned with what was expected. As the heat input temperature rises and the heat rejection temperature decreases, the COP_{th} of the unit will increase and the experimental run time will decrease.

5.4 Experimental Design

Based on the results of the modelling studies, an experimental procedure was developed for all future tests on the ClimateWell solar absorption chiller. It was determined that it is far more important to end the test during the changeover between charging and discharging as opposed after a certain amount of time has elapsed. Through simulation it was determined that the chiller should be allowed to run seven complete charging and discharging cycles. This will allow all of the stored energy to be discharged in the form of chilled water, ensuring an accurate measurement of the chiller's performance to be determined. Through simulation of different time steps and a comparison of the experimental uncertainty, based on the time averaging period of the flow meters, it was determined that readings would be taken every 30 seconds. This provided a good compromise between the required resolution to track the transient performance of the chiller while reducing the experimental uncertainty.

After determining the experimental test length and resolution, simulations were conducted to ensure the experimental apparatus was capable of testing the chiller over the desired range of test conditions. Through these simulations, it was found that at a high

heat input temperature and low heat rejection temperature, the building load simulator at the design conditions was not adequate to match the amount of cooling provided by the chiller. To match the cooling capacity with the building load simulator, it was determined that the flow rate within the loop would be increased from 15 L/min at the design conditions to 25 L/min in order to increase the heat transfer rate through HE-3. During all other desired experimental tests, the design conditions met all of the required loads and were able to provide consistent input temperatures.

The TRNSYS model of the experimental apparatus was successfully used to determine the experimental procedure, including the total testing time, the experimental time step and all special considerations across the experimental test range. This model will continue to evolve as testing begins with the experimental apparatus. The data obtained from each of the components will be used to further refine the model and the experimental results will be compared to the predicted performance of the chiller. In addition, varying power input conditions can be considered to study the transient performance of the chiller.

6 Chapter: Calibration and Uncertainty Analysis

When doing an experimental analysis, it is critical to determine the experimental error that is introduced into the results through the experimental process. Through the design process, it was imperative to take measures and integrate instrumentation into the hydraulic networks in a way that reduces the experimental error. During both the design phase and upon completion of the experimental set-up, the overall experimental error was determined for the system and where possible, steps were taken to reduce this error. This chapter describes the process of calibrating the instrumentation and the uncertainty of the key metrics of the experimental system. These metrics include, but are not limited to, the heat transfer rates in the absorption chiller and the coefficient of performance. The process used for determining the error on calibration and the overall experimental error was adapted from Figliola and Beasley [43].

Experimental error can be broken up into two categories; systematic error and random error. Random error is caused by the random scatter of measured data and is introduced through the repeatability and resolution of the measurement devices. The random standard uncertainty, $s_{\bar{x}}$, is defined by Equation 6.1, where N is the number of samples and s_x is the standard deviation of the measurements.

$$s_{\bar{x}} = \frac{s_x}{\sqrt{N}} \tag{6.1}$$

The degrees of freedom of the random standard uncertainty can be calculated using Equation 6.2.

$$v = N - 1 \tag{6.2}$$

Using the degrees of freedom and a standard t-table, a t-value for a desired confidence interval (for this experimental work, a 95% confidence interval was used) can be ascertained. Taking the t-value and the random standard uncertainty, Equation 6.3 is used to find the random uncertainty.

$$u_r = \pm t_{v,P} s_{\bar{x}} \tag{6.3}$$

The systematic error is introduced to the results by the uncertainty of the measurement devices and data acquisition equipment within the system and is dependent on the operating conditions of the system. The systematic error was determined and minimized for each of the instruments through calibration experiments, and this process is described in Section 6.1. The overall experimental error of the system is found by taking the square root of the sum of the squares of the systematic and random errors as indicated in Equation 6.4.

$$u_T = \sqrt{{u_s}^2 + {u_r}^2} \tag{6.4}$$

This chapter focuses on determining the systematic error of the system through calibration and error propagation and does not take into account the random error which is not constant and will be determined for each specific experiment.

6.1 Component Calibration and Uncertainty

To determine the overall uncertainty of the system, the instrumentation uncertainty had to be obtained. This included the uncertainty on the temperature readings of the thermocouples, on the difference in temperature readings of the thermopiles and the measured flow rates from the flow meters. The following sub-sections describe the calibration process that was undertaken for each of the instruments.

6.1.1 Thermocouples

A calibration experiment was designed and undertaken to determine the relationship between the voltage produced by the thermocouple, and the temperature, and to determine and minimize the uncertainty of the reading. Typically, thermocouples measure the temperature using a relation determined by a table of typical voltage to temperature conversions which has been developed by the National Institute of Standards and Technology (N.I.S.T.) [39]. For special limits of error (SLE) wire, this provides a temperature which is accurate to within ±0.5°C. This table does not, however include the error introduced by the data acquisition system or the cold junction compensation temperature reading.

To calibrate the thermocouples, a thermocouple was placed in a constant, uniform temperature bath (Fluke 7102) which is constant in temperature to ±0.02°C throughout the bath. The temperature of the bath was measured using a platinum resistant temperature detector (RTD), which is factory calibrated to ±0.02°C. A curve was fitted to the data provided and Equation 6.5 was determined for a range of temperatures from 0°C to 100°C.

$$T = 0.000997 * R^2 + 2.308 * R - 240.845 \qquad (6.5)$$

This equation has a coefficient of determination of 1, meaning it is a very good fit, and the error from the regression was found to be an order of magnitude smaller than the RTD error, and therefore was neglected in the calibration uncertainty analysis. The cold junction temperature was measured using a thermistor built into the National Instrument thermocouple card (NI 9142) and has a built in error of ±0.25°C [44]. A representative thermocouple was built from each of the two different spools of thermocouple wire (one

30 gauge and one 24 gauge), and immersed within the constant temperature bath. Starting at 5°C, and increasing the set-point temperature by intervals of 2°C, the bath temperature, cold junction temperature and thermocouple voltage was measured. At each temperature, a reading was taken every five seconds for three minutes, for a total of 36 readings at each temperature set-point and then averaged. In total, measurements were taken at 46 temperature set-points, and the data for the two thermocouple wires is shown in Appendix C.

The voltage produced by the thermocouple does not indicate the temperature at the tip directly, but rather the temperature difference between the tip of the thermocouple (at the point where the temperature is desired) and the cold junction compensation (CJC). A relation between the difference in temperature of the cold junction and the tip of the thermocouple and the voltage produced was determined by first subtracting the temperature of the cold junction from the temperature of the bath, and then created an ordered pair with the voltage produced by the thermocouple. This was then plotted and a curve was fit to the data. A sixth order polynomial was chosen, as LabVIEW has a prebuilt variable that calculates temperature using a sixth order polynomial. Once these equations were determined, the CJC temperature is added to the equation for the temperature difference, providing a single equation that can be used to determine the temperature reading. Using this procedure, Equation 6.6 was found for the roll of 30 gauge wire while Equation 6.7 was obtained for the roll of 24 gauge wire.

$$T = 0.00109 * \mathrm{V}^6 + 0.00615 * \mathrm{V}^5 - 0.0799 * \mathrm{V}^4 + 0.212 * \mathrm{V}^3 - 0.708 * \mathrm{V}^2 + 24.65 * \mathrm{V} - 0.186 + \mathrm{CJC} \quad (6.6)$$

$$T = 0.00258 * \mathrm{V}^6 - 0.00374 * \mathrm{V}^5 - 0.0633 * \mathrm{V}^4 + 0.227 * \mathrm{V}^3 - 0.741 * \mathrm{V}^2 + 24.68 * \mathrm{V} + 0.091 + \mathrm{CJC} \quad (6.7)$$

where:

T is temperature in °C,
V is voltage produced by the thermocouple in mV, and,
CJC is cold junction temperature in °C.

Once these equations were determined, the next step was to perform an uncertainty analysis on the calibrated temperature readings from the thermocouples. This uncertainty had to take into account both the errors associated with the calibration of the thermocouples as well as the experimental measurement process. Most of the errors come directly from the specifications of the equipment, however, some of these had to be converted to an error in temperature. Only the uncertainty as a result of the equipment was considered as the random error on the calibration experiment and was determined to be an order of magnitude smaller than the equipment error.

To determine the temperature error caused by the voltage reading of the thermocouple card, a sensitivity factor relating the change in temperature reading compared to the change in voltage was calculated by taking the derivative of the thermocouple equation with respect to voltage. Doing this, it was determined to be 21.82 °C/mV using the maximum voltage during the tests of 3.23 mV for the 30 gauge wire. Using this value and the voltage reading error of 8 nV or 0.008 mV, the error on the temperature caused by the voltage reading is 0.175°C. The same process was followed and a sensitivity of 2.59°C/ohm for the temperature reading of the RTD to the resistance

reading was obtained. The digital multi-meter (DMM) used to measure the resistance has an error of ±0.0110% on 4-wire resistance measurements. Using 139.67 ohms, the maximum resistance obtained during the experiment, a maximum error in the resistance readings was determined to be 0.0154 ohms which, when multiplied by the sensitivity factor, gave an error in the temperature reading of 0.0397°C. All of the errors were deemed independent, and therefore the total error was determined by taking the square root of the sum the squares. Table 6-1 list all sources of error on the calibration and measurement process.

Table 6-1: Error on temperature measurement

Source of Error	Error - 30 gauge (°C)	Error - 24 gauge (°C)
Cold junction temperature – calibration	0.25	0.25
Cold junction temperature – experimental	0.25	0.25
Regression prediction error	0.237	0.157
Resistance temperature detector	0.02	0.02
Resistance read error – DMM	0.0397	0.0397
Bath uniformity	0.02	0.02
Voltage error – calibration	0.175	0.175
Voltage error – experimental	0.175	0.175
Total Uncertainty	0.49	0.46

Using the calibration experiment, the error on temperature readings of the 30 gauge wire in the thermocouples within the system has an uncertainty of ±0.49°C and the 24 gauge wire has an uncertainty of ±0.46°C.

6.1.2 Thermopiles

A similar experiment to that performed for calibrating the thermocouples was performed to calibrate and determine the uncertainty of the temperature differences measured by the thermopiles within the system. Two constant temperature baths were used with the temperatures in both baths being monitored by two separate RTDs. The first bath was kept at a constant temperature, representing the cold side being measured by the thermopile, while the temperature of the second bath was increased in 5°C increments up to 95°C. Measurements of the temperature in each of the two baths and the voltage produced by the thermopiles were recorded for three minutes, at 10 second intervals for a total of 18 measurements which were then averaged. The difference in the two baths was calculated, and a set of ordered pairs was developed between the difference in temperature and the voltage produced. This was repeated with the cold bath at a temperature of 5°C to 35°C and for 60°C to 90°C, at 5°C increments. These temperatures were chosen as they represent the range of cold side temperatures that will be experienced within the experimental test set-up.

Using the data obtained 14 individual equations were determined for each of the cold temperatures. During experiments, the thermocouple installed with each side of the thermopile will be used to determine the cold side temperature which will be associated with the equation that should be used for the measurement. Because the temperature recorded from this thermocouple is only used to determine the hot and cold side temperature and the appropriate equation to use, the error on this reading will have no impact on the accuracy of the temperature difference and therefore, is not included in the uncertainty analysis.

The same RTD and digital multi-meter used in the thermocouple calibration was used to measure the temperature of the hot bath, however, a second RTD and a different digital multi-meter were used to measure the temperature of the cold bath. The second RTD was also factory calibrated to ±0.02°C, and Equation 6.8 was fitted to the data.

$$T = 0.001 * R^2 + 2.309 * R - 240.863 \quad (6.8)$$

The data obtained through this calibration procedure is presented in Appendix D and the 14 equations for each of the cold side temperatures are presented in Table 6-2 where δT is the temperature difference in °C and V is voltage in mV.

Table 6-2: Thermopile equations

Cold Side Temperature (°C)	Equation for Temperature Difference
5	$\delta T = -0.032 * V^2 + 6.32 * V + 0.087$
10	$\delta T = -0.029 * V^2 + 6.20 * V + 0.32$
15	$\delta T = -0.031 * V^2 + 6.20 * V + 0.039$
20	$\delta T = -0.029 * V^2 + 6.13 * V + 0.081$
25	$\delta T = -0.029 * V^2 + 6.08 * V + 0.030$
30	$\delta T = -0.030 * V^2 + 6.04 * V + 0.0036$
35	$\delta T = -0.031 * V^2 + 6.00 * V - 0.053$
60	$\delta T = -0.024 * V^2 + 5.71 * V + 0.036$
65	$\delta T = -0.022 * V^2 + 5.70 * V + 0.033$
70	$\delta T = -0.040 * V^2 + 5.71 * V + 0.040$
75	$\delta T = -0.029 * V^2 + 5.59 * V + 0.083$
80	$\delta T = -0.034 * V^2 + 5.54 * V + 0.051$
85	$\delta T = -0.030 * V^2 + 6.47 * V + 0.092$
90	$\delta T = 6.40 * V - 0.80$

Once the previously stated 14 equations were determined, an uncertainty analysis was performed to determine the error on the temperature difference measured by the thermopiles. Because of their high accuracy, the voltage produced by the thermopiles was measured by the thermocouple input cards even though the cold junction temperature was no longer required. To determine the effect the voltage reading error of 8 nV has on the temperature difference measured, the derivative with respect to voltage of each of the 14 equations was taken and the maximum sensitivity factor was determined to be 6.4 °C/mV. Multiplying the 0.008mV with the sensitivity factor, the error on the voltage reading was determined to be 0.051°C.

Next the error caused by the two digital-multi meters had to be determined. The sensitivity of both RTDs was determined to be the same at 2.59 °C/ohm. The temperature error on the resistance reading of the hot bath is the same as that of the thermocouple calibration, at 0.0397 °C. The uncertainty on the resistance reading for the cold bath is 0.004% of the reading plus 0.002 ohms. The highest resistance measurement for the cold side was at 90°C and was 135.77 ohms. This caused an uncertainty of ±0.00743 ohms which when multiplied by the sensitivity factor, causes an error in temperature of ±0.019 °C. All of the errors that contributed to the uncertainty on the difference in temperature readings are tabulated in Table 6-3, with the total error again being calculated using the square root of the sum of the squares.

Table 6-3: Error on thermopile measurements

Source of Error	Error (°C)
Resistance temperature detector – hot	0.02
Resistance read error – DMM – hot	0.0397
Bath uniformity – hot	0.02
Resistance temperature detector – cold	0.02
Resistance read error – DMM – cold	0.019
Bath uniformity – cold	0.02
Voltage error – calibration	0.051
Voltage error – experimental	0.051
Regression prediction error	0.117
Total Uncertainty	0.15

Through this calibration experiment and data analysis, a set of equations was determined to convert the voltage reading produced by the thermopiles into a temperature difference and the uncertainty on the temperature difference was determined to be ±0.15 °C.

6.1.3 Flow Meters

Four flow meters were installed within the system, and unlike the thermocouples and thermopiles, where the error is independent of the magnitude of the reading, the error on the flow meter readings is directly related to the flow rate. The flow meters have all been factory calibrated to 1% of the flow measurement. As discussed in Section 3.3.3, the flow meter contains two oval gears, which are calibrated to allow a certain quantity of fluid through for each rotation of the gears. The relationship between the flow and

number of pulses is related by the k-factor, and calculated using Equation 6.4. The k-factor for each of the two models of flow meters used are listed in Table 6-4

$$\dot{V} = \frac{pulses}{k * t} \tag{6.9}$$

Table 6-4: k-factor for Brooks flow meters

Flow Meter Model	k-factor (pulse/Gal)	k-factor (pulse/L)
BM07	197	52
BM10	136.3	36

The number of cycles is counted with a pulse counting module installed within the National Instruments data acquisition system and this counting creates a second error on the flow meter readings.

Although there is no error on the actual counting of the pulses as it is a discrete value, the number of pulses counted over a given period always has a fraction of a pulse at the beginning of the time period that is counted as a full pulse, while a fraction of a pulse at the end that is not counted at all. Depending on the time period and the pulse rate, this error can be significant. Within each time period of pulse counting, an error equivalent to one pulse is assumed and added to the error of 1% of the flow. This error is most noticeable at lower flows or when a small period of time is taken to count the pulses. To reduce the error caused by this additional pulse, a longer time period should be used to calculate the flow rate and an appropriately sized flow meter for the expected flow rates should be used. These errors are considered independent of each other and the total error on the flow reading is equivalent of the square root of the sum of squares of the two values. At the design flow rate of each of the hydraulic loops, the error on the flow

rate was found at 1 s, 5 s, 10 s, 30 s, 60 s and 120 s time periods for pulse counting. The results in terms of flow rate are presented in Table 6-5

Table 6-5: Error on temperature measurement

Hydraulic Loop	Design Flow Rate (L/min)	Error on Flow Rate (L/min)						
		1 s	5 s	10 s	15 s	30 s	60 s	120 s
Hot Input	25	1.68	0.42	0.30	0.27	0.26	0.25	0.25
Air Conditioning	25	1.18	0.34	0.28	0.26	0.25	0.25	0.25
Heat Rejection	55	1.75	0.64	0.57	0.56	0.55	0.55	0.55
Building Load	15	1.15	0.28	0.19	0.18	0.16	0.15	0.15

From these results, it can be seen that there is little improvement in increasing the time above 15 seconds. These results were previously used and discussed in Section 5.2.2 to determine the optimal time step for the experimental procedure. Using these results and the results from the simulations of the systems, it was determined that measurements would be taken at 30 second intervals.

6.2 Overall System Uncertainty Analysis

Once the uncertainty of each of the instruments being used to measure the temperature and flow rates within the system have been determined, the overall uncertainty of the calculations of the heat transfer rates within the absorption chiller, as well as the overall COP_{th} and $COP_{el,chiller}$ can be determined.

6.2.1 Uncertainty Calculation Procedure

To determine the uncertainty of a derived quantity, a square root of the sum of squares is taken of the uncertainty scaled by a sensitivity factor for each. For a derived quantity, R, as defined by Equation 6.10,

$$R = f(x_1, x_2, x_3 \dots x_L) \tag{6.10}$$

The sensitivity factor, θ, for any independent variable is derived using a Taylor series expansion and is determined using Equation 6.11.

$$\theta_i = \frac{\partial R}{\partial x_i} \qquad i = 1,2,3 \dots L \tag{6.11}$$

Once the sensitivity factor is determined for each of the independent variables, the overall uncertainty on the derived quantity, u_R, is calculated using Equation 6.12.

$$u_R = \left[\sum_{i=1}^{L} (\theta_i \, u_i)^2\right]^{1/2} \tag{6.12}$$

The preceding procedure was used to calculate the uncertainty on the system performance and is explained in detail in the following section.

6.2.2 Uncertainty on Heat Transfer Calculations

To calculate the heat transfer within the absorption chiller, the change in energy from the entering fluid stream to the exiting fluid stream is found using Equation 6.13.

$$\dot{Q} = \dot{V} \rho c_p \delta T \tag{6.13}$$

The volumetric flow rate, $\dot{V}$, is measured by the flow meters in the hydraulic network, while the change in temperature, ΔT, is measured by the thermopiles at the entry and exit

of the chiller. Since density, ρ, is dependent on the temperature of the fluid, Equation 6.14 was determined and defines the density of water with respect to temperature over the a temperature range of 0°C to 100°C.

$$\rho = 1.68 * 10^{-5} * T^3 - 0.0061 * T^2 + 0.022 * T + 1000 \quad (6.14)$$

The thermocouple installed at each of the inlets and exits of the absorption chiller are used to obtain the temperatures for the equation. Due to the uncertainty in the temperature reading calculated in Section 6.1.1 as well as the regression prediction error, the error in the density is ±0.25 kg/m^3. The heat capacity of water is considered constant at 4.2 kJ/kg K, with an error of 0.02 kJ/kg K, which is the maximum fluctuation in c_p over the temperature range of 0°C to 100°C.

To determine the sensitivity factor for each of the independent variables Equations 6.15 to 6.18 were used.

$$\theta_{\dot{V}} = \frac{\partial \dot{Q}}{\partial \dot{V}} = \rho c_p \delta T \quad (6.15)$$

$$\theta_{\rho} = \frac{\partial \dot{Q}}{\partial \rho} = \dot{V} c_p \delta T \quad (6.16)$$

$$\theta_{C_p} = \frac{\partial \dot{Q}}{\partial C_p} = \dot{V} \rho \delta T \quad (6.17)$$

$$\theta_{\delta T} = \frac{\partial \dot{Q}}{\partial \delta T} = \dot{V} \rho c_p \quad (6.18)$$

Using these derived equations as well as the designed conditions listed in Table 3-1, the sensitivity factors using the design conditions were determined and are tabulated in

Table 6-6. The sensitivity factor for the flow rates was calculated using the error for both 1 s and 30 s measurement periods.

Table 6-6: Sensitivity factors

Hydraulic Loop	$\theta_{\dot{V}}$-1s ($kW \cdot s/m^3$)	$\theta_{\dot{V}}$-30s ($kW \cdot s/m^3$)	θ_{ρ} ($kW \cdot m^3/kg$)	θ_{C_p} ($kg \cdot K/s$)	$\theta_{\delta T}$ (kW/K)
Hot Input	1.024	0.028	1.49×10^{-5}	0.00524	0.0623
Air Conditioning	0.412	0.00925	4.6×10^{-6}	0.00173	0.0666
Heat Rejection	0.765	0.0145	3.48×10^{-6}	0.00173	0.0666

Taking these sensitivity factors and multiplying them by the independent variable they represent, the uncertainty caused by each individual variable can be determined. Using these values with Equation 6.8, the overall uncertainty on the heat transfer rates are calculated. The uncertainty for the three heat transfer rates in the chiller using a 1s time averaging is presented in Table 6-7 while the results using a 30s time averaging are presented in Table 6-8.

Table 6-7: Uncertainty on heat transfer rates – 1 s time averaging

Hydraulic Loop	Design Heat Transfer Rate (kW)	Uncertainty on Heat Transfer (kW)	Percent Error (%)
Hot Input	15.2	1.06	7.0
Air Conditioning	8.7	0.49	5.6
Heat Rejection	24.0	0.96	4.0

Table 6-8: Uncertainty on heat transfer rates – 30 s time averaging

Hydraulic Loop	Design Heat Transfer Rate (kW)	Uncertainty on Heat Transfer (kW)	Percent Error (%)
Hot Input	15.2	0.31	2.0
Air Conditioning	8.7	0.28	3.2
Heat Rejection	24.0	0.59	2.5

Based on these results, marked reductions in the uncertainty of the heat transfer rates can be seen going from a 1 s time averaging period for the flow rates to a 30 s time averaging.

6.2.3 Uncertainty on the COPs of the Absorption Chiller

Using the calculated heat transfer rates and uncertainties, the uncertainty of the COP_{th} can be calculated. The first step was to find the sensitivity factors for each of the variables which have been derived in Equations 6.19 and 6.20.

$$\theta_{\dot{Q}_{cold}} = \frac{\partial COP_{th}}{\partial(\dot{Q}_{cold})} = \frac{1}{\dot{Q}_{hot}} \tag{6.19}$$

$$\theta_{\dot{Q}_{hot}} = \frac{\partial COP_{th}}{\partial(\dot{Q}_{hot})} = \frac{\dot{Q}_{cold}}{(\dot{Q}_{hot})^2} \tag{6.20}$$

For the design conditions, the COP_{th} of the absorption chiller was determined to be 0.575 which is consistent with the results obtained through simulation for the same conditions. Using the sensitivity factors and the uncertainties found for the heat transfer rates in Section 6.2.2, the overall uncertainty of the COP_{th} was determined to be ±0.022, or ±3.8% of the overall value.

In addition to the $COP_{th,}$ the $COP_{el,chiller}$ must also be calculated. As per the specifications for the absorption chiller, the maximum power consumption of the unit is 70 W, and the $COP_{el,chiller}$ will be calculated using this value. The power monitoring

system is accurate to ±1% of the reading, or ±0.7 W at 70 W. Sensitivity factors where determined for the electrical power and the air conditioning heat transfer rate, and using the uncertainty previously calculated for the air conditioning heat transfer rate, at the design conditions, the $COP_{el,chiller}$ was determined to be 124.8 with an uncertainty of ±4.2, or 3.3%. This value is higher than what is generally reported in literature, as it is an instantaneous measurement at the design conditions when cooling is at its peak, however, when the electricity consumed by the unit when no cooling is being produced is taken into consideration, the $COP_{el,chiller}$ will actually be lower.

7 Chapter: Conclusions and Future Work

7.1 Conclusions

Before the widespread implementation of solar cooling devices in Canada can be realized, significant research must be conducted to determine the feasibility of the systems and the optimal configuration for the Canadian climate. To determine the potential of these systems in Canada, an extensive research project was undertaken which focused on the experimental evaluation and computer simulation of an intermittent absorption chiller. This thesis focused on the design, construction and instrumentation of an experimental test apparatus to evaluate the performance of a ClimateWell solar absorption chiller. The ClimateWell chiller has been designed for use within the residential market and has a cooling capacity of approximately 9 kW.

The experimental test apparatus was designed to determine the performance of the chiller by simulating a wide range of constant, controlled heating and heat rejection temperatures and flow rates. In addition to constant steady state conditions, the system is designed to ascertain the performance of the chiller under transient conditions. A steam-to-water heat exchanger was installed along the building's existing steam line to provide a controllable heat source. This was selected instead of actual collectors as collectors cannot be controlled, and the heat collected must be dissipated if the chiller is not running. To dissipate the heat, a combination of a dry cooler installed on the roof of the building and a heat exchanger with the building's chilled water line (for summer operation) was used.

The complete experimental test set-up was then constructed including the new infrastructure in the mechanical room of the building which ties the experimental apparatus to the building systems. In addition to the heat input and heat rejection systems, a building load simulator was designed and built within the SESL. The purpose of this loop is to provide realistic cooling loads that would be experienced in an actual house, as well as to offset the cooling provided to the chiller during steady state conditions. While constructing the experimental loops, extensive instrumentation was embedded within the hydraulic network to determine the heat transfer rates to and from the chiller. To do this, the flow rates through the chiller, the temperatures at the inlet and outlets of the chiller and the temperature differences were measured.

To determine the uncertainty on the temperature and temperature difference measurements, calibration experiments were designed and undertaken to ascertain a relationship between the voltage produced by the thermocouple and the temperature at the tip of the thermocouple. A second experiment was undertaken to create relationships for the voltage produced by the thermopile compared to the temperature difference between the hot and cold side at different cold side temperatures. The uncertainty on the temperature and flow rate readings were then used to determine the uncertainty on the heat transfer rates for the heat input, air conditioning and heat rejection loop. Using these values, the COP_{th} of the chiller was calculated and the overall experimental uncertainty was determined to be ±3.8%, while the $COP_{el,chiller}$ was determined to be ±3.3%.

A model of the experimental apparatus was created in TRNSYS to determine the optimal experimental procedure and to ensure the experimental set-up will work both at the design conditions and over the entire desired test range. Through this modelling

study, the experimental procedure was determined to last seven cycles for each test with measurements taken at every 30 s interval. It was determined that when the heat rejection temperature is very low (10°C and 15°C), the cooling produced by the chiller is greater than the heat input possible from the building load simulator. As a result, when the chiller is being tested at these conditions, a higher flow rate (25 L/min) is required within the building load loop. This model also provides a first estimation of the performance of the chiller and the length of the experimental run under different operating conditions. These values will be compared to the experimental results and used to refine the TRNSYS model.

The design and commissioning of the experimental apparatus is the first step in the determining the feasibility of solar absorption chillers within the Ontario and Canadian market. The widespread implementation within the residential market could greatly reduce the amount energy consumed for mechanical cooling and consequently the amount of greenhouse gases produced. Of equal importance, the use of solar cooling has the potential to reduce the peak loading placed on the power grid during the summer months.

7.2 Future Work

This work is the first phase in a multi-phased research project to determine the feasibility of solar cooling in Canada. In conjunction with this thesis, a second project is ongoing to design and implement the control system, and create the required programs to provide both constant input and controlled transient conditions. A building automation system will be connected to the National Instruments cRIO installed within the lab to

pass signals to the individual components and to constantly monitor the state of the experimental system. This system will be used to prevent any freezing within any of the loops and will also ensure the pressure and temperature never exceed a certain level.

Experimental testing will commence once the heat input and heat rejection systems are connected in the experimental set-up. The experimental process will start by determining the performance of the chiller under steady state conditions with various heat input and heat rejection temperatures. This will allow the completion of a performance map of the chiller. The results of the steady state test will be compared to the previously conducted TRNSYS simulations to validate the chiller model. The model of the complete experimental set-up will be refined using experimental data to determine the heat loss rates and confirm the heat transfer rates in the piping network and through the heat exchangers.

Upon completion of mapping the performance of the chiller using steady state conditions, the chiller will then be evaluated under transient conditions. Using the data collected from the weather station, realistic power curves for different solar collector configurations will be determined. The derived power curves will be programmed into the building controller, controlling the flow of steam into the heat exchanger creating realistic heating input profiles. TRNSYS simulations will be conducted with an identical heat input profile and simulation results will be compared to the measured chiller performance to validate the TRNSYS model under transient conditions. Once complete, the validated model will be implemented into a complete building model where, through simulation, the optimal system configuration and seasonal performance of the chiller can be determined. Additionally, comparisons between solar thermal systems paired with an

absorption chiller should be compared to the annual performance of a typical cooling system powered by photovoltaic panels within different climate zones of Canada.

Although the experimental set-up has been created to evaluate the performance of the chiller, future modifications could be made to the experimental apparatus to more accurately represent the chiller's operation within an actual residential setting. An air handler could be used to distribute the air conditioning provided by the chiller as opposed to the series of water-to-water heat exchangers. This will provide an accurate representation of any losses that would be experienced within the cooling distribution network. The second improvement that could be made to the experimental set-up is the integration of solar thermal storage into the apparatus on both the hot and cold side of the system. Although the chiller is able to internally store cooling potential, the integration of thermal storage will allow for prolonged periods of little or no solar input and this change will allow for system testing with the new configuration.

References

[1] Natural Resources Canada, "Energy Use Handbook - 1990 to 2010," Office of Energy Efficiency, Natural Resources Canada, Ottawa, 2012. [Online]. Available: http://oee.nrcan.gc.ca/publications/statistics/handbook2010/handbook2013.pdf

[2] Independent Electrical Service Operator, "18-Month Outlook - From June 2013 to November 2014," Toronto, 2013. [Online]. Available: http://www.ieso.ca/imoweb/pubs/marketReports/18MonthOutlook_2013may.pdf

[3] I. Urgursal and A. Farhat, "Greenhouse Gas Emmision Intensity Factors for Marginal Electricity Generation in Canada," *Dalhousie University,* 2009.

[4] H. Henning, "Solar assisted air conditioning of buildings - an overview," *Applied Thermal Engineering,* 2006.

[5] J. Deng, R. Wang and G. Han, "A review of thermally activated cooling technologies for combined cooling, heating and power systems," *Progress in Energy and Combustion Science,* Vol. 37, pp 172-203. 2011.

[6] K. Herold, R. Radermacher and S. Klein, Absorption Chillers and Heat Pumps, Boca Raton: CRC Press, 1996.

[7] D. Jaehnig, "Market Available Components for Systems for Solar Heating and Cooling with a Cooling Capacity <20kW," *A technical report of subtask A of the IEA-SHC Task 38,* 2009.

[8] M. Moran and H. Shapiro, Fundamentals of Engineering Thermodynamics, 6th edition, John Wiley & Sons, Inc, 2008.

[9] C. Bales and S. Nordlander, "TCA Evaluation; Lab Measurements, Modelling and System Simulations," Thesis, Solar Energy Research Center, 2005.

[10] ClimateWell AB, "Design Guidelines for Solar Cooling," 2010. [Online]. Available: http://www.dew-kylsystem.com/Design-Guidelines-ClimateWell-Solar-Chiller.pdf

[11] J. Duffie and W. Beckman, Solar Engineering of Thermal Processes, Third Edition, Hoboken, New Jersey: John Wiley & Sons, Inc., 2006.

[12] International Energy Agency "About the IEA Solar Heating & Cooling Programme," [Online]. Available: http://www.iea-shc.org/about/. [Accessed 2012].

[13] H.-M. Henning and J. Albers, "Decision Scheme for the Selection of the Appropriate Technology using Solar Thermal Air-Conditioning," *IEA Solar Heating and Cooling; Task 25: Solar-Assisted Air-Conditiong of Buildings,* 2004.

[14] "Ongoing Research Relevant for Solar Assisted Air Conditioning Systems," *IEA Solar Heating and Cooling; Task 25: Solar-Assisted Air-Conditioning of Buildings,* 2002.

[15] H.-M. Henning, Solar-Assisted Air Conditioning in Buildings - A Handbook for Planners, New York: Springer Wien, 2004.

[16] H.-M. Henning, "Solar Cooling Position Paper," *IEA SHC Task 38 Solar Air-Conditioning and Refrigeration,* 2011.

[17] W. Sparber, A. Napolitano and P. Melograno, "Overview on world wide installed solar cooling systems," in *Proceeding of the 2nd International Conference Solar Air Conditioning*, Tarragona, Spain, 2007.

[18] "Check-List Method for the Selection and the Seccess in the Integration of a Solar Cooling System in Buildings," [Online]. Available: http://www.tecsol.fr/checklist/.

[19] D. Jaehnig and A. Thuer, "Monitoring Results," *A technical report of subtask A of the IEA-SHC Task 38,* 2011.

[20] A. Napolitano, W. Sparber, A. Thur, P. Finocciaro and B. Nocke, "Monitoring Procedure for Solar Cooling Systems," *A joint technical report of subtask A and B of the IEA-SHC Task 38,* 2011.

[21] D. Mugnier and U. Jakob, "Keeping Cool with the Sun," *International Sustainable Energy Review,* vol. 6, no. 1, pp. 28-30, 2012.

[23] N. Kalkan, E. Young and A. Caliktas, "Solar thermal air conditioning technology reducing the footprint of solar thermal air conditioning," *Renewable and Sustainable Energy Reviews,* vol. 16, pp. 6353-6382, 2012.

[24] G. Johnson, "Design and Commissioning of an Experiment to Characterize the Performance of a Lithium-Bromide Absorption Chiller," Master's Thesis, Carleton University, Ottawa, 2008.

[25] C. Edwards, "Performance Assessment of Solar Absorption Cooling for Ontario Housing," Master's Thesis, Carleton University, Ottawa, 2009.

[26] A. Rosato and S. Sibilio, "Preliminary experimental characterization of a three-phase absorption heat pump," *International Journal of Refrigeration,* vol. 36, pp. 717-729, 2012.

[27] G. Angrisani, A. Rosato, C. Roselli, M. Sasso and S. Sibilio, "Experimental results of micro-trigeneration installation," *Applied Thermal Engineering,* vol. 38, pp. 78-90, 2012.

[28] Z. M. Hasib, "A residential micro tri-generation system basen on a gas fired stirling engine CHP and therm-chemical accumulator (TCA)," Toronto, 2013.

[29] N. Ekrami, "Feasibility of residential combined cooling, heating and power generation systems in Canada," Toronto, 2013.

[30] T. Mateus and A. C. Oliveira, "Energy and economic analysis of an integrated solar absorption cooling and heating system in different building types and climates," *Applied Energy,* pp. 949-957, 2008.

[31] S. Udomsri, C. Bales, A. Martin and V. Martin, "Decentralized cooling in district heating network: System simulation and parametric study," *Applied Energy,* vol. 92, pp. 175-184, 2012.

[32] S. Thomas, S. Hennaut, S. Mass and P. Andre, "Experimentation and simulation of a small-scale adsorption cooling system in temperate climate," *Energy Procedia,* vol. 30, pp. 704-714, 2012.

[33] ClimateWell AB, "Solar Cooling of a Detached House in Madrid," [Online]. Available: http://www.climatewell.com/Documents/Case-Studies/WISIONS_ClimateWell.pdf. [Accessed November 2013].

[34] D. Borge-Diez, A. Colmenar-Santos, C. Perez-Molina and M. Castro-Gil, "Experimental validation of a fully solar-driven triple-state absorption system in small residential buildings," *Energy and Buildings,* vol. 55, pp. 227-237, 2012.

[35] J. Nowag, F. Boudehenn, A. Le Denn, F. Lucas, O. Marc, M. Raduslescu and P. Papillon, "Calculation of performance indicators for solar cooling, heating and domestic hot water systems," *Energy Procedia,* vol. 30, pp. 937-946, 2012.

[36] Grudfos Pumps Corporation, "Grundfos Data Booklet - UP Series Circulators," [Online]. Available: http://ca.grundfos.com/content/dam/GCA/Literature/Product%20Guide/LUPPG001_0113_UP.pdf. [Accessed January, 2013].

[37] Grundfos Pumps Corporation, "Grudfos Product Guide - MAGNA UPE Series 2000 Circulator Pumps," [Online]. Available: http://ca.grundfos.com/content/gca/en_CA/products/find-product/large-variable-speed-circulator-pump-magna-series/_jcr_content/tabbedpanel/brochures/par2/downloads/download_1/file/file.res/LMAGPG01_0312_Magna.pdf. [Accessed January, 2013].

[38] Grundfos Pumps Corporation, "Grundfos Product Guide - CR, CRI, CRN, CRE, CRIE, CRNE Vertical multistage centrifugal pumps," [Online]. Available: http://ca.grundfos.com/content/dam/GCA/Literature/Product%20Guide/LCRPG001_0212_CR.pdf. [Accessed January, 2013].

[39] Omega "Revised Thermocouple Reference Tables - Type T Refence Tables," [Online]. Available: http://www.omega.ca/temperature/Z/pdf/z207.pdf.

[40] S. Klein and et.al., TRNSYS 17 - A TRaNsient SYstem Simulation Program - User Manual, Madison, WI.: Solar Energy Laboratory, University of Wisconsin - Madison, 2010.

[41] DOW Chemical Corporation, "Engineering and Operating Guide for DOWFROST and DOWFROSTHD inhibited Ethylene Glycol-based Heat Transfer Fluids," 2008. [Online]. Available: http://msdssearch.dow.com/PublishedLiterature DOWCOM/dh_010e/0901b8038010e417.pdf?filepath=/heattrans/pdfs/noreg/180-01286.pdf&fromPage=GetDoc. [Accessed July 2013].

[42] Energy Research Centre of the Netherlands, Engineering Tools, PolySMART, 2010.

[43] R. Figliola and D. Beasley, Theory and Design for Mechanical Measurements - Fifth Edition, John Wiley & Sons, Inc., 2011.

[44] National Instruments, "Operating Instructions and Specifications - NI 9214," [Online]. Available: http://www.ni.com/pdf/manuals/375138b.pdf.

Appendices

Appendix A Weather Station

In addition to the infrastructure designed and installed within the SESL, a weather station was installed on a neighboring building's roof to record actual temperatures and solar radiation experienced at Carleton University. Solar radiation measurements are taken facing due south with an angle from the horizontal of 0°, 18°, 30°, 45°, and 90° at 15 minute time steps. This data will be used in a future project to create a program within the control system and building automation system that will automatically regulate the flow of steam into the steam-to-water heat exchanger to create power profiles. These profiles will mimic the power created by different sized and configured solar arrays for any day of the year, up to the maximum capacity of the heat input system.

In addition to measuring the solar radiation and temperature, the relative humidity, rain fall, wind speed and the snow accumulation are also monitored and recorded. These values could be used to validate weather files and building simulations. The weather station was built as a stand-alone system that uses a battery and a solar panel to power the data acquisition system and the sensors. To retrieve data, a two way radio system has been installed to send data between computers in the lab and the weather station. Figure A-1 shows an image of the installed weather station, while Figure A-2 shows the installed pyranometers at the different angles. The instruments, as well as their purpose and accuracy are listed in Table A-1.

Table A-1: Weather Station

Instrument Type	Model	Purpose	Number installed	Accuracy of sensor
Pyranometer	Kipp & Zonen CMP6	Record solar radiation	5	±5%
Temperature and humidity probe	HC2-S3	Measure temperature and relative humidity	1	±0.1°C ±0.8% RH
Tipping rain bucket	TE525M	Record quantity of rainfall	1	±1%
Sonic ranger	SR50A	Monitor snow accumulation	1	±1cm
Anemometer	RM Young 05103	Measure wind speed and direction	1	±0.3m/s ±3°
Data acquisition	CR3000	Record and transmit data back to lab	1	NA

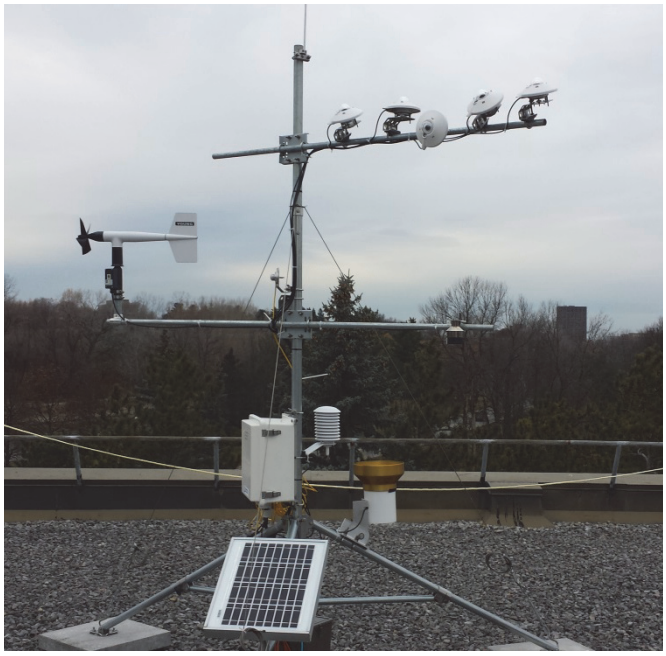

Figure A-1: Installed weather station

Figure A-2: Pyranometers installed (from left to right) at 30°, 0°, 90°, 45°, and 18°

Appendix B TRNSYS Deck File

To conduct a simulation in TRNSYS, a file is created by the simulation studio which lists all of the simulation conditions, the Types used within the model, all of the connections made between Types and the initial conditions for each variable in each Type. This file, called the Deck file is then read in by the TRNSYS simulation engine, which takes processes the data within the Deck file and runs the simulation, and upon completion, an output file is created with the results of the simulation. A new Deck file is created for each simulation, outlining all of the simulation conditions. The following is an example of the deck file created by the TRNSYS model of the experimental set-up. In this case the heat input was set to run for 20.7 hours at a temperature of 80°C and the auxiliary cooler was set to 15°C. The total simulation was set to last 25 hours, at 30 s time steps.

```
VERSION 17
**********************************************************************
*** TRNSYS input file (deck) generated by TrnsysStudio
*** on Sunday, December 08, 2013 at 12:58
*** from TrnsysStudio project: C:\Trnsys17\MyProjects\Project12\Lab Setup 30-07-13 - Tests.tpf
***
*** If you edit this file, use the File/Import TRNSYS Input File function in
*** TrnsysStudio to update the project.
***
*** If you have problems, questions or suggestions please contact your local
*** TRNSYS distributor or mailto:software@cstb.fr
***
**********************************************************************


**********************************************************************
*** Units
**********************************************************************

**********************************************************************
*** Control cards
**********************************************************************
* START, STOP and STEP
CONSTANTS 3
```

```
START=0
STOP=25
STEP=0.008333334
* User defined CONSTANTS

SIMULATION     START  STOP    STEP    ! Start time          End time             Time step
TOLERANCES 0.01 0.01                   ! Integration         Convergence
LIMITS 30 500 50                                ! Max iterations   Max warnings      Trace limit
DFQ 1                                  ! TRNSYS numerical integration solver method
WIDTH 80                               ! TRNSYS output file width, number of characters
LIST                                   ! NOLIST statement
                                       ! MAP statement
SOLVER 0 1 1                           ! Solver statement            Minimum        relaxation        factor
          Maximum relaxation factor
NAN_CHECK 0                            ! Nan DEBUG statement
OVERWRITE_CHECK 0                      ! Overwrite DEBUG statement
TIME_REPORT 0                          ! disable time report
EQSOLVER 0                             ! EQUATION SOLVER statement

* Model "Heater Control" (Type 14)
*

UNIT 33 TYPE 14            Heater Control
*$UNIT_NAME Heater Control
*$MODEL .\Utility\Forcing Functions\General\Type14h.tmf
*$POSITION 111 220
*$LAYER Main #
PARAMETERS 8
0                  ! 1 Initial value of time
1                  ! 2 Initial value of function
20.7               ! 3 Time at point-1
1                  ! 4 Value at point -1
20.7               ! 5 Time at point-2
0                  ! 6 Value at point -2
100                ! 7 Time at point-3
0                  ! 8 Value at point -3
*-------------------------------------------------------------------------------

* Model "Chiller Control Unit" (Type 826)
*

UNIT 38 TYPE 826          Chiller Control Unit
*$UNIT_NAME Chiller Control Unit
*$MODEL .\ClimateWell\Type826_SolarChiller_control.tmf
*$POSITION 575 353
*$LAYER Main #
PARAMETERS 8
1                  ! 1 OM
0.1                ! 2 swapdur
2                  ! 3 Min_swap_int
0.9                ! 4 LC_Full
.1                 ! 5 LC_Empty
.7                 ! 6 SOC_minswap
.05                ! 7 wait_time
110                ! 8 T_SP_Max
INPUTS 31
```

```
0,0             ! [unconnected] mcc
0,0             ! [unconnected] Tcc
6,2             ! P3:Outlet flow rate ->mrc
6,1             ! P3:Outlet fluid temperature ->Trc
0,0             ! [unconnected] mcd
0,0             ! [unconnected] Tcd
0,0             ! [unconnected] mrd
0,0             ! [unconnected] Trd
0,0             ! [unconnected] Cmd
0,0             ! [unconnected] Heat_rec_per
0,0             ! [unconnected] Tset_cooling
0,0             ! [unconnected] Tset_heating
0,0             ! [unconnected] Tamb
17,2            ! HE-4:Source side flow rate ->mhs
17,1            ! HE-4:Source side outlet temperature ->Thso
8,2             ! P2:Outlet flow rate ->mac
8,1             ! P2:Outlet fluid temperature ->Taco
37,4            ! Barrel A:Tsucxo ->TcxoA
37,2            ! Barrel A:Tsurxo ->TrxoA
36,4            ! Barrel B:Tsucxo ->TcxoB
36,2            ! Barrel B:Tsurxo ->TrxoB
37,17           ! Barrel A:SOC ->SOCA
36,17           ! Barrel B:SOC ->SOCB
0,0             ! [unconnected] free
37,13           ! Barrel A:Tre ->TreA
37,14           ! Barrel A:Tce ->TceA
36,13           ! Barrel B:Tre ->TreB
36,14           ! Barrel B:Tce ->TceB
0,0             ! [unconnected] MwatA
0,0             ! [unconnected] MwatB
0,0             ! [unconnected] PACin
*** INITIAL INPUT VALUES
900 30 900 30 900 30 900 30 -1 0 5 30 22 1800 30 1200 15 12 35 45 75 0.421 0.1 0 40 40
30 30 20 25 1
*-------------------------------------------------------------------------------

* Model "HE-3" (Type 5)
*

UNIT 27 TYPE 5 HE-3
*$UNIT_NAME HE-3
*$MODEL .\Heat Exchangers\Counter Flow\Type5b.tmf
*$POSITION 894 314
*$LAYER Main #
PARAMETERS 4
2               ! 1 Counter flow mode
4.19            ! 2 Specific heat of source side fluid
4.19            ! 3 Specific heat of load side fluid
0               ! 4 Not used
INPUTS 5
38,28           ! Chiller Control Unit:Taci ->Source side inlet temperature
38,26           ! Chiller Control Unit:mac ->Source side flow rate
38,27           ! Chiller Control Unit:Thsi ->Load side inlet temperature
38,25           ! Chiller Control Unit:mhs ->Load side flow rate
0,0             ! [unconnected] Overall heat transfer coefficient of exchanger
*** INITIAL INPUT VALUES
```

```
20.0 100.0 20.0 100.0 1011.599973
*-------------------------------------------------------------------------------

* Model "P3" (Type 3)
*

UNIT 6 TYPE 3    P3
*$UNIT_NAME P3
*$MODEL .\Hydronics\Pumps\Single Speed\Type3d.tmf
*$POSITION 308 340
*$LAYER Main #
PARAMETERS 4
1500            ! 1 Maximum flow rate
4.190           ! 2 Fluid specific heat
900             ! 3 Maximum power
0.05            ! 4 Conversion coefficient
INPUTS 3
34,1            ! Heat Input:Outlet fluid temperature ->Inlet fluid temperature
34,2            ! Heat Input:Outlet flow rate ->Inlet mass flow rate
33,2            ! Heater Control:Instantaneous value of function over the timestep ->Control signal
*** INITIAL INPUT VALUES
90 1500 1.0
*-------------------------------------------------------------------------------

* Model "Heat Input" (Type 659)
*

UNIT 34 TYPE 659          Heat Input
*$UNIT_NAME Heat Input
*$MODEL .\HVAC Library (TESS)\Auxiliary Heater (Fluid)\Type659.tmf
*$POSITION 273 206
*$LAYER Main #
*$# AUXILIARY HEATER (FLUID)
PARAMETERS 2
71999.994673            ! 1 Rated capacity
4.19            ! 2 Specific heat of fluid
INPUTS 7
38,4            ! Chiller Control Unit:Trco ->Inlet fluid temperature
38,3            ! Chiller Control Unit:mrco ->Inlet flow rate
33,2            ! Heater Control:Instantaneous value of function over the timestep ->Control function
0,0             ! [unconnected] Set point temperature
0,0             ! [unconnected] Overall loss coefficient
0,0             ! [unconnected] Boiler efficiency
0,0             ! [unconnected] Temperature of surroundings
*** INITIAL INPUT VALUES
80 1500 1 80 0.0 1.0 20.0
*-------------------------------------------------------------------------------

* Model "Chiller Performance" (Type 65)
*

UNIT 23 TYPE 65           Chiller Performance
*$UNIT_NAME Chiller Performance
*$MODEL .\Output\Online Plotter\Online Plotter With File\TRNSYS-Supplied Units\Type65a.tmf
*$POSITION 128 460
*$LAYER Main #
```

```
PARAMETERS 12
3               ! 1 Nb. of left-axis variables
6               ! 2 Nb. of right-axis variables
0.0             ! 3 Left axis minimum
3500            ! 4 Left axis maximum
0.0             ! 5 Right axis minimum
100             ! 6 Right axis maximum
1               ! 7 Number of plots per simulation
12              ! 8 X-axis gridpoints
0               ! 9 Shut off Online w/o removing
31              ! 10 Logical Unit for output file
2               ! 11 Output file units
0               ! 12 Output file delimiter
INPUTS 9
38,3            ! Chiller Control Unit:mrco ->Left axis variable-1
38,25           ! Chiller Control Unit:mhs ->Left axis variable-2
38,26           ! Chiller Control Unit:mac ->Left axis variable-3
38,4            ! Chiller Control Unit:Trco ->Right axis variable-1
38,27           ! Chiller Control Unit:Thsi ->Right axis variable-2
38,28           ! Chiller Control Unit:Taci ->Right axis variable-3
6,1             ! P3:Outlet fluid temperature ->Right axis variable-4
17,1            ! HE-4:Source side outlet temperature ->Right axis variable-5
8,1             ! P2:Outlet fluid temperature ->Right axis variable-6
*** INITIAL INPUT VALUES
mrco mhs mac Trco Thsi Taci Outlet Source Outlet
LABELS  3
"Flow Rates"
"Temperatures"
"Chiller"
*** External files
ASSIGN "C:\Users\CHRIS\Documents\Modelling Results Files\Chiller Performance" 31
*|? What file should the online print to? |1000
*-------------------------------------------------------------------------------

* Model "HE-2" (Type 5)
*

UNIT 24 TYPE 5 HE-2
*$UNIT_NAME HE-2
*$MODEL .\Heat Exchangers\Counter Flow\Type5b.tmf
*$POSITION 948 433
*$LAYER Main #
PARAMETERS 4
2               ! 1 Counter flow mode
4.19            ! 2 Specific heat of source side fluid
4.19            ! 3 Specific heat of load side fluid
0               ! 4 Not used
INPUTS 5
27,1            ! HE-3:Source side outlet temperature ->Source side inlet temperature
27,2            ! HE-3:Source side flow rate ->Source side flow rate
28,3            ! Hot Water Tank:Temperature to load ->Load side inlet temperature
28,4            ! Hot Water Tank:Flowrate to load ->Load side flow rate
0,0             ! [unconnected] Overall heat transfer coefficient of exchanger
*** INITIAL INPUT VALUES
20.0 100.0 20.0 100.0 1007.999973
*-------------------------------------------------------------------------------
```

```
* Model "P2" (Type 3)
*

UNIT 8 TYPE 3    P2
*$UNIT_NAME P2
*$MODEL .\Hydronics\Pumps\Single Speed\Type3d.tmf
*$POSITION 974 540
*$LAYER Main #
PARAMETERS 4
1500            ! 1 Maximum flow rate
4.190           ! 2 Fluid specific heat
900             ! 3 Maximum power
0.05            ! 4 Conversion coefficient
INPUTS 3
24,1            ! HE-2:Source side outlet temperature ->Inlet fluid temperature
24,2            ! HE-2:Source side flow rate ->Inlet mass flow rate
38,40           ! Chiller Control Unit:PAC ->Control signal
*** INITIAL INPUT VALUES
20.0 1500 1
*-------------------------------------------------------------------------------

* Model "Barrel B" (Type 825)
*

UNIT 36 TYPE 825        Barrel B
*$UNIT_NAME Barrel B
*$MODEL .\ClimateWell\Type825_SolarChiller_barrel.tmf
*$POSITION 640 620
*$LAYER Main #
PARAMETERS 6
4               ! 1 Mwat0
20              ! 2 Tre0
20              ! 3 Tce0
3.76            ! 4 Cprxf
3.76            ! 5 Cpcxf
0               ! 6 Mice0
INPUTS 5
38,18           ! Chiller Control Unit:mrxB ->mrx
38,19           ! Chiller Control Unit:TrxiB ->Tsurxi
38,16           ! Chiller Control Unit:mcxB ->mcx
38,17           ! Chiller Control Unit:TcxiB ->Tsucxi
38,20           ! Chiller Control Unit:Tamb B ->Tamb
*** INITIAL INPUT VALUES
900 30 900 30 22
*-------------------------------------------------------------------------------

* Model "Barrel A" (Type 825)
*

UNIT 37 TYPE 825        Barrel A
*$UNIT_NAME Barrel A
*$MODEL .\ClimateWell\Type825_SolarChiller_barrel.tmf
*$POSITION 449 620
*$LAYER Main #
PARAMETERS 6
```

```
4                   ! 1 Mwat0
20                  ! 2 Tre0
20                  ! 3 Tce0
3.76                ! 4 Cprxf
3.76                ! 5 Cpcxf
0                   ! 6 Mice0
INPUTS 5
38,11               ! Chiller Control Unit:mrxA  ->mrx
38,12               ! Chiller Control Unit:TrxiA ->Tsurxi
38,9                ! Chiller Control Unit:mcxA ->mcx
38,10               ! Chiller Control Unit:TcxiA ->Tsucxi
38,13               ! Chiller Control Unit:Tamb A ->Tamb
*** INITIAL INPUT VALUES
900 30 900 30 22
*-------------------------------------------------------------------------------

* Model "P4" (Type 3)
*

UNIT 7 TYPE 3   P4
*$UNIT_NAME P4
*$MODEL .\Hydronics\Pumps\Single Speed\Type3d.tmf
*$POSITION 788 166
*$LAYER Main #
PARAMETERS 4
3300                ! 1 Maximum flow rate
4.190               ! 2 Fluid specific heat
2682                ! 3 Maximum power
0.05                ! 4 Conversion coefficient
INPUTS 3
27,3                ! HE-3:Load side outlet temperature ->Inlet fluid temperature
27,4                ! HE-3:Load side flow rate ->Inlet mass flow rate
38,41               ! Chiller Control Unit:PHS ->Control signal
*** INITIAL INPUT VALUES
30 3300 1.0
*-------------------------------------------------------------------------------

* Model "Heat Transfer HXN" (Type 65)
*

UNIT 31 TYPE 65           Heat Transfer HXN
*$UNIT_NAME Heat Transfer HXN
*$MODEL .\Output\Online Plotter\Online Plotter With File\TRNSYS-Supplied Units\Type65a.tmf
*$POSITION 1061 633
*$LAYER Main #
PARAMETERS 12
1                   ! 1 Nb. of left-axis variables
2                   ! 2 Nb. of right-axis variables
0.0                 ! 3 Left axis minimum
120000.0                    ! 4 Left axis maximum
-20000              ! 5 Right axis minimum
0                   ! 6 Right axis maximum
1                   ! 7 Number of plots per simulation
12                  ! 8 X-axis gridpoints
0                   ! 9 Shut off Online w/o removing
33                  ! 10 Logical Unit for output file
```

```
2                   ! 11 Output file units
0                   ! 12 Output file delimiter
INPUTS 3
17,5                ! HE-4:Heat transfer rate ->Left axis variable
27,5                ! HE-3:Heat transfer rate ->Right axis variable-1
24,5                ! HE-2:Heat transfer rate ->Right axis variable-2
*** INITIAL INPUT VALUES
Water/Glycol 5kW 3.5kW
LABELS  3
"Heat transfer rates"
"Heat transfer rates"
"HXN"
*** External files
ASSIGN "C:\Users\CHRIS\Documents\Modelling Results Files\Heat Transfer Rates" 33
*|? What file should the online print to? |1000
*-------------------------------------------------------------------------------

* Model "State of Charge" (Type 65)
*

UNIT 25 TYPE 65             State of Charge
*$UNIT_NAME State of Charge
*$MODEL .\Output\Online Plotter\Online Plotter With File\TRNSYS-Supplied Units\Type65a.tmf
*$POSITION 367 553
*$LAYER Main #
PARAMETERS 12
2                   ! 1 Nb. of left-axis variables
0                   ! 2 Nb. of right-axis variables
0.0                 ! 3 Left axis minimum
1                   ! 4 Left axis maximum
0.0                 ! 5 Right axis minimum
1000.0              ! 6 Right axis maximum
1                   ! 7 Number of plots per simulation
12                  ! 8 X-axis gridpoints
0                   ! 9 Shut off Online w/o removing
35                  ! 10 Logical Unit for output file
2                   ! 11 Output file units
0                   ! 12 Output file delimiter
INPUTS 2
37,17               ! Barrel A:SOC ->Left axis variable-1
36,17               ! Barrel B:SOC ->Left axis variable-2
*** INITIAL INPUT VALUES
SOCA SOCB
LABELS  3
"SOC"
" "
"SOC"
*** External files
ASSIGN "C:\Users\CHRIS\Documents\Modelling Results Files\SOC Values" 35
*|? What file should the online print to? |1000
*-------------------------------------------------------------------------------

* Model "HE-4" (Type 5)
*

UNIT 17 TYPE 5 HE-4
```

```
*$UNIT_NAME HE-4
*$MODEL .\Heat Exchangers\Counter Flow\Type5b.tmf
*$POSITION 881 220
*$LAYER Main #
PARAMETERS 4
2               ! 1 Counter flow mode
4.19            ! 2 Specific heat of source side fluid
3.56            ! 3 Specific heat of load side fluid
0               ! 4 Not used
INPUTS 5
7,1             ! P4:Outlet fluid temperature ->Source side inlet temperature
7,2             ! P4:Outlet flow rate ->Source side flow rate
22,1            ! Cooling Unit:Outlet fluid temperature ->Load side inlet temperature
22,2            ! Cooling Unit:Outlet flow rate ->Load side flow rate
0,0             ! [unconnected] Overall heat transfer coefficient of exchanger
*** INITIAL INPUT VALUES
20.0 100.0 20.0 100.0 11149.199705
*------------------------------------------------------------------------------

* Model "P1" (Type 3)
*

UNIT 20 TYPE 3 P1
*$UNIT_NAME P1
*$MODEL .\Hydronics\Pumps\Single Speed\Type3d.tmf
*$POSITION 1108 473
*$LAYER Main #
PARAMETERS 4
1500            ! 1 Maximum flow rate
4.190           ! 2 Fluid specific heat
900             ! 3 Maximum power
0.05            ! 4 Conversion coefficient
INPUTS 3
24,3            ! HE-2:Load side outlet temperature ->Inlet fluid temperature
24,4            ! HE-2:Load side flow rate ->Inlet mass flow rate
38,40           ! Chiller Control Unit:PAC ->Control signal
*** INITIAL INPUT VALUES
20.0 100.0 1.0
*------------------------------------------------------------------------------

* Model "P5" (Type 3)
*

UNIT 18 TYPE 3 P5
*$UNIT_NAME P5
*$MODEL .\Hydronics\Pumps\Single Speed\Type3d.tmf
*$POSITION 961 113
*$LAYER Main #
PARAMETERS 4
3300            ! 1 Maximum flow rate
3.56            ! 2 Fluid specific heat
2681.999819             ! 3 Maximum power
0.05            ! 4 Conversion coefficient
INPUTS 3
17,3            ! HE-4:Load side outlet temperature ->Inlet fluid temperature
17,4            ! HE-4:Load side flow rate ->Inlet mass flow rate
```

```
38,41               ! Chiller Control Unit:PHS ->Control signal
*** INITIAL INPUT VALUES
30 3300 1.0
*--------------------------------------------------------------------------------

* Model "Hot Water Tank" (Type 4)
*

UNIT 28 TYPE 4 Hot Water Tank
*$UNIT_NAME Hot Water Tank
*$MODEL .\Thermal Storage\Stratified Storage Tank\Fixed Inlets\Uniform Losses\Type4a.tmf
*$POSITION 1137 393
*$LAYER Water Loop #
PARAMETERS 49
1                   ! 1 Fixed inlet positions
.27                 ! 2 Tank volume
4.190               ! 3 Fluid specific heat
1000.0              ! 4 Fluid density
3.0                 ! 5 Tank loss coefficient
0.05                ! 6 Height of node-1
0.05                ! 7 Height of node-2
0.05                ! 8 Height of node-3
0.05                ! 9 Height of node-4
0.05                ! 10 Height of node-5
0.05                ! 11 Height of node-6
0.05                ! 12 Height of node-7
0.05                ! 13 Height of node-8
0.05                ! 14 Height of node-9
0.05                ! 15 Height of node-10
0.05                ! 16 Height of node-11
0.05                ! 17 Height of node-12
0.05                ! 18 Height of node-13
0.05                ! 19 Height of node-14
0.05                ! 20 Height of node-15
0.05                ! 21 Height of node-16
0.05                ! 22 Height of node-17
0.05                ! 23 Height of node-18
0.05                ! 24 Height of node-19
0.05                ! 25 Height of node-20
0.05                ! 26 Height of node-21
0.05                ! 27 Height of node-22
0.05                ! 28 Height of node-23
0.05                ! 29 Height of node-24
0.05                ! 30 Height of node-25
0.05                ! 31 Height of node-26
0.05                ! 32 Height of node-27
0.05                ! 33 Height of node-28
0.05                ! 34 Height of node-29
0.05                ! 35 Height of node-30
1                   ! 36 Auxiliary heater mode
3                   ! 37 Node containing heating element 1
1                   ! 38 Node containing thermostat 1
60                  ! 39 Set point temperature for element 1
5.0                 ! 40 Deadband for heating element 1
16199.998801                ! 41 Maximum heating rate of element 1
15                  ! 42 Node containing heating element 2
```

```
15                  ! 43 Node containing thermostat 2
55.0                ! 44 Set point temperature for element 2
5.0                 ! 45 Deadband for heating element 2
16199.998801                ! 46 Maximum heating rate of element 2
0.0                 ! 47 Not used (Flue UA)
20.0                ! 48 Not used (Tflue)
100.0               ! 49 Boiling point
INPUTS 7
0,0                 ! [unconnected] Hot-side temperature
0,0                 ! [unconnected] Hot-side flowrate
20,1                ! P1:Outlet fluid temperature ->Cold-side temperature
20,2                ! P1:Outlet flow rate ->Cold-side flowrate
0,0                 ! [unconnected] Environment temperature
0,0                 ! [unconnected] Control signal for element 1
0,0                 ! [unconnected] Control signal for element 2
*** INITIAL INPUT VALUES
45.0 100.0 20.0 100.0 22.0 1.0 1.0
DERIVATIVES 30
50                  ! 1 Initial temperature of node-1
50                  ! 2 Initial temperature of node-2
50                  ! 3 Initial temperature of node-3
50                  ! 4 Initial temperature of node-4
50                  ! 5 Initial temperature of node-5
50                  ! 6 Initial temperature of node-6
50                  ! 7 Initial temperature of node-7
50                  ! 8 Initial temperature of node-8
50                  ! 9 Initial temperature of node-9
50                  ! 10 Initial temperature of node-10
50                  ! 11 Initial temperature of node-11
50                  ! 12 Initial temperature of node-12
50                  ! 13 Initial temperature of node-13
50                  ! 14 Initial temperature of node-14
50                  ! 15 Initial temperature of node-15
50                  ! 16 Initial temperature of node-16
50                  ! 17 Initial temperature of node-17
50                  ! 18 Initial temperature of node-18
50                  ! 19 Initial temperature of node-19
50                  ! 20 Initial temperature of node-20
50                  ! 21 Initial temperature of node-21
50                  ! 22 Initial temperature of node-22
50                  ! 23 Initial temperature of node-23
50                  ! 24 Initial temperature of node-24
50                  ! 25 Initial temperature of node-25
50                  ! 26 Initial temperature of node-26
50                  ! 27 Initial temperature of node-27
50                  ! 28 Initial temperature of node-28
50                  ! 29 Initial temperature of node-29
50                  ! 30 Initial temperature of node-30
*-------------------------------------------------------------------------------

* Model "Cooling Unit" (Type 1246)
*

UNIT 22 TYPE 1246       Cooling Unit
*$UNIT_NAME Cooling Unit
*$MODEL .\HVAC Library (TESS)\Auxiliary Cooler\Type1246.tmf
```

```
*$POSITION 1131 166
*$LAYER Main #
*$# AUXILIARY COOLER (FLUID)
PARAMETERS 2
107999.992122               ! 1 Rated capacity
3.56                ! 2 Specific heat of fluid
INPUTS 6
18,1                ! P5:Outlet fluid temperature ->Inlet fluid temperature
18,2                ! P5:Outlet flow rate ->Inlet flow rate
0,0                 ! [unconnected] Control function
0,0                 ! [unconnected] Set point temperature
0,0                 ! [unconnected] Overall loss coefficient
0,0                 ! [unconnected] Temperature of surroundings
*** INITIAL INPUT VALUES
15 10000.0 1 15 0.0 20.0
*-------------------------------------------------------------------------------

* Model "Tank Temperature Profile" (Type 65)
*

UNIT 29 TYPE 65             Tank Temperature Profile
*$UNIT_NAME Tank Temperature Profile
*$MODEL .\Output\Online Plotter\Online Plotter With File\TRNSYS-Supplied Units\Type65a.tmf
*$POSITION 1110 286
*$LAYER Main #
PARAMETERS 12
10                  ! 1 Nb. of left-axis variables
0                   ! 2 Nb. of right-axis variables
0.0                 ! 3 Left axis minimum
100                 ! 4 Left axis maximum
0.0                 ! 5 Right axis minimum
1000.0              ! 6 Right axis maximum
1                   ! 7 Number of plots per simulation
12                  ! 8 X-axis gridpoints
0                   ! 9 Shut off Online w/o removing
32                  ! 10 Logical Unit for output file
2                   ! 11 Output file units
0                   ! 12 Output file delimiter
INPUTS 10
28,13               ! Hot Water Tank:Temperature of node 1+-1 ->Left axis variable-1
28,16               ! Hot Water Tank:Temperature of node 1+-4 ->Left axis variable-2
28,19               ! Hot Water Tank:Temperature of node 1+-7 ->Left axis variable-3
28,22               ! Hot Water Tank:Temperature of node 1+-10 ->Left axis variable-4
28,25               ! Hot Water Tank:Temperature of node 1+-13 ->Left axis variable-5
28,28               ! Hot Water Tank:Temperature of node 1+-16 ->Left axis variable-6
28,31               ! Hot Water Tank:Temperature of node 1+-19 ->Left axis variable-7
28,34               ! Hot Water Tank:Temperature of node 1+-22 ->Left axis variable-8
28,37               ! Hot Water Tank:Temperature of node 1+-25 ->Left axis variable-9
28,40               ! Hot Water Tank:Temperature of node 1+-28 ->Left axis variable-10
*** INITIAL INPUT VALUES
Temperature Temperature Temperature Temperature Temperature Temperature
Temperature Temperature Temperature Temperature
LABELS  3
"Temperatures"
" "
"Stratification"
```

```
*** External files
ASSIGN "C:\Users\CHRIS\Documents\Modelling Results Files\Tank Stratification" 32
*|? What file should the online print to? |1000
*-------------------------------------------------------------------------------

END
```

Appendix C Thermocouple Calibration Data and Graphs

A calibration experiment was conducted to derive a relationship between the temperature and the voltage reading of the thermocouples (see Section 3.3.1 for complete experimental details). This Appendix presents the recorded data and the graphs used to derive the relationship for each of the two types of thermocouple wire. Table C-1 and Figure C-1 present the results for the 30 gauge Type-T thermocouple wire while Table C-2 and Figure C-2 present the results for the 24 gauge thermocouple wire. Each table shows the average of the 36 measurements taken for the RTD temperature, CJC temperature and voltage produced by the thermocouple at each bath set-point. The bath was first set at 5°C and subsequently increased by 2°C increments. While the bath was set to a whole number, the internal thermometer has limited accuracy and therefore the bath temperature was measured using the much more accurate RTD.

Table C-1: Recorded temperatures and voltages for calibration of 30 gauge wire

Bath Temperature (°C)	CJC Temperature (°C)	Temperature Difference (°C)	Voltage (V)	Standard Deviation on Voltage Reading (V)
5.143	21.032	-15.889	-6.239E-04	4.200E-07
7.145	21.051	-13.906	-5.464E-04	4.819E-07
9.133	21.115	-11.982	-4.706E-04	9.734E-07
11.121	21.102	-9.981	-3.917E-04	4.506E-07
13.109	21.183	-8.073	-3.159E-04	6.538E-07
15.097	21.134	-6.037	-2.349E-04	4.580E-07
16.880	21.136	-4.255	-1.645E-04	2.109E-06
18.821	21.100	-2.279	-8.530E-05	2.925E-06
20.836	20.852	-0.016	6.312E-06	3.536E-06
22.848	20.681	2.167	9.511E-05	2.808E-06
24.851	20.663	4.188	1.778E-04	2.409E-06
26.848	20.925	5.923	2.491E-04	1.066E-06
28.839	21.117	7.722	3.234E-04	1.333E-06
30.824	21.076	9.747	4.073E-04	1.526E-06
32.807	20.910	11.897	4.963E-04	1.433E-06

34.793	20.836	13.957	5.820E-04	1.586E-06
36.772	20.762	16.010	6.677E-04	1.112E-06
38.759	21.055	17.704	7.391E-04	4.726E-07
40.747	21.249	19.498	8.149E-04	9.503E-07
42.741	21.291	21.450	8.970E-04	2.291E-06
44.735	21.121	23.614	9.880E-04	1.071E-06
46.729	21.001	25.728	1.077E-03	1.965E-06
48.714	20.862	27.852	1.168E-03	1.583E-06
50.706	20.767	29.939	1.257E-03	1.632E-06
52.700	20.706	31.994	1.345E-03	1.276E-06
54.689	20.636	34.052	1.434E-03	1.419E-06
56.665	20.534	36.131	1.524E-03	1.658E-06
58.647	20.468	38.179	1.612E-03	1.131E-06
60.626	20.367	40.259	1.702E-03	1.049E-06
62.599	20.295	42.303	1.792E-03	1.069E-06
64.573	20.241	44.331	1.880E-03	1.070E-06
66.554	20.187	46.368	1.970E-03	9.781E-07
68.525	20.176	48.349	2.057E-03	9.274E-07
70.511	20.313	50.198	2.140E-03	1.304E-06
72.447	20.380	52.067	2.223E-03	1.083E-06
74.812	20.355	54.456	2.331E-03	1.125E-06
76.719	20.882	55.837	2.395E-03	3.739E-06
78.773	20.888	57.886	2.488E-03	2.715E-06
80.755	20.801	59.954	2.582E-03	1.998E-06
82.753	20.409	62.344	2.688E-03	1.356E-06
84.664	20.295	64.370	2.780E-03	1.674E-06
86.644	20.239	66.405	2.873E-03	2.544E-06
88.575	20.285	68.290	2.960E-03	2.251E-06
90.490	20.253	70.237	3.050E-03	2.841E-06
92.467	20.167	72.300	3.144E-03	2.659E-06
94.349	20.139	74.210	3.233E-03	3.302E-06

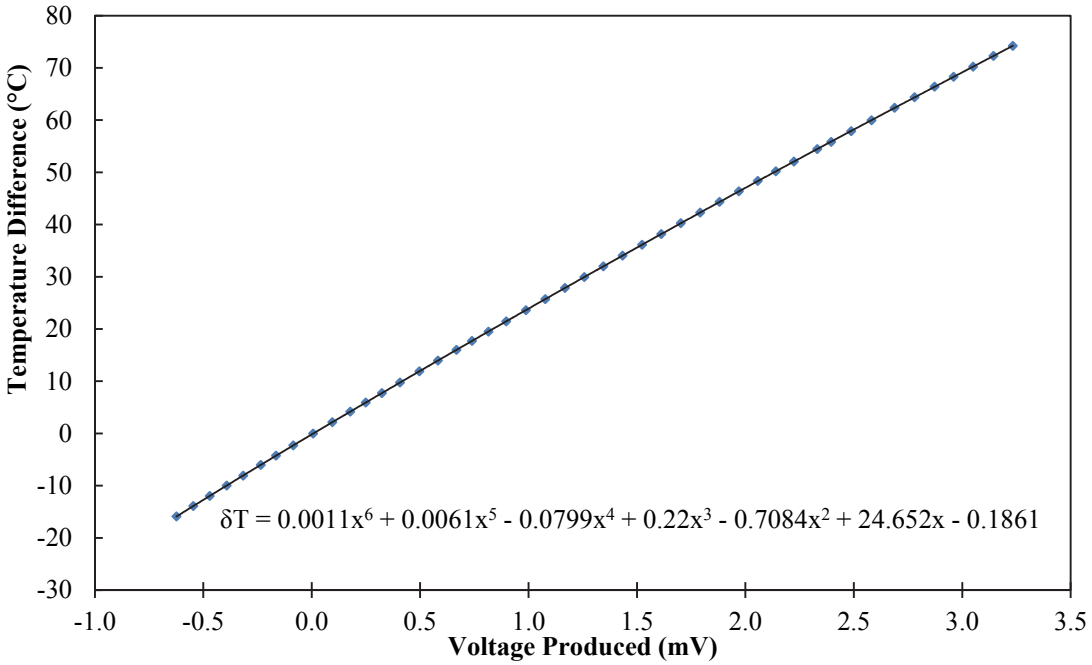

Figure C-1: Plot of temperature difference and voltage with trend line for 30 gauge wire

Table C-2: Recorded temperatures and voltages for calibration of 24 gauge wire

Bath Temperature (°C)	CJC Temperature (°C)	Temperature Difference (°C)	Voltage (V)	Standard Deviation on Voltage Reading (V)
5.143	21.024	-15.881	-6.333E-04	4.933E-07
7.145	21.042	-13.897	-5.558E-04	4.278E-07
9.133	21.108	-11.974	-4.803E-04	9.915E-07
11.121	21.096	-9.975	-4.016E-04	4.899E-07
13.109	21.175	-8.066	-3.259E-04	6.349E-07
15.097	21.122	-6.025	-2.450E-04	6.171E-07
16.880	21.132	-4.252	-1.753E-04	2.161E-06
18.821	21.100	-2.279	-9.675E-05	3.071E-06
20.836	20.853	-0.017	-5.076E-06	3.660E-06
22.848	20.680	2.168	8.375E-05	3.076E-06
24.851	20.658	4.193	1.664E-04	2.499E-06
26.848	20.922	5.926	2.377E-04	1.406E-06
28.839	21.116	7.723	3.119E-04	1.740E-06
30.824	21.076	9.747	3.956E-04	1.898E-06
32.807	20.909	11.898	4.846E-04	1.612E-06
34.793	20.833	13.960	5.703E-04	1.580E-06
36.772	20.763	16.009	6.558E-04	1.146E-06
38.759	21.059	17.700	7.268E-04	4.150E-07
40.747	21.255	19.492	8.024E-04	1.116E-06
42.741	21.289	21.453	8.852E-04	2.368E-06
44.735	21.142	23.593	9.751E-04	9.463E-07
46.729	21.000	25.729	1.065E-03	2.031E-06
48.714	20.862	27.852	1.155E-03	1.470E-06
50.706	20.765	29.942	1.245E-03	1.658E-06
52.700	20.703	31.997	1.332E-03	1.394E-06
54.689	20.633	34.055	1.421E-03	1.446E-06
56.665	20.530	36.135	1.511E-03	1.702E-06
58.647	20.463	38.184	1.599E-03	1.226E-06
60.626	20.362	40.264	1.689E-03	1.053E-06
62.599	20.289	42.309	1.779E-03	1.034E-06
64.573	20.235	44.338	1.867E-03	1.115E-06
66.554	20.178	46.376	1.957E-03	1.127E-06
68.525	20.165	48.360	2.044E-03	9.123E-07
70.511	20.308	50.204	2.126E-03	1.138E-06
72.447	20.372	52.076	2.210E-03	1.077E-06
74.812	20.352	54.459	2.318E-03	1.007E-06
76.719	20.875	55.844	2.382E-03	3.454E-06
78.773	20.893	57.880	2.474E-03	2.112E-06
80.755	20.796	59.959	2.568E-03	1.792E-06
82.753	20.401	62.353	2.674E-03	9.397E-07

84.664	20.285	64.380	2.767E-03	1.404E-06
86.644	20.227	66.417	2.859E-03	1.835E-06
88.575	20.272	68.303	2.947E-03	1.707E-06
90.490	20.242	70.248	3.037E-03	1.983E-06
92.467	20.153	72.314	3.131E-03	1.923E-06
94.349	20.132	74.217	3.220E-03	2.602E-06

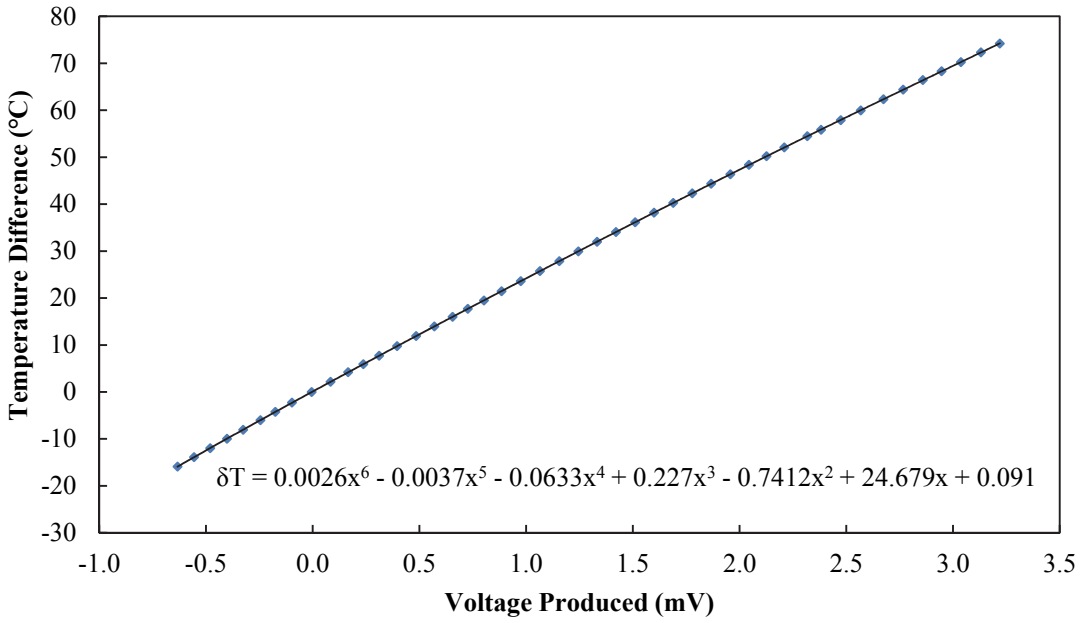

Figure C-2: Plot of temperature difference and voltage with trend line for 24 gauge wire

Appendix D Thermopile Calibration Results

A second calibration experiment was conducted to determine the relationship between the temperature difference between the two sides of the thermopiles and the voltage produced. This relationship changes depending on the temperature of the cold side of the thermopile, and therefore was replicated over a range of cold side temperatures. Figure D-1 shows the different combinations of hot and cold side bath set point temperatures that were tested.

Cold Side(°C)	Hot Side (°C)																	
5	5	10	15	20	25	30	35	40	45	50	55	60	65	70	75	80	85	90	95
10	10	15	20	25	30	35	40	45	50	55	60	65	70	75	80	85	90	95	
15	15	20	25	30	35	40	45	50	55	60	65	70	75	80	85	90	95		
20	20	25	30	35	40	45	50	55	60	65	70	75	80	85	90	95			
25	25	30	35	40	45	50	55	60	65	70	75	80	85	90	95				
30	30	35	40	45	50	55	60	65	70	75	80	85	90	95					
35	35	40	45	50	55	60	65	70	75	80	85	90	95						
60	60	65	70	75	80	85	90	95											
65	65	70	75	80	85	90	95												
70	70	75	80	85	90	95													
75	75	80	85	90	95														
80	80	85	90	95															
85	85	90	95																
90	90	95																	

Figure D-1: Cold and hot side temperature set points

The results for each cold side calibration run are presented in Table D-1 to Table D-14. These tables show the voltage produced by the thermopile and the measured hot and cold side temperatures along with the calculated temperature difference. These results were used to derive the equations for each cold sided temperature presented in Table 6-2.

Table D-1: Thermopile calibration results - cold side 5°C

Voltage Produced (mV)	Cold Side (°C)	Hot Side (°C)	Temperature Difference (°C)
0.001	5.08	5.10	0.02
0.791	5.09	10.15	5.05
1.582	5.10	15.11	10.01
2.379	5.10	20.07	14.97
3.187	5.10	25.04	19.95
4.009	5.10	30.02	24.92
4.829	5.09	34.99	29.90
5.663	5.09	39.94	34.85
6.464	5.09	44.72	39.62
7.312	5.10	49.68	44.58
8.166	5.10	54.63	49.53
9.025	5.09	59.58	54.48
9.889	5.09	64.49	59.40
10.760	5.09	69.43	64.34
11.634	5.10	74.35	69.25
12.510	5.10	79.24	74.14
13.399	5.10	84.14	79.04
14.294	5.10	89.04	83.94
15.334	5.10	94.58	89.48

Table D-2: Thermopile calibration results - cold side 10°C

Voltage Produced (mV)	Cold Side (°C)	Hot Side (°C)	Temperature Difference (°C)
-0.002	10.07	10.43	0.35
0.706	10.07	14.72	4.65
1.526	10.07	19.78	9.71
2.349	10.07	24.82	14.75
3.177	10.08	29.84	19.77
4.014	10.07	34.81	24.74
4.846	10.07	39.78	29.70
5.685	10.07	44.74	34.67
6.530	10.07	49.70	39.63
7.385	10.07	54.66	44.59
8.247	10.07	59.62	49.55
9.119	10.07	64.55	54.48
9.978	10.07	69.43	59.36
10.853	10.07	74.38	64.31
11.732	10.07	79.22	69.15
12.621	10.07	84.15	74.08
13.527	10.07	89.04	78.97
14.536	10.07	94.51	84.44

Table D-3: Thermopile calibration results - cold side 15°C

Voltage Produced (mV)	Cold Side (°C)	Hot Side (°C)	Temperature Difference (°C)
0.007	15.05	15.08	0.04
0.807	15.05	20.08	5.02
1.574	15.05	24.80	9.75
2.397	15.05	29.82	14.77
3.229	15.05	34.80	19.75
4.060	15.05	39.77	24.72
4.898	15.05	44.74	29.69
5.744	15.05	49.71	34.66
6.595	15.05	54.66	39.61
7.458	15.05	59.61	44.56
8.317	15.05	64.54	49.49
9.185	15.05	69.47	54.42
10.064	15.05	74.37	59.32
10.939	15.05	79.24	64.20
11.811	15.05	84.08	69.03
12.726	15.05	89.04	73.99
13.627	15.05	93.92	78.87

Table D-4: Thermopile calibration results - cold side 20°C

Voltage Produced (mV)	Cold Side (°C)	Hot Side (°C)	Temperature Difference (°C)
0.774	20.03	24.83	4.80
1.600	20.03	29.83	9.80
2.427	20.03	34.81	14.78
3.256	20.03	39.78	19.75
4.096	20.03	44.76	24.73
4.946	20.03	49.72	29.69
5.793	20.03	54.68	34.65
6.657	20.03	59.63	39.60
7.524	20.03	64.57	44.54
8.396	20.03	69.51	49.48
9.272	20.03	74.42	54.39
10.148	20.03	79.30	59.27
11.028	20.03	84.15	64.11
11.939	20.03	89.14	69.11
12.831	20.03	93.98	73.95
0.774	20.03	24.83	4.80

Table D-5: Thermopile calibration results - cold side 25°C

Voltage Produced (mV)	Cold Side (°C)	Hot Side (°C)	Temperature Difference (°C)
0.005	25.00	25.04	0.04
0.795	25.00	29.85	4.85
1.625	25.00	34.84	9.84
2.456	24.99	39.80	14.81
3.296	25.00	44.78	19.78
4.143	25.00	49.75	24.76
4.999	25.00	54.72	29.72
5.859	25.00	59.66	34.66
6.722	25.00	64.61	39.61
7.600	25.00	69.56	44.56
8.474	25.00	74.47	49.47
9.358	25.00	79.38	54.38
10.239	25.00	84.24	59.25
11.151	25.00	89.23	64.23
12.038	25.00	94.05	69.05

Table D-6: Thermopile calibration results - cold side 30°C

Voltage Produced (mV)	Cold Side (°C)	Hot Side (°C)	Temperature Difference (°C)
-0.005	29.98	29.96	-0.01
0.804	29.98	34.83	4.85
1.640	29.98	39.79	9.82
2.478	29.97	44.76	14.79
3.327	29.98	49.73	19.75
4.181	29.98	54.69	24.71
5.039	29.98	59.64	29.66
5.899	29.98	64.57	34.59
6.774	29.98	69.52	39.55
7.653	29.98	74.44	44.46
8.533	29.97	79.34	49.37
9.423	29.97	84.23	54.25
10.297	29.97	89.08	59.10
11.332	29.97	94.50	64.52

Table D-7: Thermopile calibration results - cold side 35°C

Voltage Produced (mV)	Cold Side (°C)	Hot Side (°C)	Temperature Difference (°C)
0.007	34.96	34.95	-0.01
0.826	34.96	39.85	4.90
1.669	34.95	44.85	9.90
2.519	34.96	49.84	14.89
3.379	34.95	54.81	19.86
4.237	34.95	59.76	24.80
5.106	34.95	64.72	29.77
5.977	34.95	69.65	34.70
6.845	34.95	74.57	39.61
7.721	34.96	79.46	44.51
8.599	34.95	84.32	49.37
9.484	34.96	89.19	54.23
10.492	34.95	94.40	59.45

Table D-8: Thermopile calibration results - cold side 60°C

Voltage Produced (mV)	Cold Side (°C)	Hot Side (°C)	Temperature Difference (°C)
-0.013	59.808	59.759	-0.049
0.849	59.812	64.673	4.862
1.719	59.815	69.617	9.802
2.599	59.814	74.530	14.715
3.483	59.815	79.427	19.612
4.368	59.814	84.306	24.492
5.255	59.805	89.147	29.342
6.131	59.816	93.949	34.133

Table D-9: Thermopile calibration results - cold side 65°C

Voltage Produced (mV)	Cold Side (°C)	Hot Side (°C)	Temperature Difference (°C)
0.002	64.76	64.79	0.03
0.850	64.76	69.60	4.84
1.720	64.77	74.52	9.75
2.610	64.77	79.43	14.66
3.499	64.77	84.35	19.58
4.368	64.77	89.17	24.41
5.253	64.77	93.99	29.21

Table D-10: Thermopile calibration results - cold side 70°C

Voltage Produced (mV)	Cold Side (°C)	Hot Side (°C)	Temperature Difference (°C)
-0.027	69.72	69.65	-0.08
0.841	69.72	74.51	4.78
1.724	69.73	79.42	9.69
2.589	69.73	84.34	14.61
3.482	69.74	89.27	19.52
4.384	69.73	93.99	24.26

Table D-11: Thermopile calibration results - cold side 75°C

Voltage Produced (mV)	Cold Side (°C)	Hot Side (°C)	Temperature Difference (°C)
-0.055	74.66	74.44	-0.22
0.828	74.65	79.34	4.69
1.709	74.65	84.20	9.55
2.609	74.65	89.14	14.49
3.503	74.66	93.97	19.31

Table D-12: Thermopile calibration results - cold side 80°C

Voltage Produced (mV)	Cold Side (°C)	Hot Side (°C)	Temperature Difference (°C)
-0.025	79.62	79.54	-0.09
0.852	79.63	84.38	4.75
1.749	79.62	89.24	9.63
2.730	79.62	94.54	14.92

Table D-13: Thermopile calibration results - cold side 85°C

Voltage Produced (mV)	Cold Side (°C)	Hot Side (°C)	Temperature Difference (°C)
-0.038	84.53	84.41	-0.12
0.836	84.53	89.20	4.66
1.702	84.51	93.91	9.39

Table D-14: Thermopile calibration results - cold side 90°C

Voltage Produced (mV)	Cold Side (°C)	Hot Side (°C)	Temperature Difference (°C)
0.085	89.54	89.28	-0.25
0.858	89.51	94.21	4.69